THE EFFECTS OF POROSITY AND CROSSLINKING OF A COLLAGEN BASED ARTIFICIAL SKIN ON WOUND HEALING

by

Elizabeth Hsiu-Yun Chen

B.S.E., University of Pennsylvania
(1979)

SUBMITTED IN PARTIAL FULFILLMENT

OF THE REQUIREMENTS FOR THE

DEGREE OF MASTER OF

SCIENCE

at the

MASSACHUSETTS INSTITUTE OF

TECHNOLOGY

June, 1982

Signature of Author.....
Department of Mechanical Engineering
May 7, 1982

Certified by.....
Ioannis V. Yannas
Thesis Supervisor

Accepted by.....
Chairman, Department Committee
Warren M. Rohsenow

THE EFFECTS OF POROSITY AND CROSSLINKING OF A COLLAGEN BASED ARTIFICIAL SKIN ON WOUND HEALING

by

Elizabeth Hsiu-Yun Chen

Submitted to the Department of Mechanical Engineering on May 7, 1982 in partial fullfillment of the requirements for the Degree of Master of Science.

ABSTRACT

The effects of two parameters, crosslink density and porosity on the bilayer artificial skin (stage 1) were studied. Two materials of different crosslink density were manufactured by processing the porous collagenous, bottom layer of the artificial skin with and without glutaraldehyde treatment. Materials with three different porosities were manufactured by varying the concentration of collagen in the porous foam-like layer. Pore structures were quantitated by a method using reflected light microscopy and computerized stereology. Increasing the collagen concentration had two major effects on the porosity of the collagen foam, 1) a decrease in the mean pore width and narrower distributions of pore widths of the "pan side" of the foam, and 2) a higher degree of orientation of pores in the edge view.

Wound healing responses to changes in both crosslink density and porosity were determined by grafting full thickness skin wounds in guinea pigs with each of the materials manufactured. Increased crosslinked density decreased the rates of collagen degradation and wound closure. More subtle decreases in these rates were observed with increased collagen concentration. The more concentrated collagen grafts with narrower distributions of pore widths and mean pore widths of 80μ and 100μ inhibited the migration of mesenchymal cells into the grafts. A highly porous collagen surface with a broad distribution of pore widths containing a significant number of widths as large as 500μ and a mean pore width of 150μ allowed rapid cellular infiltration.

These studies have shown that variations in the crosslink density of the collagen foams may be a more effective way of controlling collagen degradation and wound contraction than alterations in the collagen concentration.

Thesis Supervisor: Ioannis V. Yannas

Title: Professor of Polymer Science and Engineering

ACKNOWLEDGEMENTS

I would like to thank Professor Yannas for his guidance in this project. His experience was a great aid at many points in my research.

I am particularly grateful for all the help and encouragement I received from Eugene Skrabut. Without his help I would still be trying to finish this thesis.

My thanks also go to Jude Colt, Jim Dowd, David Zahnizer, and my sister, Dorothy Rogers, for the many hours of work they contributed to this effort. The support they gave me made the long hours more enjoyable.

Finally I would like to thank Susan Lonergan for helping me type this thesis.

TABLE OF CONTENTS

LIST OF FIGURES

LIST OF TABLES

1. INTRODUCTION AND BACKGROUND

Skin envelops the entire body covering an area of approximately 1.7 square meters on an adult human. Acting as a barrier it prevents bacteria, toxic materials and ultraviolet radiation from entering the body and reduces the loss of fluid, electrolytes and other essential materials [1]. Skin also serves as a sensory organ and regulates body temperature. It is the body's primary defense against the environment and thus, is highly subject to trauma.

There are two major layers comprising skin, the epidermis and the dermis, see Figure 1.1.1. The epidermis has four layers. The innermost layer, the stratum malpighi contains a basal layer from which basal cells mature to form the other layers of the epidermis. The outer layer, the stratum corneum contains anucleated cells which are highly oriented parallel to the surface of the skin. As the basal cells mature and migrate upwards, they produce fibrillar and amorphous proteins forming the keratin of the stratum corneum and lose their mitotic ability, see Figure 1.1.2. Between the inner and outermost layers of the epidermis are the stratum granulosum and the stratum lucidum. The stratum granulosum contains keratohyalin granules which are thought to be the precursors of keratin [2]. The stratum lucidum is a hyalin layer found in thick epidermis.

The dermis predominantly contains collagen and ground substance reinforced with elastic and reticular fibers. Fibroblasts, mast cells, histiocytes and nerve endings sensitive to pain, pressure, and temperature are also found in the dermis. Epidermal appendages such as sweat glands and hair follicles, penetrate into the dermis from the epidermis.

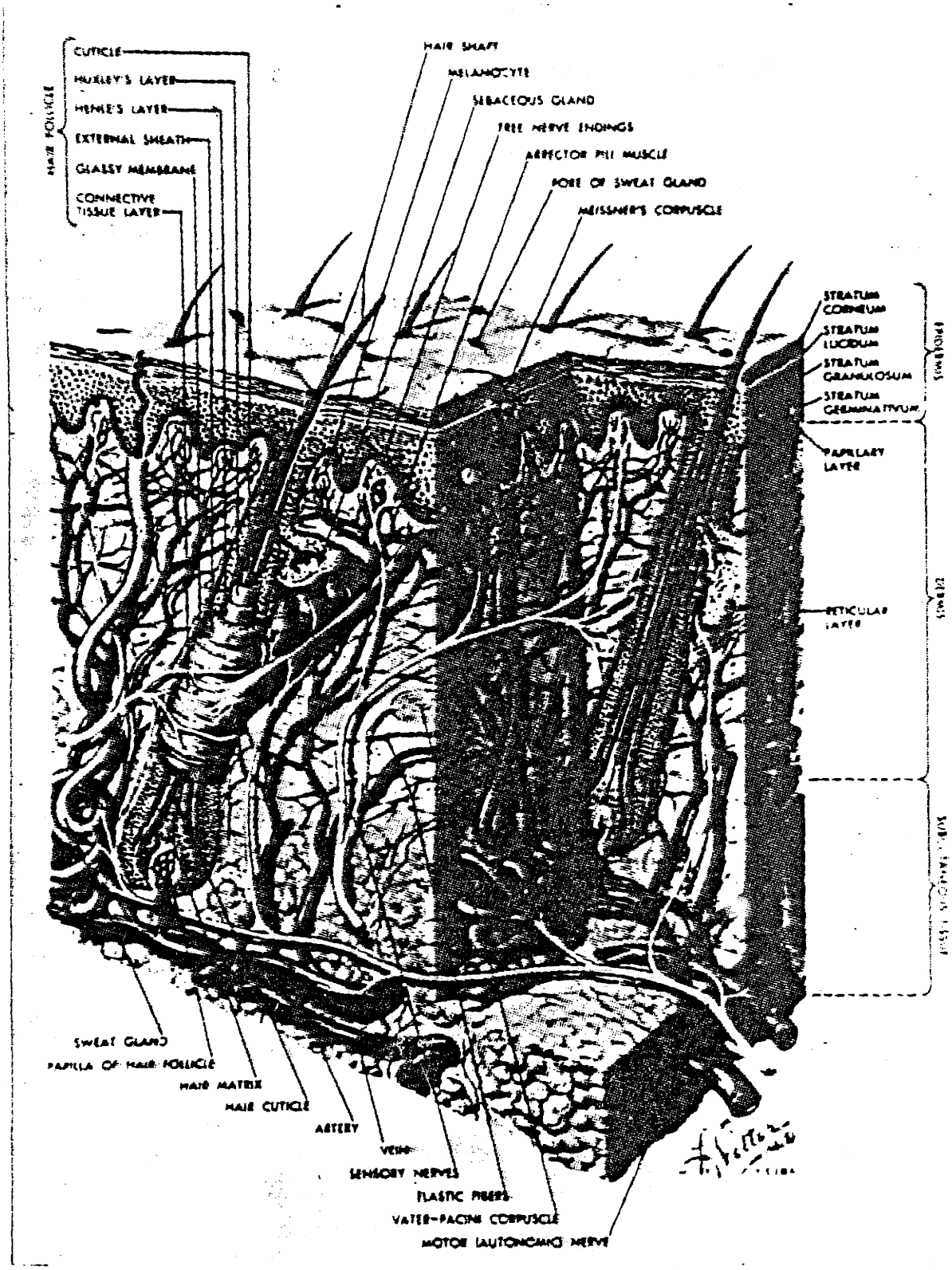

Figure 1.1.1 Three dimensional cross section of human skin (CIBA Pharmaceutical Co., Division of CIBA-GEIGY Corporation, illustrated by Frank H. Netter, M.D.)

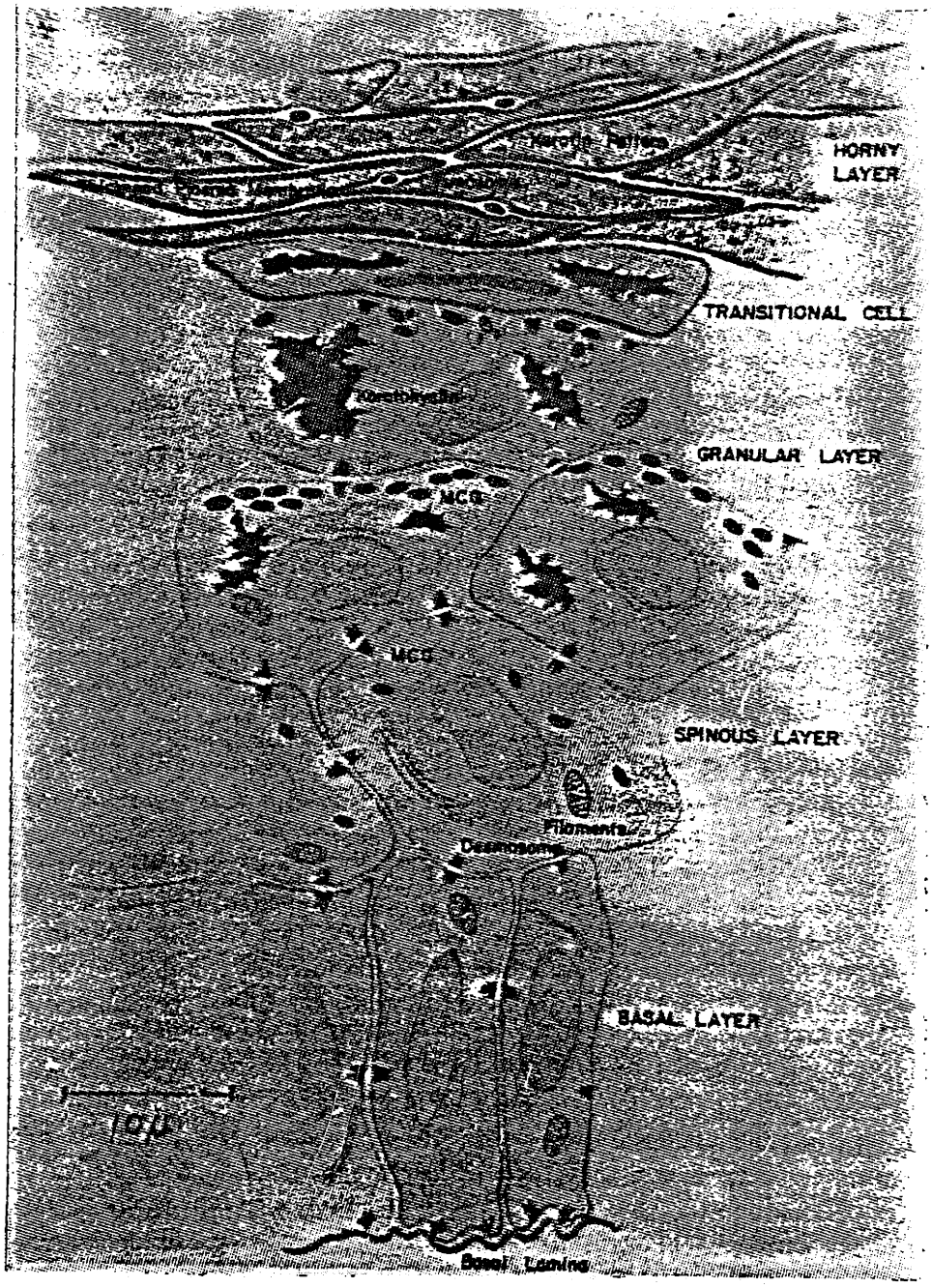

Figure 1.1.2 Schematic diagram showing the layers of the epidermis and the maturation of the basal cells [2].

Each year approximately 130,000 individuals are hospitalized for treatment of wounds from exposure to fire [3]. Many others suffer from chemical or mechanical injuries causing severe skin loss. These injuries inflict extensive damage to the body and are often life threatening. The greatest threats are from fluid loss and bacterial infection. Those patients that survive the initial trauma must live with deep, massive scars and severe contractures, possibly resulting in deformity and loss of joint function.

There is an obvious need for skin replacements. Autografting, one of the best treatment methods for skin loss, leaves no contractures. However, the low availability of autografts for a patient with over 50% skin loss and the additional trauma due to removal of the autograft reduces the feasibility of autografting for the excessively burned patient.

Allografts and xenografts (e.g., porcine skin grafts) are effective for only a short time before rejection of the grafts occurs leaving the wound open once again. The availability of allografts is poor. Porcine skin grafts are commercially available; however, they must be excised every 3 to 4 days before adhesion between the wound and the xenograft takes place and rejection begins [1].

Membranes made from reconstituted collagen or synthetic polymers have been used to treat burns [4-8]. However, none have been widely accepted. In order to design such a skin replacement, careful consideration of the physical and chemical parameters is necessary. Over the last decade an artificial skin (Stage 1) has been developed which successfully serves as a temporary coverage for full thickness wounds [9]. [10] The Stage 1 artificial skin is a bilayer membrane composed of a collagen-

glycosaminoglycan (GAG) foam bottom layer and a silicone rubber top layer. The artificial skin wets the surface of the wound well, draping over the contours leaving no dead spaces in which bacteria may breed. The collagen-GAG foam serves as a scaffolding into which mesenchymal cells migrate, infiltrate, and multiply forming a "neodermis." Epidermal cells also may migrate from the edges of the wound between the silicone and collagen-GAG layer provided intimate contact between the graft and the intact epidermis is obtained. Collagen is also available in large quantities and the products of its biodegradation are nontoxic. GAG is available commercially from mammalian and chondrichthyes sources. The silicone rubber layer acts as a barrier to moisture and environmental bacteria, reducing the fluid loss and infection at the wound site. The collagen foam undergoes degradation as fibroblasts infiltrate the membrane producing collagenase which chemically attacks the collagen matrix. Vascularization also occurs. After several weeks, the silicone layer can be easily peeled off, and in clinical use autoepidermis is mesh grafted over the wound. The result is a neodermis covered with an epidermal layer. The regenerated area is soft, pliable, and elastic and closely resembles normal skin.

Grafting of full thickness wounds in guinea pigs has given information on contraction kinetics, cell-matrix interaction, and scar formation. Contraction can be defined as "the process whereby the intact skin bordering the deficit is drawn inwards, reducing the area of the wound." [11]. Compared to the open wound response, the bilayer membrane retards contraction, see Figure 1.1.3. However, the scar areas at 60 days postgrafting of these treatments show no difference.

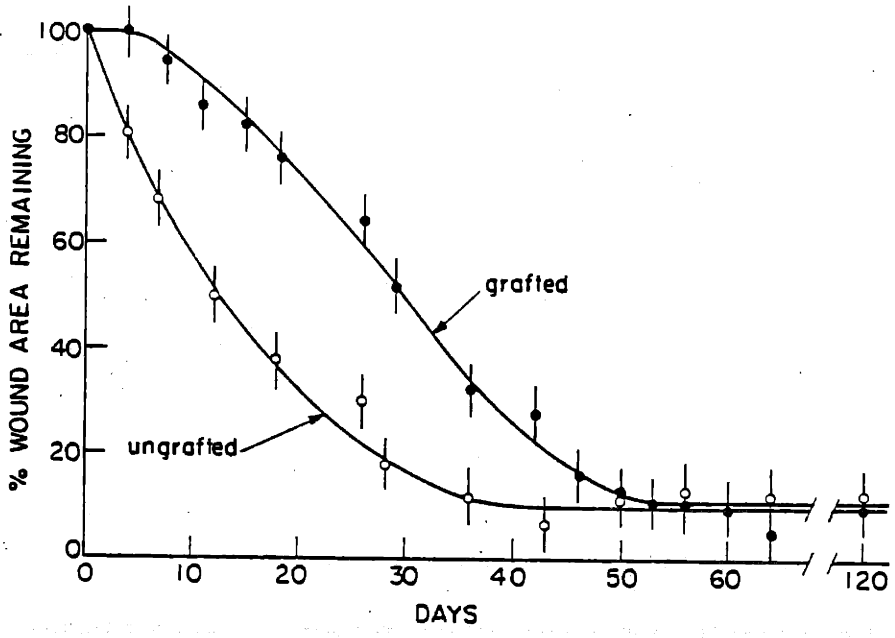

Figure 1.1.3 Reduction in area of full thickness skin wounds in guinea pigs. The graft used is a standard, crosslinked collagen graft, Stage 1. From Yannas [12].

Previous studies have shown the importance of crosslink density and the porosity of the collagen-GAG foams on degradation and wound healing. Hijar [13] demonstrated that crosslinking of collagen decreases the rate of enzymatic degradation in vitro. Both Chvapil, et al. [14] and White, et al. [15] have shown the rate of in vivo resorption of collagen decreased as the amount of crosslinking with glutaraldehyde was increased. Many studies have shown better cellular ingrowth with highly porous implants when compared with non-porous materials, but quantitative measurements of the porosity were not reported [16-18]. Stasikelis [19] has shown improved cellular response when a freeze dried porous sheet rather than a dense filtered sheet of collagen-GAG composite was subcutaneously implanted. The dense filtered sheet became surrounded by fibrotic sac, whereas the

cells infiltrated the porous material. Chvapil et al. [20] have demonstrated that a highly porous material greatly enhances penetration by connective tissues and vascularization in a subcutaneous implantation when compared with a dense, compact material.

Control of wound contraction kinetics and the optimization of cell growth in the collagen foam is necessary for the improvement of the artificial skin. This thesis studies the effects of crosslink density and the porosity of the collagen foam on contraction kinetics, scar formation and cellular interaction. Due to the complex chemistry and physics of these parameters it is difficult to separate them completely. However, two experiments have been designed to isolate these variables as much as possible.

In order to investigate the effect of crosslink density, collagen-GAG foams were prepared with and without crosslinking in aqueous glutaraldehyde solution. The foam treated with glutaraldehyde had the same crosslink density as the standard stage 1 material. The foam not treated with glutaraldehyde had a lower crosslink density than the Stage 1 material. To determine whether a difference in crosslink density would create a significantly different in vivo response, both materials were grafted on guinea pigs with full thickness skin wounds.

As mentioned previously, Stasikelis' experiments [19] with porosity showed a profound difference in cell infiltration when the porosity was changed from that of 5μ in a dense, non-porous sheet to that of 150μ in a highly porous foam. However, a marked increase in the rate of degradation was also seen with increased porosity. In order to understand the relationship between cellular interaction, in vivo degradation, and

porosity, two collagen-GAG foams of varying porosities that lie between the two extremes in Stasikelis' experiments were manufactured. The porosity was varied by increasing the concentration of collagen-GAG in the foams. These foams were grafted on animals with full thickness skin wounds to evaluate the *in vivo* response.

2. MATERIALS AND METHODS

2.1 MATERIALS

The collagen was supplied by H.I. Sinnamon (U.S. Dept. of Agriculture, Philadelphia, PA) and was prepared from fresh, uncured bovine hide as described by Komanowsky, et al [21]. The hides were limed, cut into very small pieces and then treated with acid. The collagen was separated from the water and then it was lyophilized. The collagen was received in this form and was stored at 4°C until it was used.

Chondroitin-6-sulfate (sodium salt, Type C, Sigma Chemical Co., St. Louis, MO) was the glycosaminoglycan (GAG) used.

Deionized water was prepared with a deionizing organic adsorption system (Hydro Services and Supplies, Inc., Durham, NC) see Figure 2.1.1.

Acetic acid (0.05M, pH3) used to process the collagen was made from deionized water and glacial acetic acid (Fisher Scientific, Medford, MA).

The silicone rubber for the top layer of the artificial skin is Silastic^{R} Medical Adhesive, Silicone Type A (Dow Corning, Midland, MI). The curing procedure which occurs at room temperature, requires moisture and produces acetic acid.

A solution of practical grade glutaraldehyde (J.T. Baker Chemical Co., Phillipsburg, NJ) in 0.05M acetic acid was used to crosslink the collagen-GAG composite at pH 3.

The completed artificial skin was stored in 70% isopropanol made from isopropanol (Matheson, Coleman and Bell, Norwood, OH) and deionized water.

MODEL 4NC2-18
ORGANIC ADSORPTION AND DEIONIZATION SYSTEM

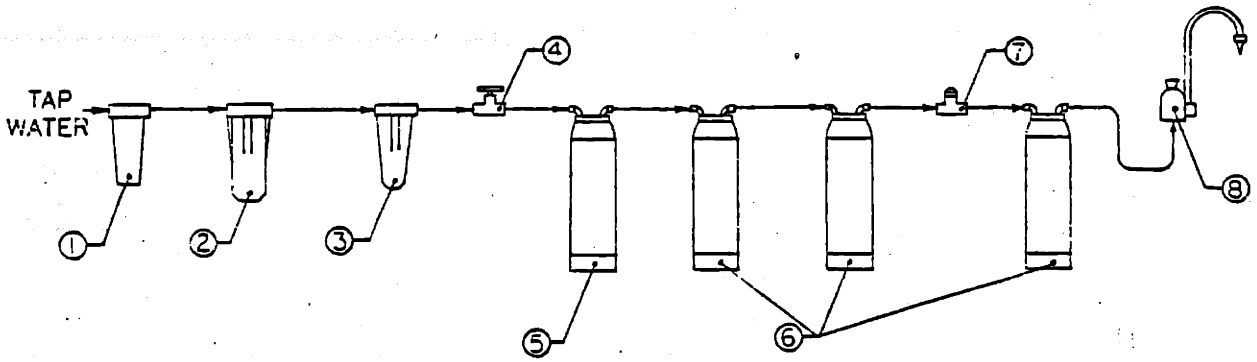

Number	Description
1	Fulflo filter 20 micron effective pore size
2	Filter .45 micron pore size
3	Sterilization filter .22 micron pore size
4	Pressure Reducer
5	Activated Carbon
6	Ion Exchange (Deionization)
7	Conducting Cell
8	Faucet

Figure 2.1.1 Deionizing Organic Adsorption System, Hydro Services, illustrated by Susan Flynn.

2.2 METHODS

The stage 1 artificial skin as described by Yannas [22-24] which has 0.5% w/w solids in the dispersion state was prepared and used as a standard or control in the following experiments. Three other materials were manufactured to investigate the effects of crosslinking and porosity. For the crosslinking study, the crosslink density was lowered by deleting the glutaraldehyde treatment of the standard material. Although this altered collagen-GAG foam has a measurable crosslink density, it will be referred to as the "noncrosslinked" material.

In order to study the effects of porosity, two materials were prepared with higher concentrations of collagen-GAG in the porous foam layer (0.8% and 1.3% w/w solids). These 0.8% and 1.3% foams are 1.6 and 2.6 times the concentration of the standard stage 1 material respectively, see Table 2.2.1. The porosities of the 1.0x, 1.6x and 2.6x materials were quantitated using scanning electron and reflected light microscopies (JSM-U3 Scanning electron microscope, Jeolco Co., Japan and Olympus Mettallurgical microscope, model BHM with photomicrographic system camera, model PM 10-A, Olympus Optical Co., Ltd., Tokyo, Japan) and stereological methods.

The molecular weight between crosslinks was measured for all four materials. Each material was grafted on guinea pigs and histology and contraction kinetics were studied, see Figure 2.2.2.

The preparation of the artificial skin may be broken down into three parts, 1) collagen-GAG dispersion preparation, 2) freeze drying procedure, and 3) siliconizing and crosslinking procedures as described

Figure 2.2.2 GENERAL PROTOCOL

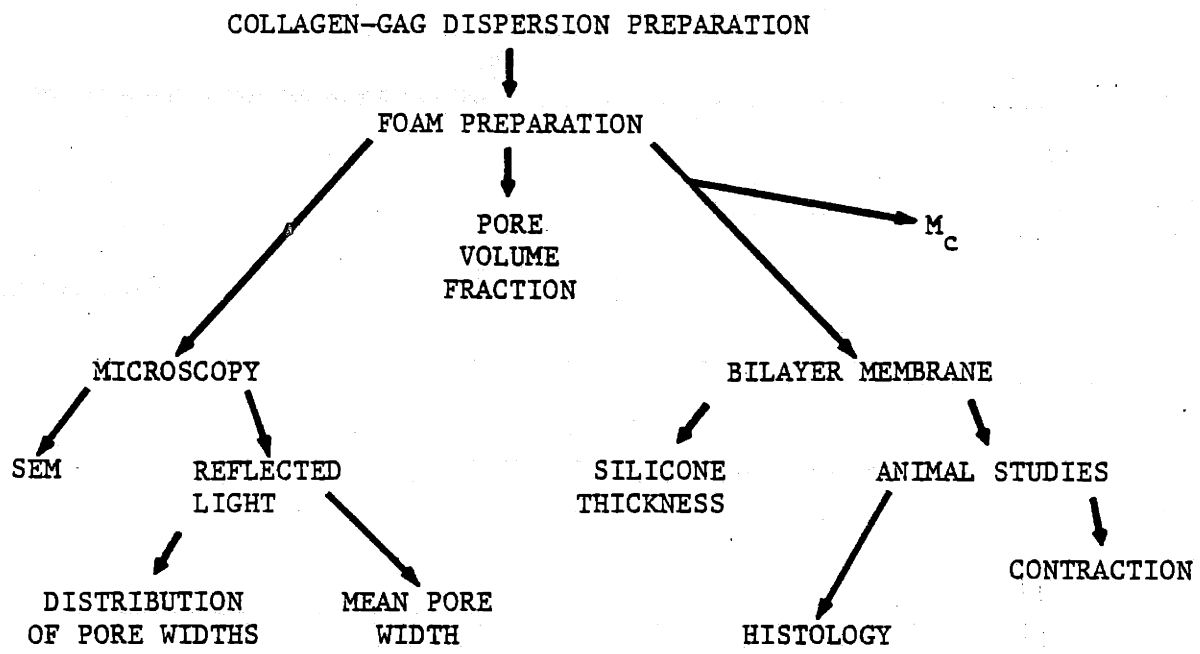

below. Refer to figures 2.2.3 through 2.2.5 for the flow charts corresponding to these three parts.

Table 2.2.1 Collagen Concentration Notation

% w/w Solids	Notation Used Here
0.5	1.0x
0.8	1.6x
1.3	2.6x

2.2.1 Collagen-GAG Dispersion Preparation

The bovine hide collagen (BHC) was comminuted in a Wiley Mill (Arthur J. Thomas Co., Philadelphia, PA) with liquid nitrogen to a 20 mesh particle size. The powdered BHC (0.55g hydrated weight. 0.50g dry weight) was dispersed in 200 ml of 0.05M acetic acid (Glacial acetic acid, Fisher Scientific, Medford, MA) for one hour in a jacketed semi-micro blender (model 8590, Eberbach Corporation, Ann Arbor, MI) mounted on a two speed blender motor through a variable power transformer (Staco, Inc., Dayton, OH, model 3PN 1010) set at 50% of 120 volts. The blenders were cooled using a Lauda/Brinkman Bath, model RC-2T (Brinkman, Westbury, NY) at 3°C. Forty milliliters of a 0.1% w/v solution of chondroitin-6-sulfate in 0.05M HOAc was added dropwise over five minutes to the blending collagen dispersion. The collagen-GAG dispersion was blended for an additional ten minutes. For all but the 2.6x material the dispersion was centrifuged for one hour at 2300 rpm (1300 g) in a CRU-5000 centrifuge (Damon, International Equipment Co., Needham Heights, MA) to concentrate the collagen-GAG mixture. For the standard, the noncrosslinked, and the

Figure 2.2.3 COLLAGEN-GAG DISPERSION PREPARATION

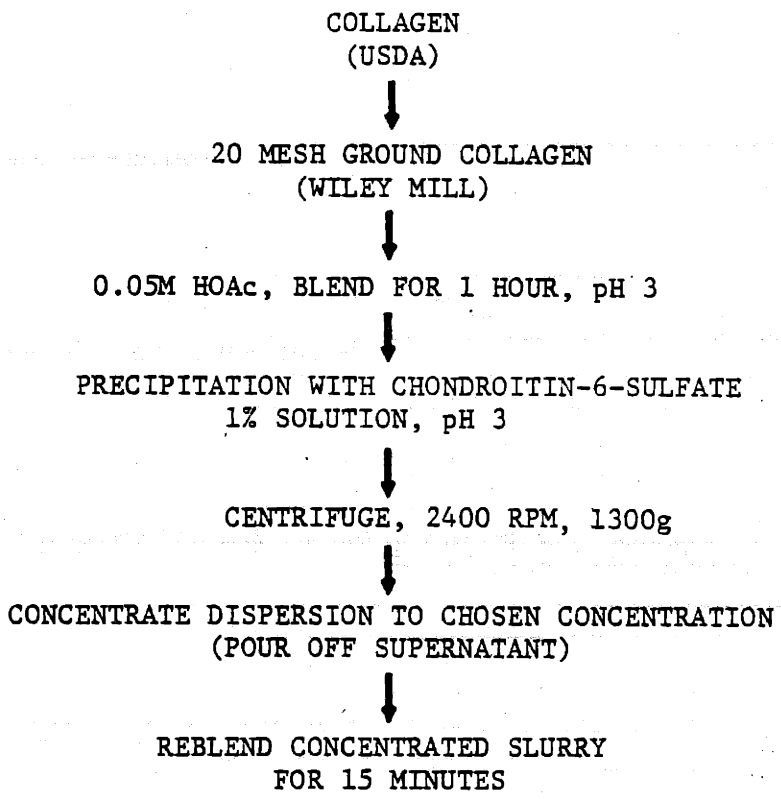

Figure 2.2.4 FREEZE DRYING PROTOCOL

(FOAM PREPARATION)

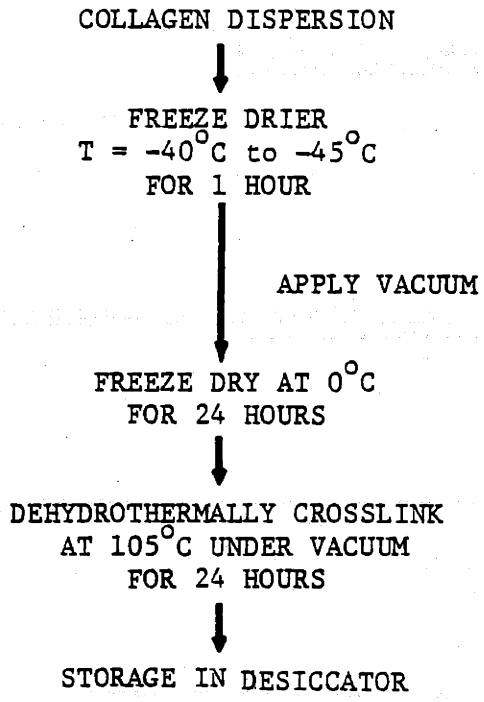

Figure 2.2.5 SILICONIZING AND CROSSLINKING PROCEDURE
(BILAYER MEMBRANE PREPARATION)

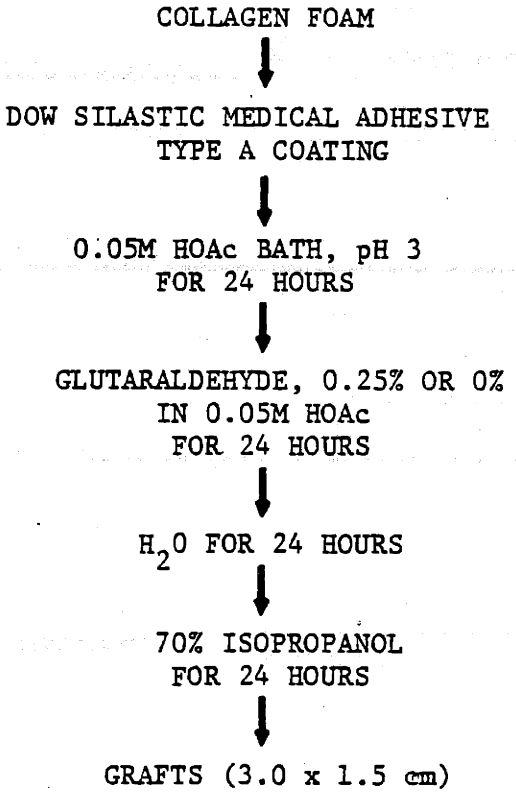

Figure 2.2.6 REFLECTED LIGHT MICROSCOPY

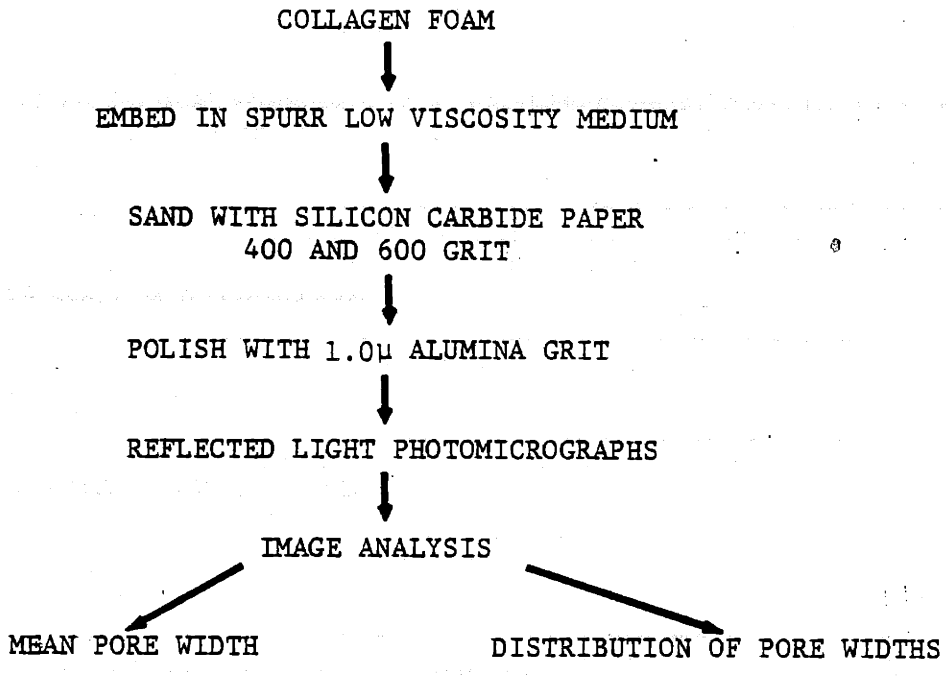

1.6x dispersions 140 ml, 140 ml, and 175 ml of supernatant were poured off respectively. Each pellet was reblended in the Eberbach blenders for fifteen minutes at the same settings. In order to concentrate the dispersion to 1.3% solids for the 2,6x material, a J-21B centrifuge with a JA 10 rotor (Beckman Instruments, Inc., Palo Alto, CA) was used at 10,000 rpm (17000g) for one hour. All the supernatant was decanted and enough supernatant was re-added to bring the volume to 133 ml. This concentrated pellet was too viscous to reblend in the Eberbach blender and was redispersed with a magnetic stirrer (Thermix, Fisher Scientific, Medford, MA) with a two inch Teflon stir bar and the speed set at 4.5 for fifteen minutes.

A dry weight determination was performed on the reblended collagen dispersion. A small aliquot weighing 3 to 5 grams was weighed in a pre-weighed aluminum boat and placed in a vacuum oven (Fisher Isotemp Vacuum oven, Fisher Scientic, Medford, MA) set at 105°C and -30mmHg for 24 hours. The desiccated sample was weighed. The dry weight is the ratio of the dry weight ot the wet weight of the collagen dispersion only. It is equal to a measure of the percent solids of the dispersion.

2.2.2 Freeze Drying Protocol

After the dispersion had been reblended, it was placed in a freezing tray (2 ml/sq. in.). The sheet of dispersion was frozen in the freeze drier (Virtis 10MRPC freeze drier and Freeze Mobile 12, Virtis, Inc., Gardner, NY) with the shelf maintained between -45°C and -40°C for one hour. The vacuum was then applied. When the pressure in the chamber was reduced to between 100 and 200 millitorr, the shelf temperature was

raised to room temperature and allowed to equilibrate for a half hour. Then the freeze drier was repressurized to atmospheric pressure. The freeze dried, collagen sheets (foams) were removed and each foam was placed in an aluminum foil pouch with one end open. The collagen foams were dehydrothermally crosslinked (DHT) and sterilized in a vacuum oven (Fisher Isotemp Vacuum Oven, Fisher Scientific, Medford, MA) set 105°C and -30 mmHg for 24 hours. Then the foil packages were sealed and the foams were stored in a desiccator at room temperature.

2.2.3 Siliconizing and Crosslinking Procedure

After DHT treatment the foams were handled sterilly throughout the remaining procedures. Solutions were sterilized by filtering with a Nalgene sterilization filter unit, type LS (Sybron Corp., Rochester, NY). Each foam was covered with a layer of uncured silicone adhesive approximately 0.0040" thick. The silicone was applied to the side of the foam that was in contact with the air during the freeze drying. The "air" surface is usually more collapsed than the "pan" surface and the more porous surface should be placed next to the wound bed. The layer of silicone was spread on the foam with the flat end of a metal spatula. The coated foam was then placed collagen side down into a bath of 0.05M HOAc for 15 to 30 seconds to allow rehydration of the foam. The foam was then turned over so that the silicone side faced down to let the silicone cure for 24 hours. Most of the air bubbles were removed from the foam by gently pushing on the foam with a sterile, gloved hand. The HOAc was drained off and one liter of 0.25% glutaraldehyde (one liter of 0.05M HOAc in the case of noncrosslinked foams) was added to crosslink

the collagen for 24 hours. Then the glutaraldehyde was drained off and the bilayer was washed twice with 500 ml of deionized water. The one liter of deionized water was added and the bilayer was soaked for 24 hours. The bilayer was removed from the water and the edges were trimmed 1.0 cm. The bilayer was placed in a sterile bag with 70% isopropanol and stored at 4°C until it was used.

2.2.4 Silicone Thickness Measurements

The silicone layer thickness was measured for each siliconized foam. For each one, 5 specimens of one square centimeter area were cut and placed in water at 80°C for 15 minutes. The gelatinized collagen was then peeled and/or rubbed off by hand. Then the samples were cooled to room temperature and each one was measured with a micrometer (L.S. Starnett, model 230, Athol, MA). The micrometer was tightened down until all light was eliminated between the platens of the micrometer and the sample.

2.2.5 Molecular Weight between Crosslinks

In order to quantitate the number of crosslinks in the collagen-GAG foams, the molecular weight between crosslinks, M_c, was measured. When the bilayer membrane was prepared, a portion of the foam was not covered with silicone. This rehydrated and crosslinked portion was used for M_c testing. The small strain mechanical properties of denatured collagen can be represented by the theory of rubber elasticity [25-26] using the equation

$$\sigma = \frac{\rho RT}{M_c} (v_2)^{1/2} (\alpha - 1/\alpha^2)$$

where, σ = equilibrium force on the gelatinized specimen divided by the unstrained cross sectional area
α = ratio of the stretched to the unstretched lengths of the gelatinized specimen
v_2 = volume fraction of polymer (see below)
ρ = density of polymer = 1.3 g/cc
T = absolute temperature
R = universal gas constant
M_c = molecular weight between crosslinks

If a graph of σ versus $(\alpha - 1/\alpha^2)$ is plotted, the M_c can be determined from the slope of the curve.

$$M_c = \frac{\rho RT(v_2)^{1/3}}{\text{slope}}$$

Stress relaxation tests were performed on gelatinized samples of the foams using a table top, screw driven, mechanical testing machine (Instron Corp., Canton, MA). Rectangular specimens 0.4" x 2" were placed in 80°C 0.15M NaCl for five minutes in order to denature the collagen. The specimen reduced in size and became yellow. The specimen was placed in the grips using a gauge length of one inch. A 3.8 liter Dewar flask filled with 0.15M NaCl at 80°C was raised to completely cover the specimen by atleast 1.5". The Instron was zeroed, balanced, and calibrated to 10g per inch of travel so that a graph of force versus time could be plotted. Each specimen was strained in tension three times at increments of 5% strain (0.05"). Between each additional increment of strain the specimen was allowed to relax for atleast four minutes to obtain an equilibrium stress. Three specimens of each type of foam were tested.

After the three equilibrium stresses were obtained in this manner

the specimen was measured for width and thickness. Thickness measurements were taken using a pressure sensitive micrometer (Mitutoyo, model 227-111, Paramus, NJ). v_2 is the volume fraction of polymer or the ratio of dry volume of the specimen to the wet volume of the specimen. In order to calculate v_2, wet and dry weight measurements were performed. The sections of the specimen that were compressed by the grips were removed. The specimen was reimmersed in the 80°C saline solution for fifteen seconds, quickly blotted on a paper towel, and then weighed to 0.1 mg. A dry weight was obtained from the same specimen after drying in an oven at 105°C for 24 hours. The densities of dry collagen and saline are 1.3 g/cc and 1.0 g/cc respectively.

$$v_2 = \frac{\text{dry polymer weight}/1.3}{\frac{\text{wet weight-dry weight}}{1.0} + \frac{\text{dry weight}}{1.3}}$$

A graph of σ versus $(\alpha - 1\alpha^2)$ was plotted for each specimen using the equilibrium forces from the stress relaxation tests and assuming that $\alpha = 0$ when $(\alpha - 1/\alpha^2) = 0$. A linear regression was performed to determine the slope. Using the values of v_2 and slope, M_c was calculated for each specimen.

2.2.6 Scanning Electron Microscopy (SEM)

Three surfaces of each foam were viewed in the SEM, the air side, pan side, and the vertical edge of the foam. Samples were mounted on aluminum studs with silver paint and then coated first with carbon and then gold in an evaporator (CVC vacuum evaporator, CVC Products, Rochester, NY). All surfaces were photographed.

2.2.7 Embedding and Reflected Light Microscopy

In order to quantitate the pore structure of the 1.0x, 1.6x, and 2.6x materials, the foams were embedded in a low viscosity epoxy (Spurr low viscosity embedding medium, Polysciences, Inc., Warrington, PA), cut, and polished so that the pan and edge surfaces of the foam were on the surface of the epoxy block. The epoxy polishes to a fine shiny surface. When viewed in reflected light microscopy, the epoxy reflects the light without scattering it whereas the collagen, due to its rough surface, scatters the light. Therefore, through the microscope, the pores filled with epoxy appear white and the collagen appears black. The Olympus metallurgical microscope (Olympus Optical Co., Ltd., Tokyo) has an internal light source. The light beam travels from the source to a prism which directs the light beam through the objective to the specimen. The specimen reflects the light back through the objective to the oculars and the specimen can be viewed. This procedure enables the viewer to observe a cross section of the pore structure cross section through one plane only. The two dimensional view allows stereological analysis to quantitate the pore structure. This procedure was modified from a standard technique used for analyzing the structure of trabecular bone [27]. The defatting procedures were eliminated and the embedding medium was changed from methyl methacrylate to Spurr Medium.

Five one centimeter square specimens of each type of foam were cut from five non-adjacent areas in a 2" x 3" sample for each type of dry foam. These 5 specimens were immersed in 95% ethanol (U.S. Industrial Chemical Co., NY, NY) for 24 hours to dehydrate the specimen thoroughly.

Then the specimens were placed in propylene oxide (J.T. Baker Chemical Co., Phillipsburg, NJ) and shaken until all the specimens sank. Spurr medium is obtained in a kit containing four ingredients and was prepared by mixing the ingredients in the order and ratios shown below. With the addition of each ingredient the mixture was stirred for 30 seconds.

Unox Epoxide 206 or ERL 4206 (vinyl cyclohexene dioxide).....10.0g
Hardner NSA (nonenyl succinic anhydride.....26.0g
Plasticizer DER 736 (diglycidyl ether of propylene glycol).....6.0g
Accelerator S-1 (DMAE: Dimethyl amino ethanol).....0.4g

A mixture of Spurr and propylene oxide (ratio 1:1) was made. The propylene oxide (PPO) was removed from the specimens and the 1:1 mixture was added. The specimens were covered and placed on a shaker table for three hours. After the first hour the specimens were uncovered to allow the PPO to evaporate. Following the third hour the mixture was removed from the shaker table. Pure Spurr was added to the specimens and they were placed on the shaker table for another three hours. The Spurr was poured off and fresh Spurr was added. Each specimen was placed pan surface down in a polyethylene mold (Peel-a-way tissue embedding molds, Peel-A-Way Scientific, El Monte. CA), and the mold was filled with fresh, pure Spurr. A wire was placed inside each mold lightly pressing on the specimen to keep it from floating to the surface or changing orientation during the polymerization. Each specimen was labelled by inserting a label into the mold. The molds were placed in an oven at 60°C for 24 hours.

After unmolding, the specimens were machined to 1" diameter cylinders in order to fit the polishing holders. First, the pan surface was

sanded with 400 grit silicon carbide paper (Tufbak, Chandler and Farquhar, Inc., Boston, MA) to remove the excess epoxy, and then 600 grit paper until all the 400 grit scratches were removed. Then 1.0μ alumina grit was used to polish the pan surface in an automatic polishing machine (Syntron vibrating polishing machine, model LP-01, type C, Syntron Co., Homer City, PA). The polished sample was then inspected in a reflected light microscope. If the collagen did not appear on the surface, the sample was sanded and polished again until the collagen surface was apparent.

All samples were photographed with reflected light microscopy with Panatomic X film (Eastman Kodak, Rochester, NY). After the pan surfaces were photographed, each sample was cut in half with a band saw and the cut surfaces were sanded, polished and photographed. The pictures were enlarged to 100x magnification and printed on Kodabromide high contrast paper no. 4, single weight, (Eastman Kodak, Rochester, NY).

Each photograph was drawn into tracing paper to eliminate any extraneous black dots, lines, or shading in the picture. A black border was placed around the frame of each traced picture.

2.2.8 Porosity Measurements

Analysis of the porosities of the 1.0x, 1.6x and 2.6x materials was performed by measuring the distances between the wall of collagen that make up the interconnecting pores of the foam. A DeAnza IP5000 image processing system (DeAnza System, Inc., San Jose, CA) and a television camera (Eyecom) were used to display and digitize the traced photographs, (Tufts New England Medical Center, Image Analysis Laboratory, John Brenner, director). The TV camera was used to produce a signal of each

picture which was then digitized and placed in computer memory (Vax 11/780, Digital Equipment Co., Maynard, MA). The picture digitization is 256 x 256 pixels (256 vertical lines and 256 horizontal lines). The magnification of the TV camera was set so that 1 pixel was equivalent to 3μ. The computer then scanned each horizontal line and measured the distances between intersections of the scan line with a black line. These measurements were accumulated for all 256 rows. The mean and standard deviation of these measurements were calculated, and a histogram is plotted. Then the computer scanned vertically and calculated the mean, standard deviation, and histogram for this direction. For a given orientation of the tracing, the computer produced two scans, one horizontally and one vertically. Figure 2.2.7 demonstrates one scan of the computer through a schematic of a traced photograph. The scan line (horizontal line) intersects the collagen (black curving lines) five times and is divided into six segments. Each of these segments is measured by the computer and is added to the histogram of measurements from other scan lines.

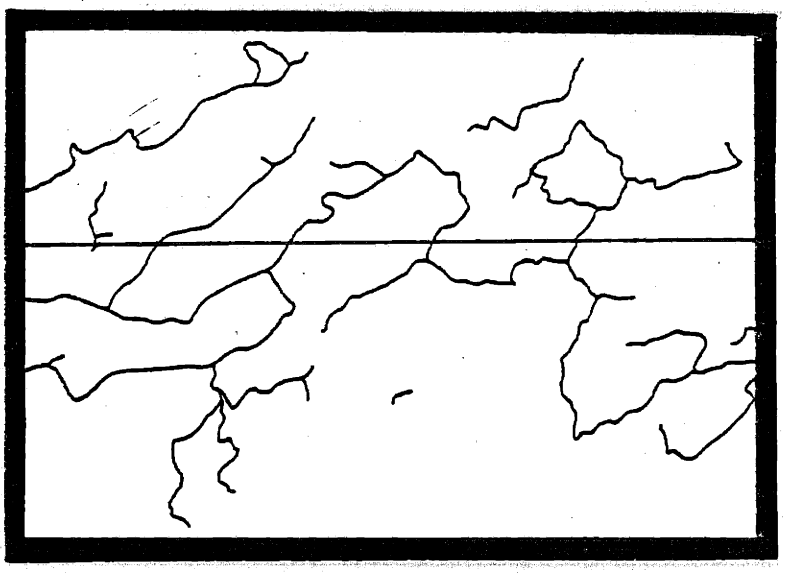

2.2.7 Schematic Diagram of computerized scan of traced reflected light photomicrograph

Only the pan surface and the edge view were analyzed since their structures are important for cellular infiltration. The pan surfaces were photographed at random orientation with respect to the axis perpendicular to the pan surface. Therefore, the computer scans were also at random orientations. For each material manufactured atleast four tracings of the pan surfaces each photographed from a different specimen, were analyzed. Two sets of results were obtained for each tracing. All eight histograms were averaged and the mean and the standard deviation of the average histogram were calculated. The variation between samples was calculated by finding the average of the mean pore widths of all samples of the same type of material and the respective standard deviation.

The edge views were analyzed in a slightly different manner. Since a specific alignment of pores was detected in the more concentrated materials, the degree of orientation was measured. A black piece of paper with a circular hole (7.5 cm in diameter) in the center was placed on each tracing. Computer scans were taken at an arbitrarily assigned angle (labelled 0°) and at 90° to the first scan. The circular tracing was then rotated 30° about its center and the measurements were taken at 30° and 120°. This rotation was repeated for scans at 60° and 150°. The angle which gave the maximum mean pore width was recorded, if a maximum was observed. Additional scans were performed at angle 5° greater and 5° less than this angle to obtain the maximum mean pore width and angle of orientation. The mean pore distances were plotted versus the angle of orientation. If a maximum was detected in the curve, then the pores were aligned in a particular orientation. If there was no maximum in the curve, then the pores of the tracing were

not oriented. For each curve of mean pore width versus angle of scan, the height of the peak, the standard deviation of the peak, and the kurtosis were measured. The kurtosis is a measure of the deviation of a curve from a normal distribution. A normal distribution has a kurtosis of 3.0. If the kurtosis is less than 3.0, the peak is flatter than a normal distribution. If the kurtosis is greater than 3.0, the peak is sharper than a normal distribution. Figure 2.2.8 shows curves with various values of kurtosis. These parameters will give an indication of the extent of orientation for each material. The standard deviation of the peak and kurtosis were calculated using a computer program [28].

The mean aspect ratio of the pores, a ratio of the maximum mean pore width to the minimum mean pore width was calculated for each sample to indicate the average shape of the pores in the three different materials, see Figure 2.2.9. The average of the mean pore widths at all angles of scan for each sample was calculated for each kind of material.

2.2.9 Pore Volume Fraction

The pore volume fraction was measured for the 1.0x, 1.6x, and 2.6x materials before rehydration and crosslinking. One centimeter square samples were cut from the dry foam. More accurate values of the length, width, and thickness of each sample were measured using dial calipers (Mitutoyo, model D-6"-T, Japan) and a micrometer (L.S. Starrett, model no. 230, Athol, MA). Each measurement was taken by reducing the distance between the surface of the sample and the platens until all light was eliminated from this gap. The samples were then weighed to 0.1 mg. Pore volume fraction was calculated using the following formula.

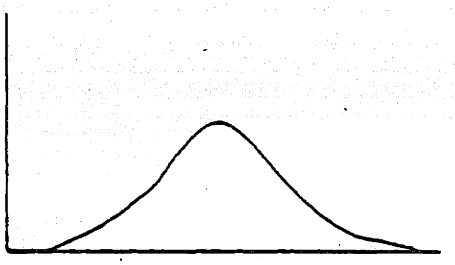

a) Normal distribution, kurtosis = 3

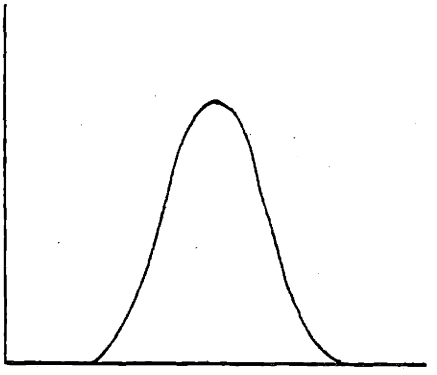

b) Kurtosis > 3

c) Kurtosis < 3

Figure 2.2.8 Effect of Peak Shape on Kurtosis

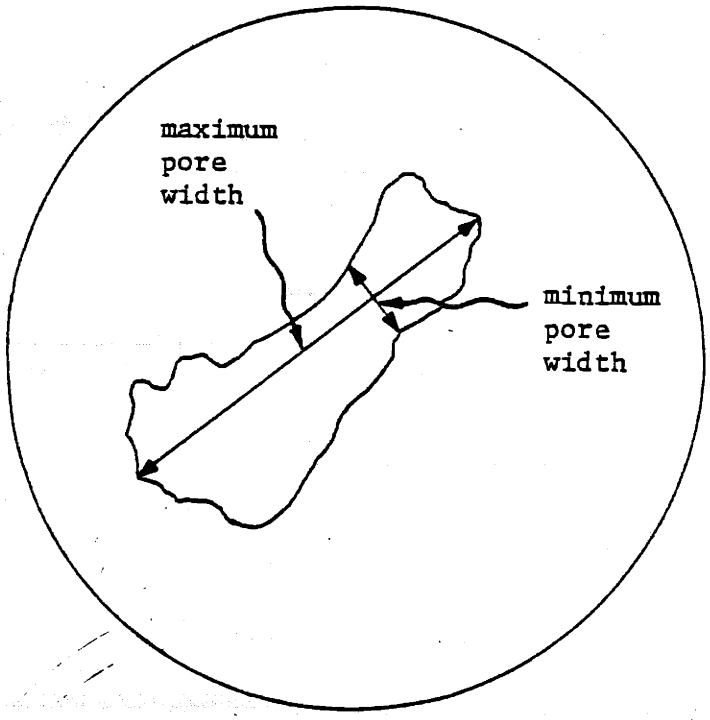

Figure 2.2.9 Pore Aspect Ratio

$$v_1 \text{ (dry)} = 1 - \frac{m/\rho}{t\ L\ w}$$

where, v_1 (dry = volume fraction of pores of the dry sample
m = weight of foam sample
ρ = density of collagen-GAG = 1.3 g/cc
t - average measured thickness
L = average measured length
w = average measured width

and m/ρ = volume of the solid phase
tLw = apparent volume of the foam

2.2.10 In Vivo Response

Wound healing response was obtained by grafting guinea pigs with each of the materials manufactured. Grafts (3.0 x 1.5 cm) stored in 70% isopropanol were cut under sterile conditions and placed in normal saline in a Twirl-A-Pak bag (American Scientific Products, Bedford, MA). The grafts were shaken and massaged to remove the 70% isopropanol from the pores, and then were placed in another Twirl-a-Pak bag of sterile normal saline and the massaging and shaking was repeated. The grafts were placed in fresh normal saline and were ready for grafting.

White, female, Camm-Hartley guinea pigs (Camm, Wayne, NJ) weighing 300-400g each were shaved and dehaired with Nair (Carter Products, Division of Carter-Wallace, Amer. Hosp. Supply, Irvine, CA). Each guinea pig was given an intramuscular injection of Tetracyn in the hind quarter (intramuscular tetracycline, Pfizer, 0.035 mg in 1 ml, 0.1 mg/kg) as a prophylactic antibiotic, approximately one half hour before surgery. The anesthesia was 1-3% Fluothane (Halothane, Halocarbon Labs., Inc., Hackensack, NJ) in oxygen. For the 1.6x and 2.6x materials a full thick-

ness excision (1.5 x 3.0 cm) was made up to but not including the panniculus carnosus on the left side of the back of the guinea pig. A graft was placed on the wound with the collagen-GAG surface against the wound bed, and was sutured in place with ten black monofilament nylon sutures, see figure 2.2.10.

For the materials that were treated with and without glutaraldehyde, a direct comparison was made by grafting each animal with two 1.5 x 3.0 cm grafts. The left side was grafted with material crosslinked with glutaraldehyde while the right was grafted with the noncrosslinked material.

The animals were bandaged after surgery with sterile gauze and a double layer of Elastoplast bandages (Beiersdorf, Inc., South Norwalk, Conn.)

The closure rate of the grafted wounds was followed at three or four day intervals. The animals were unbandaged, observed and photographed. A Nikkormat camera with Macro Nikkor lens, 55mm, f3.5 (Nikon, Japan) was used to photograph the grafts with Kodachrome ASA64 color slide film (Eastman Kodak, Rochester, NY). The slides were projected and the pink area of the graft was traced onto white paper. The pink area is the area underneath the silicone layer which has not epithelialized or contracted. Thus, the pink area is a measure of both the contraction and epithelialization (C/E), see Figure 2.2.11. Areas were calculated by cutting out and weighing the tracings. Area data is presented graphically by plotting the percentage of the original area versus time post-surgery.

The 50% closure day is the day post surgery when the pink area

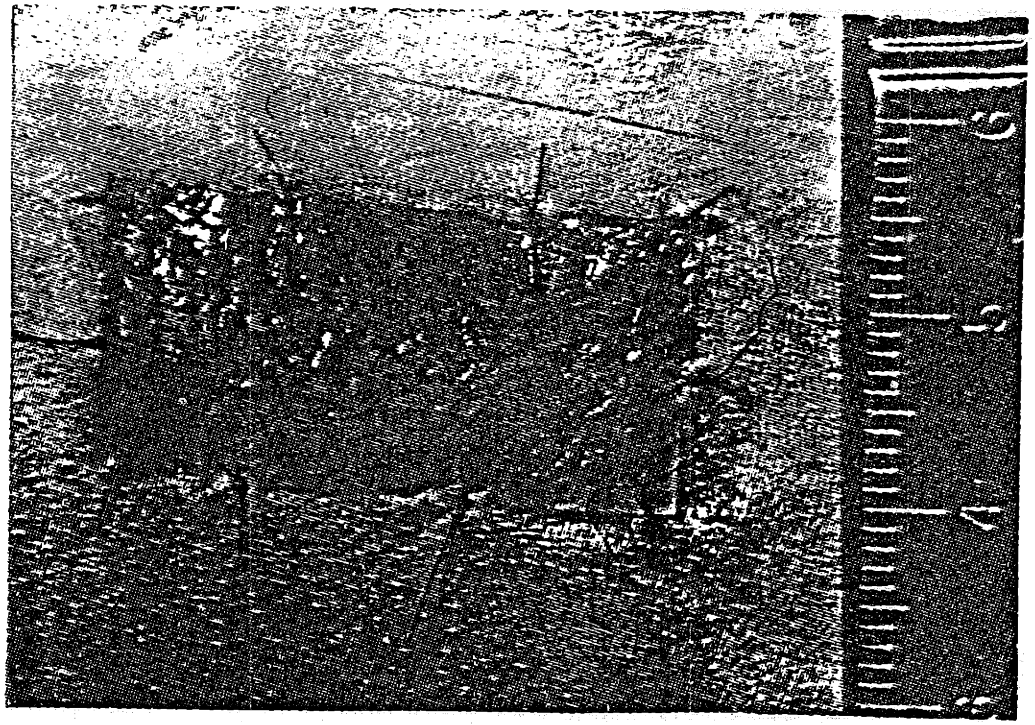

Figure 2.2.10 Full thickness wound grafted with the bilayer membrane, Day 0.

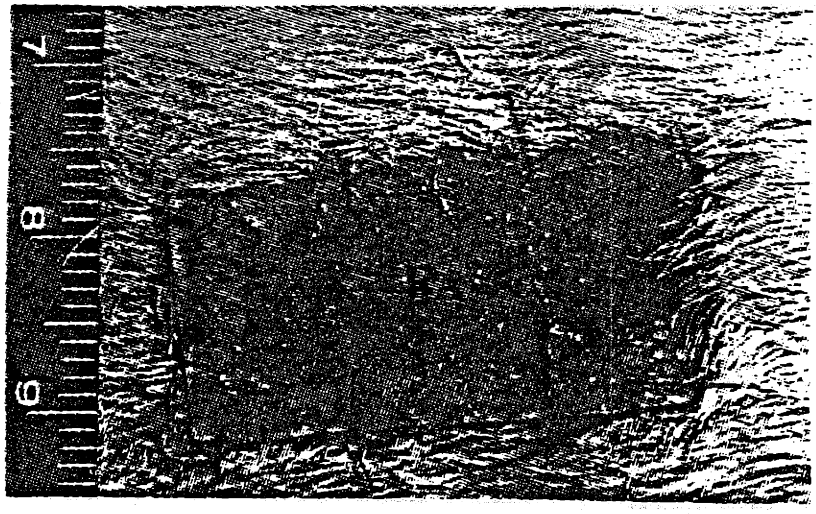

Figure 2.2.11 Pink area under the silicone layer, PA - pink area.

(open area) under the silicone reaches 50% of its original area. The 50% closure day was measured for all material manufactured.

The day when the silicone was ejected and the pink area (open area) was zero, was labelled the day of closure. The day of closure was recorded for each type of material.

The areas of the long term external scars were measured by tracing along the edge of the hairless area of the remains of the graft site, cutting these areas out, and weighing them. The scar is considered long term when it does not change appreciably over a period of two weeks.

Histological samples were taken at varying time intervals post-surgery. The animal was anesthetized with Diabutol and the graft and atleast a one centimeter border of surrounding skin was excised. A full thickness skin sample, including the panniculus carnosus was removed mounted on an index card indicating anterior and posterior directions, and placed in 10% buffered formalin (Fisher Scientific, Medford, MA). The guinea pig was sacrificed with an overdose of Diabutol injected in the heart. The sample was split into three parts, anterior, middle and posterior, dehydrated in ethanol baths, cleared in xylene, and embedded in parafin. Microtomed sections of 6μ thickness were produced and mounted on microscope slides. Sections cut serially perpendicular to the anterior-posterior direction were taken from the middle part of the graft. Sections cut parallel to the anterior-posterior direction were taken from the anterior and posterior parts. The parafin was removed; the sections were rehydrated and stained with hematoxylin and eosin. Finally the sections were dehydrated and cleared in xylene, and a cover slip was mounted on the sections with Permount (Fisher Scientific, Medford, MA).

3. RESULTS

3.1 Thickness Measurements

The thickness of the silicone layer for each material grafted on guinea pigs was measured. Values are shown in Table 3.1.1. Since the silicone layer was applied to each foam by hand, there were ridges and thin areas that created a large range of values. The mean thicknesses for each material range from 0.0338" to 0.0415" whereas the range of thickness varied from 0.0206" to 0.0620". There was no significant difference of the thicknesses for the different materials.

Table 3.1.1 Silicone Thickness Measurements

Type of Material	Mean	Std. Dev.	n
1.0x noncrosslinked	0.0396"	0.0114"	19
1.0x crosslinked	0.0415"	0.0091"	15
1.6x	0.0391"	0.0117"	10
2.6x	0.0338"	0.0090"	15

3.2 Molecular Weight between Crosslinks, M_c

3.2.1 M_c: Crosslinked versus Noncrosslinked

The M_c values were measured for the crosslinked and noncrosslinked materials, see Table 3.2.1. The M_c values for the crosslinked standard materials were slightly below the normal range of values (8×10^3 to 20×10^3 daltons) [29] due to the thickness measurements of the samples tested. The pressure sensitive micrometer was used to measure the thickness of each specimen. It applied approximately 200 grams to the specimen during each measurement. This force is larger than the force

that has been used in the past (50g) [29] and results in smaller thickness measurements and thus, lower values of M_c. For the standard crosslinked material a range of 4×10^3 to 12×10^3 daltons was measured and calculated for the molecular weight between crosslinks.

The values of M_c for the noncrosslinked foams were significantly larger than the values for the crosslinked foams ($p < 0.0005$, $n = 5, 9$, in an unpaired, one-tailed, t-test [30]), indicating a lower crosslink density for the material that was not treated with glutaraldehyde. The average M_c of the noncrosslinked material was 5.0 times the average M_c of the crosslinked material.

The values of v_2, the volume fraction of gelatinized collagen, were not significantly different for the noncrosslinked and crosslinked materials (two-tailed, t-test, $p > 0.5$ [30]).

3.2.2 M_c: Variation with Concentration

The M_c values were measured for the 1.0x, 1.6x, and 2.6x materials. As for the values of M_c for the crosslinked and noncrosslinked foams, the values are below the normal range (8×10^3 to 20×10^3 daltons) [29] due to the thickness measurements with the pressure sensitive micrometer. The values for M_c and v_2 are presented in Table 3.2.2. The average values of M_c for the 1.0x, 1.6x, and 2.6x materials were 7.6×10^3, 8.7×10^3, and 8.2×10^3 daltons respectively. These three values are not significantly different (all $p > 0.5$, one-way analysis of variance), thus, the average molecular weight between crosslinks is independent of collagen concentration of the foam.

The values of v_2 for the 1.0x material were not significantly

Table 3.2.1 Molecular Weight between Crosslinks, M_c

Type of Material	Mean (daltons)	Std. Dev. (daltons)	v_2	Std. Dev.	n
crosslinked	7.9×10^3	2.7×10^3	0.055	0.026	9
noncrosslinked	3.9×10^3	2.0×10^3	0.066	0.068	4

Table 3.2.2 Molecular Weight between Crosslinks, M_c

Type of Material	Mean (daltons)	Std. Dev. (daltons)	v_2	Std. Dev.	n
1.0x	7.6×10^3	2.8×10^3	0.052	0.023	12
1.6x	8.7×10^3	0.4×10^3	0.044	0.006	3
2.6x	8.2×10^3	4.0×10^3	0.069	0.012	9

3.3 Scanning Electron Microscopy (SEM)

Scanning electron photomicrographs were taken of the foams that were produced. Since the SEM can only be performed on dry specimens, the samples for SEM were prepared from the collagen-GAG foams before rehydration. Therefore, the crosslinked and noncrosslinked foams looked identical and were labelled 1.0x.

The pan surfaces were photographed and the results are shown in figure 3.3.1 a,b,c. The pores along the pan surface decrease in size as the concentration of the collagen increases. The 1.0x and 1.6x materials have similar structures. The pores are separated from each other by thin collagen sheets, although the pores are smaller in the 1.6x foam. The 2.6x material has an entirely different structure. There are fewer pores at the surface. Between the pores are broad sheets of collagen indicating a much denser surface. In both the 1.6x

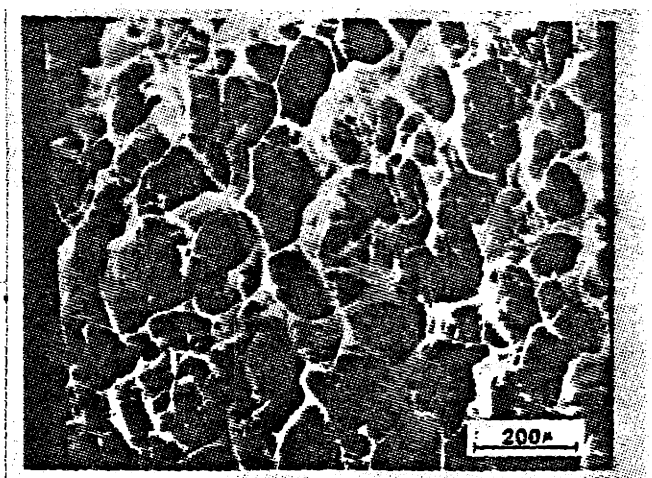

Figure 3.3.1 Pan surfaces of collagen foams photographed in scanning electron microscopy.

a) 1.0x concentration

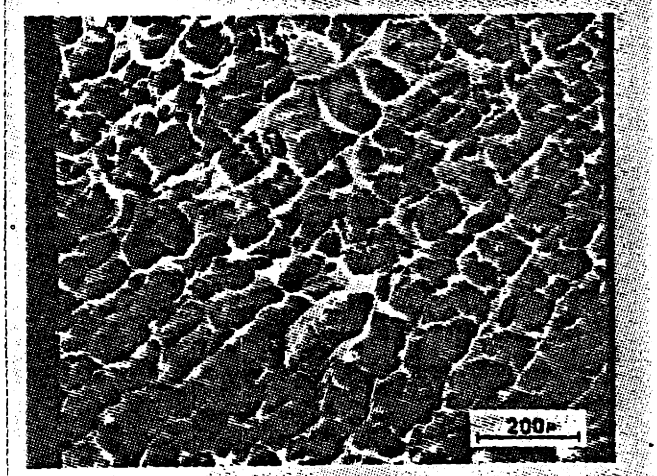

b) 1.6x concentration

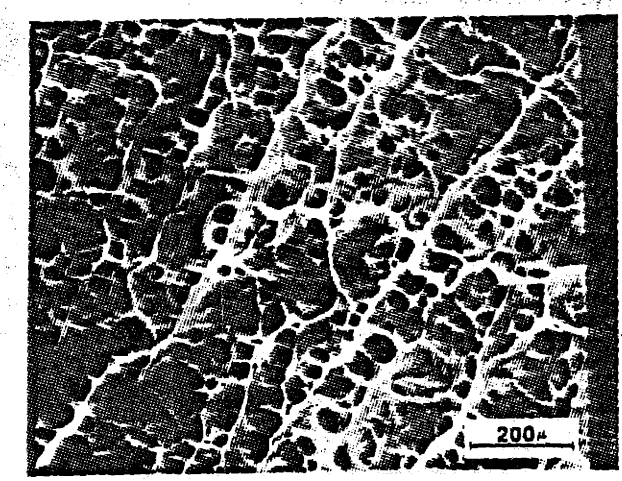

c) 2.6x concentration

and 2.6x surfaces there are regions where the pores seemed to be oriented in a particular directions. This orientation is rarely observed in the 1.0x material.

The air surfaces of the three materials were photographed and are shown in Figure 3.3.2 a, b, c. There is a large difference in the appearance of the 1.0x and the higher concentration materials. The 1.0x foam shows a porous structure which is slightly more collapsed than its pan surface. In contrast the 1.6x and 2.6x foams have a very dense, low porosity surface. The pores are few and very small. Again an alignment of the collagen plates can be seen whereas the 1.0x material has a random pore structure.

The edge views (perpendicular to the pan and air surfaces) are shown in Figures 3.3.3 and 3.3.4. As would be expected the density of collagen in the cross section increases with increasing collagen concentration in the foam. Once more there is a distinct orientation of the pores in the 1.6x and 2.6x foams. In general the 2.6x material is more highly oriented than the 1.6x material. In some sections, there are regions of randomly oriented pores near the pan surface comprising roughly 20% of the thickness of the foam. However, pores aligned completely from the air surface to the pan surface have also been observed. Some sections of the foams have revealed a denser region near the pan surface.

Figure 3.3.2 Air surface of collagen foams photographed in scanning electron microscopy

a) 1.0x concentration

b) 1.6x concentration

c) 2.6x concentration

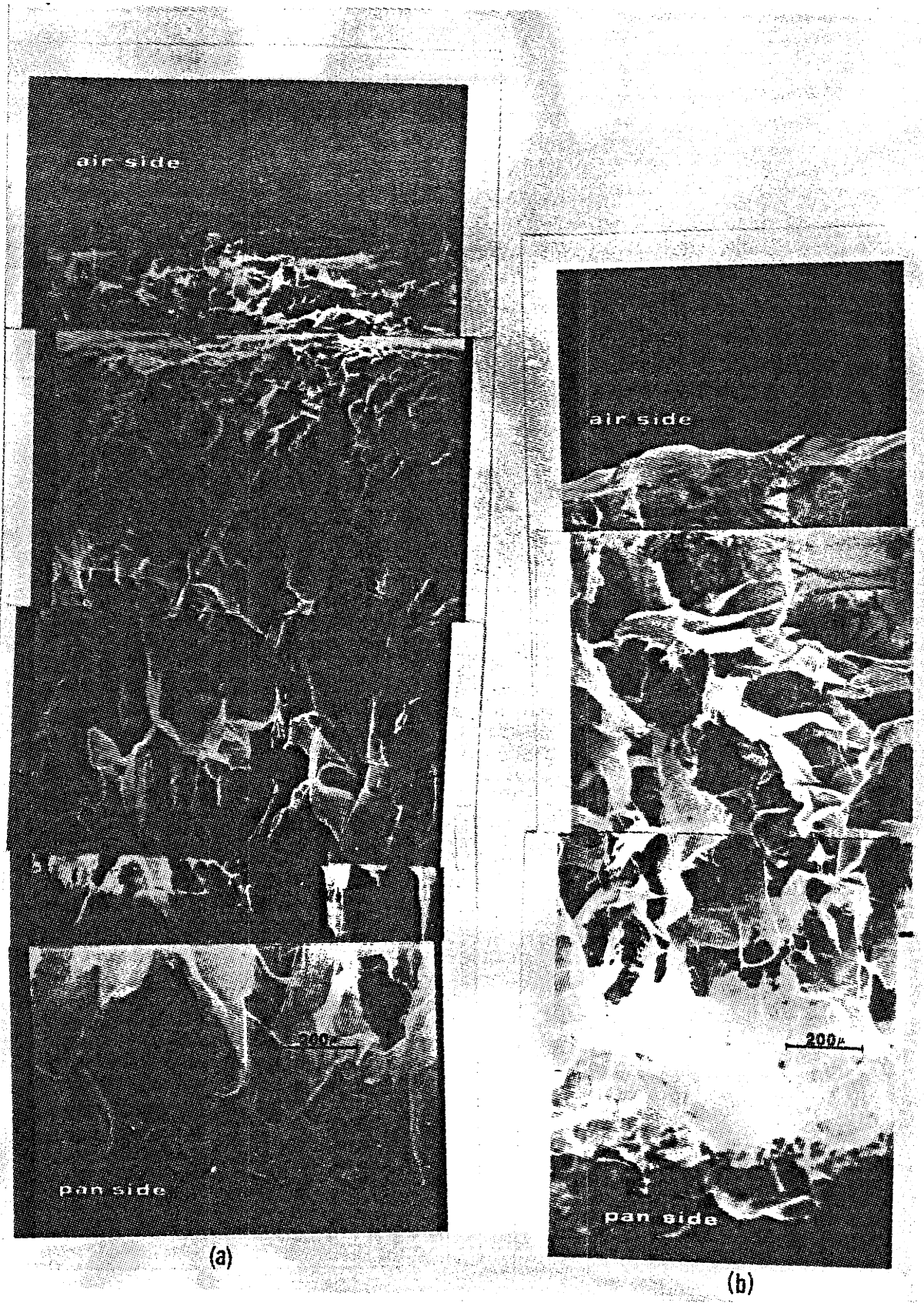

Figure 3.3.3 Edge view of collagen foam photographed in scanning electron microscopy, a) 1.0x concentration, b) 1.6x concentration

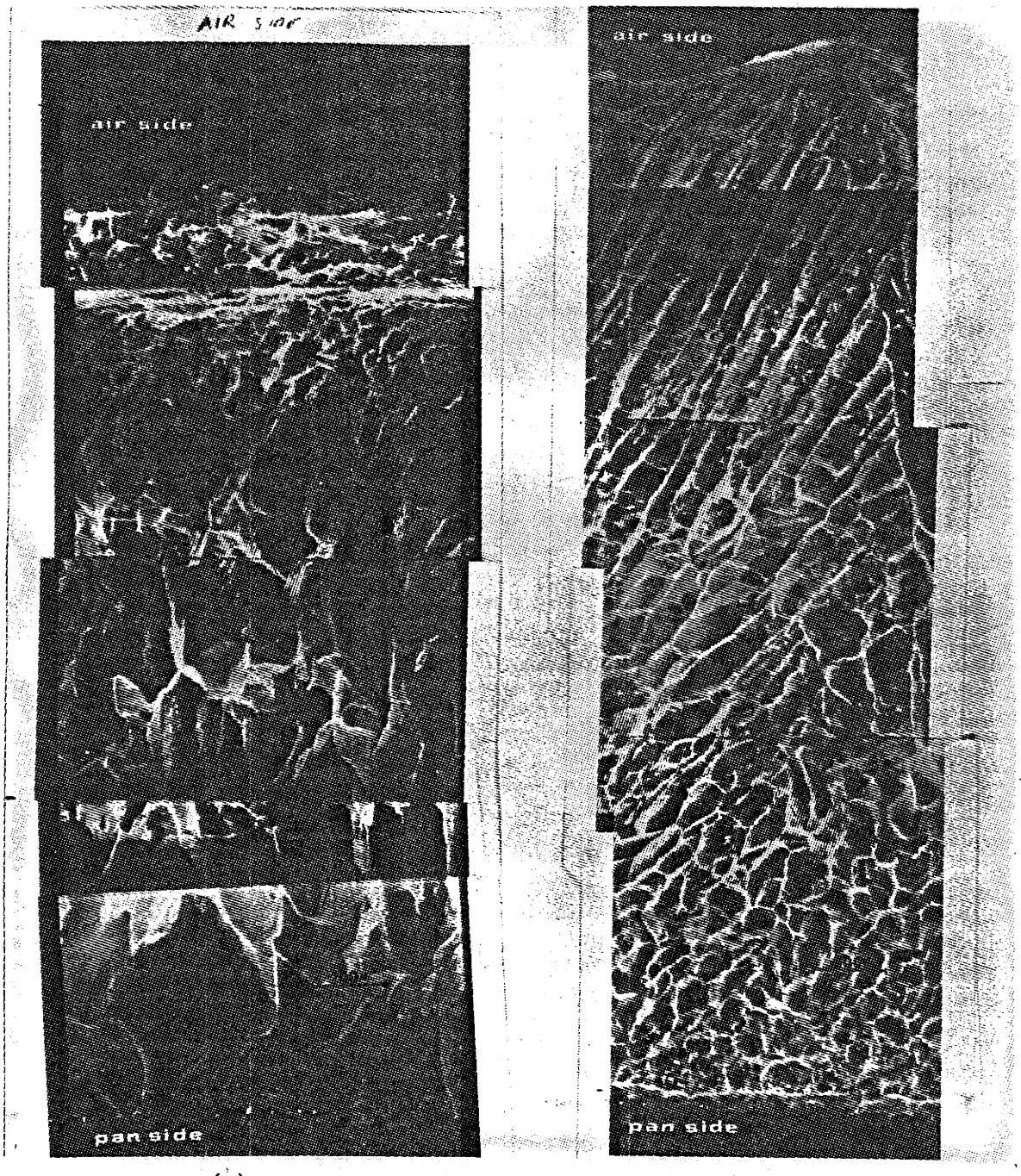

(a) (b)

Figure 3.3.4 Edge view of collagen foam photographed in scanning electron microscopy, a) 1.0x concentration, b) 2.6x concentration

3.4 Porosity

3.4.1 Pore Width Measurements

3.4.1.1 Pan Side

The pan sides of the 1.0x, 1.6x, and 2.6x materials were quantitated using computerized image analysis. Figures 3.4.1 through 3.4.3 show examples of the reflected light photomicrographs of the pan side for each type of material and its traced image. Measurements of the distance between collagen plates forming the interconnecting pores of the embedded foams were performed.

Averaged, normalized distributions of pore widths are presented in Figure 3.4.4 through 3.4.6 for the 1.0x, 1.6x, and 2.6x foams. The average histogram for each material is the average of all the histograms from the individual samples for the 1.0x material. For example, there were seven traced samples for the 1.0x material. Each sample was analyzed for pore widths and the data were plotted as a histogram. All seven histograms were averaged by the following procedure. The heights of all the first bar intervals (0 - 50μ) of the seven histograms were added and divided by seven to determine the height of the average histogram bar for the first interval (0 -50μ). The same procedure was used to determine the height of the average histogram bars for the other intervals. The result was an average histogram of all seven samples. To normalize the average histogram, divide the height of each bar of the average histogram by the sum of the heights of all the bars of the average histogram. The resulting normalized, average histogram had a total area of the bars equal to one.

The average, noramlized histograms became more narrow as the concentration of collagen in the foam is increased as indicated by the decrease

(a)

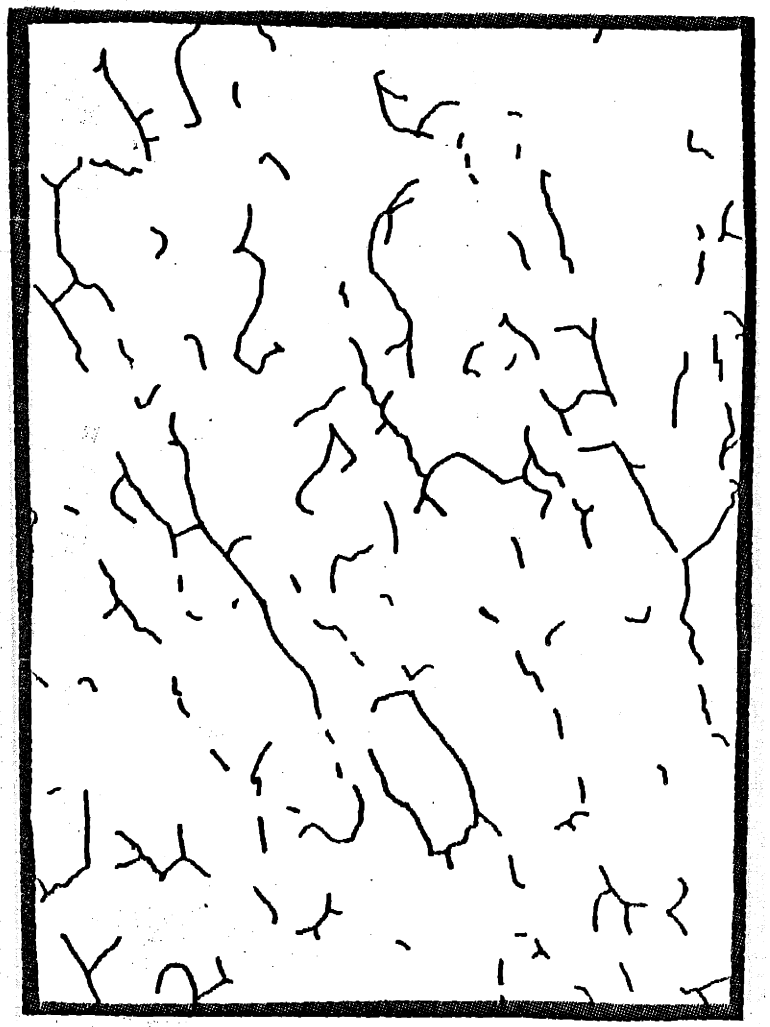

(b)

Figure 3.4.1 1.0x concentration pan side a) reflected light photomicrograph, b) tracing of photomicrograph

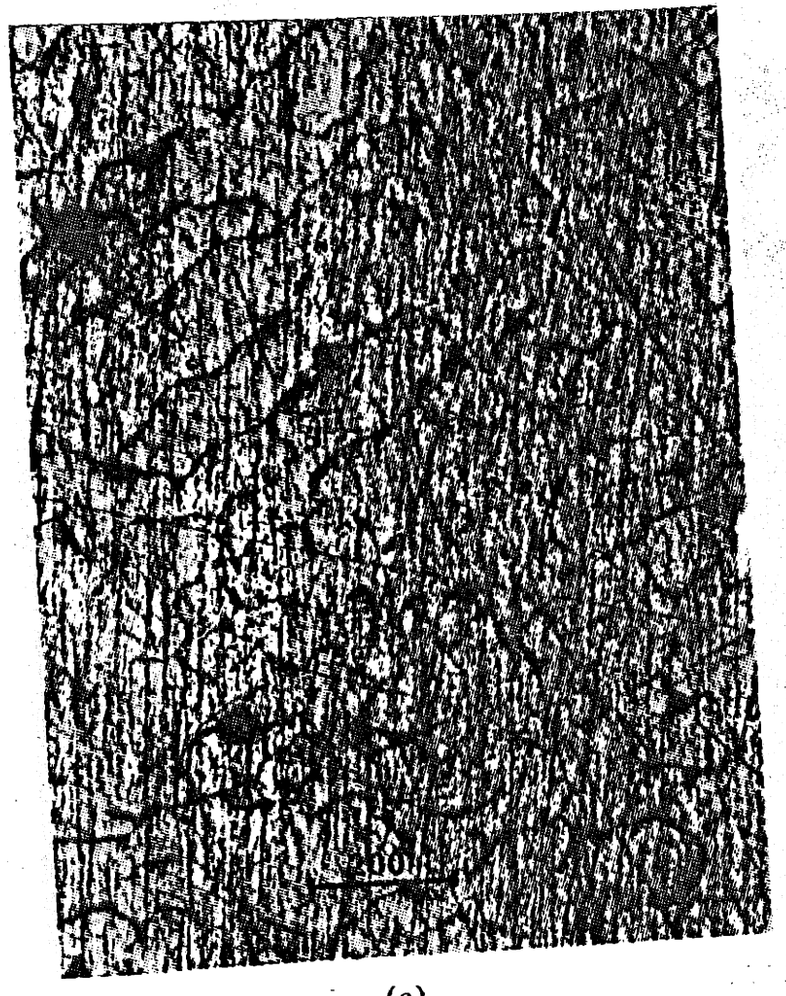

(a)

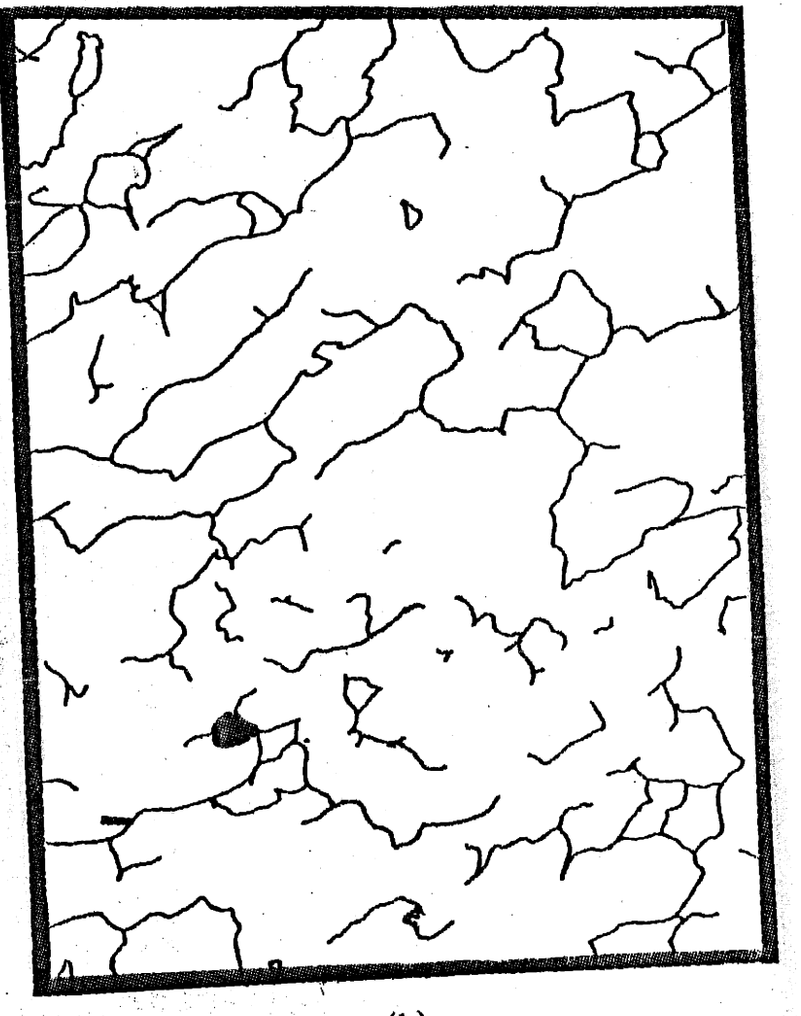

(b)

Figure 3.4.2 1.6x concentration pan side a) reflected light photomicrograph, b) tracing of photomicrograph

(a)

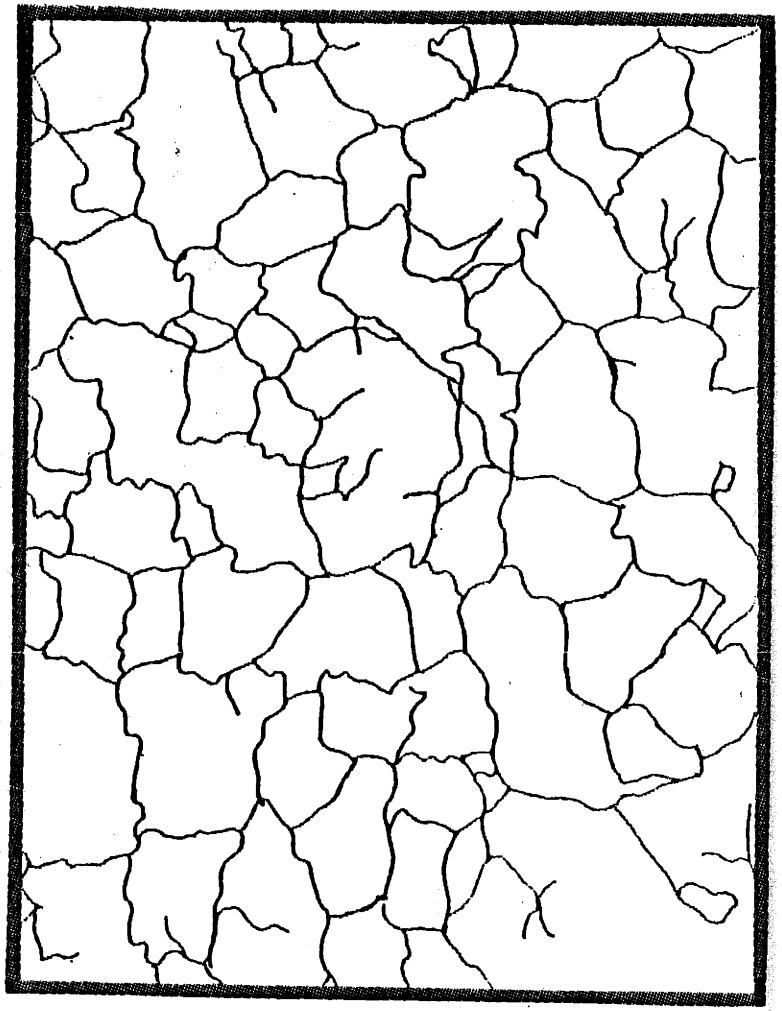

(b)

Figure 3.4.3 2.6x concentration pan side a) reflected light photomicrograph, b) tracing of photomicrograph

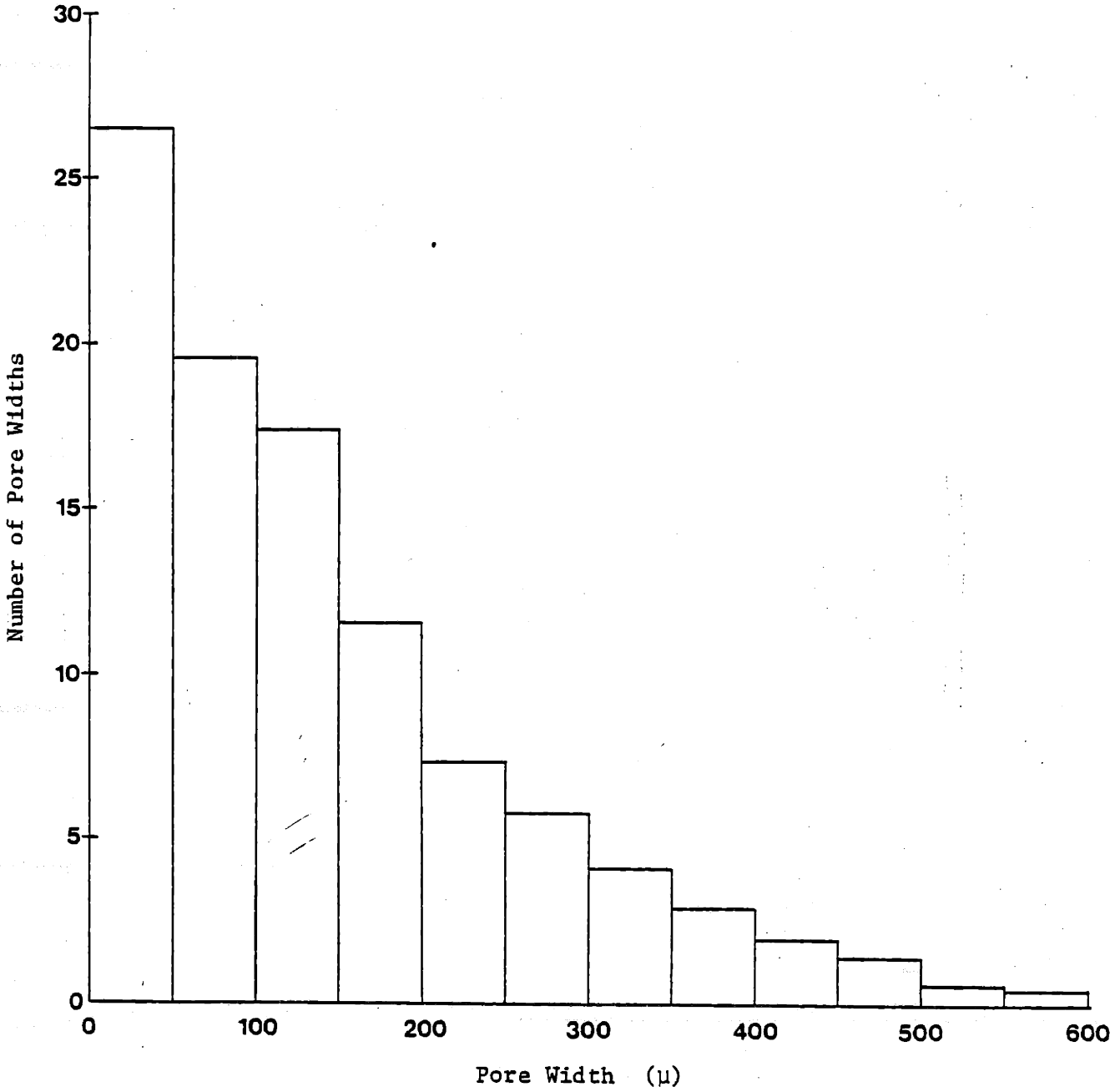

Figure 3.4.4 Average Histogram of Pore Widths of Pan Side, 1.0x

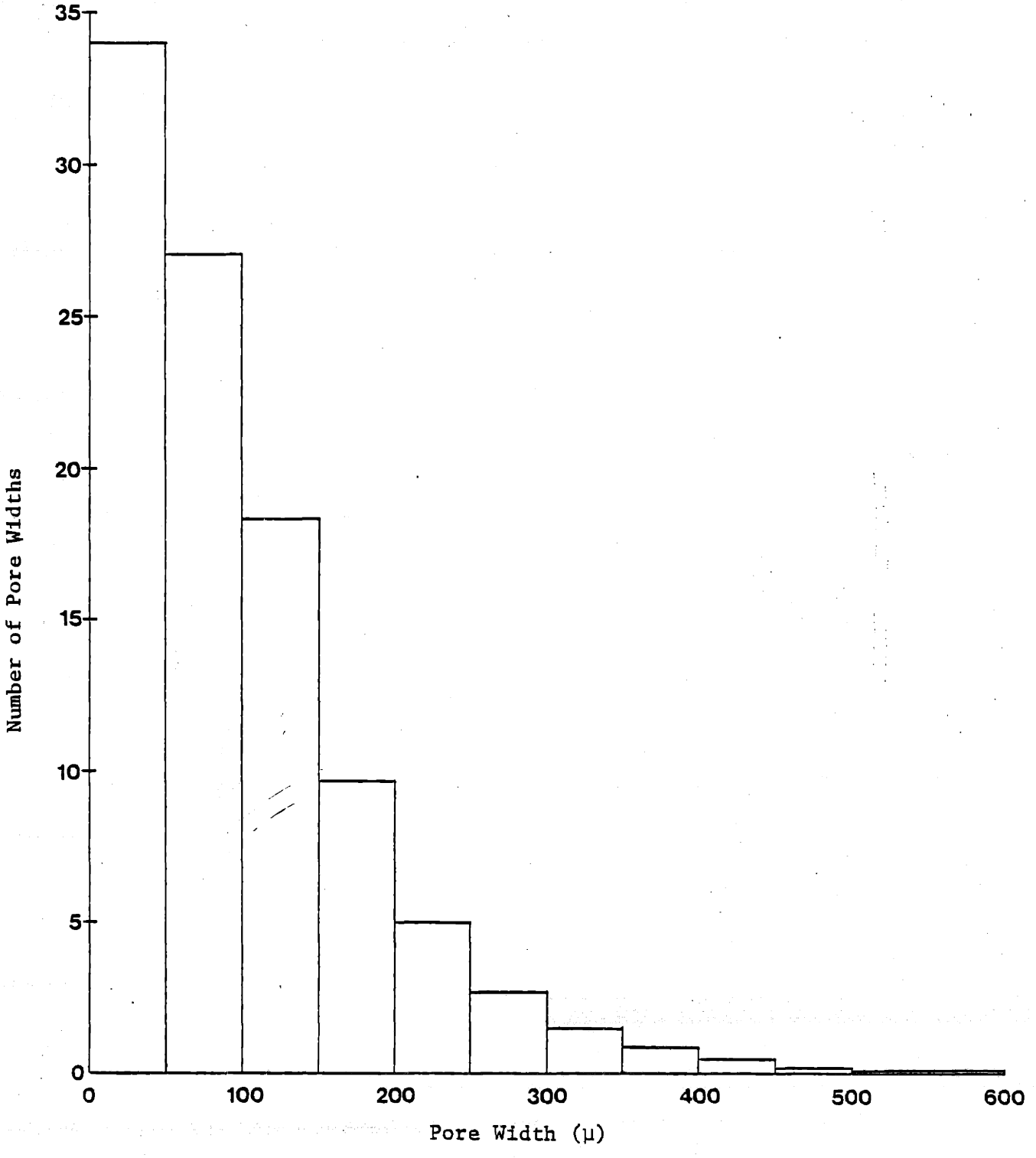

Figure 3.4.5 Average Histogram of Pore Widths of Pan Side, 1.6x

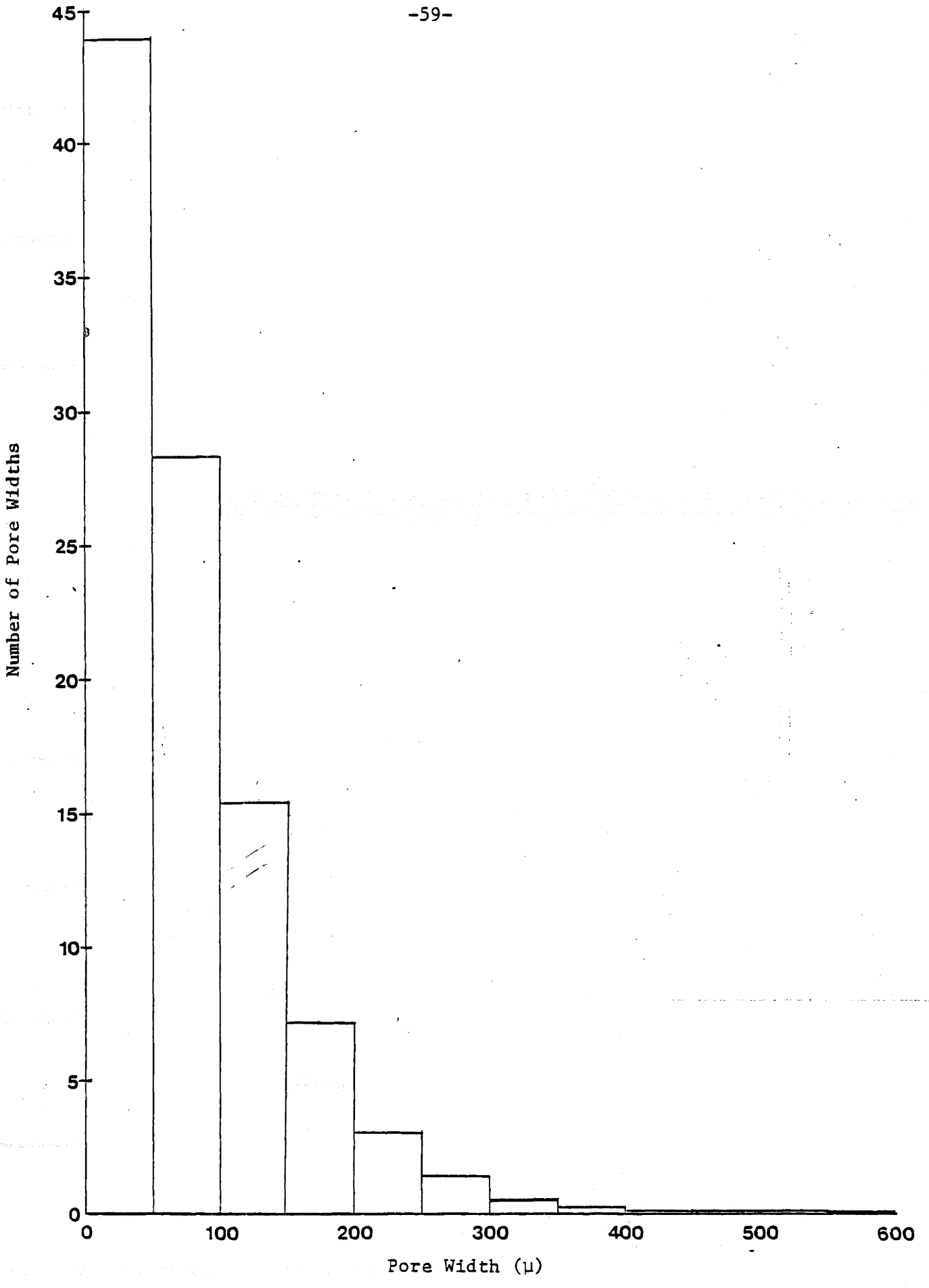

Figure 3.4.6 Average Histogram of Pore Widths of Pan Side, 2.6x

in the standard deviations, σ_h, for the more concentrated materials. The mean of the average histogram, P_h, for the 1.0x, 1.6x, and 2.6x foams were 145μ (σ_h = 131μ), 100μ (σ_h = 29μ), and 77μ (σ_h = 73μ) respectively, see Table 3.4.1.

In order to measure the variations between samples of the same type of material, the mean of the histograms of individual samples were averaged and the standard deviation was calculated. For example, seven means were calculated from the seven histograms for the 1.0x material. The average, P_i, and standard deviation, σ_i, of these seven means were calculated. The standard deviations, σ_i, indicates the sample to sample variation for each type of material. P_i and σ_i were calculated for the 1.0x, 1.6x, and 2.6x materials and the results are also shown in Table 3.4.1. Both the 1.6x and 2.6x materials were significantly different from the 1.0x when their values of P_i were compared in one-tailed t-tests, (1.0x versus 1.6x, n = 7, 9, $p < 0.0005$; 1.0x versus 2.6x, n = 7, 18, $p < 0.0005$). The 1.6x and 2.6x materials were significantly different when their values of P_i were compared in a one-tailed t-test (1.6x versus 2.6x, n = 9, 18, $p < 0.0005$).

Table 3.4.1 Mean Pore Width: Pan Side

Type of Material	P_h (μ)	σ_h (μ)	P_i (μ)	σ_i (μ)
1.0x	145	131	148	15
1.6x	100	86	103	19
2.6x	77	73	78	8

P_h = mean of the average histogram of pore widths.

σ_i = standard deviation of the average histogram

P_i = average of the mean pore widths of individual samples

σ_i = standard deviation of the mean pore widths of individual samples

Thus, the mean pore width of the pan side decreases with increasing collagen concentration. Figure 3.4.7 shows a graph of mean pore width versus concentration. An exponential relationship is observed. Figure 3.4.8 is a graph of the ln(mean pore width) versus concentration. A linear correlation of -0.97 was calculated for the equation.

$$P = 206 \exp(-0.76C)$$

where, P = mean pore width, μ
C = collagen concentration, % w/w solids

It should be noted that there are only three points to each curve, and more information must be obtained before this relationship may be generalized.

3.4.1.2 Edge View

The edge views show a difference in orientation of the pores between the standard 1.0x material and the higher concentrations. The pores of the 1.0x material appear randomly oriented compared with the pores of the 2.6x foam which are arranged in columns. The 1.6x material was not as highly oriented as the 2.6x material. Sections of pores with random structure as well as orientation were observed. The angle between the major orientation direction and the axis perpendicular to the pan surface was not constant for a particular material. The range of this angle was between 0° and 60°.

The pore orientation was quantitated by plotting mean pore width versus angle of scan and curves representative of each material are shown in Figure 3.4.9 a, b, c. The curves for the 1.6x and 2.6x materials have narrower and sharper peaks than the curve for the 1.0x foam,

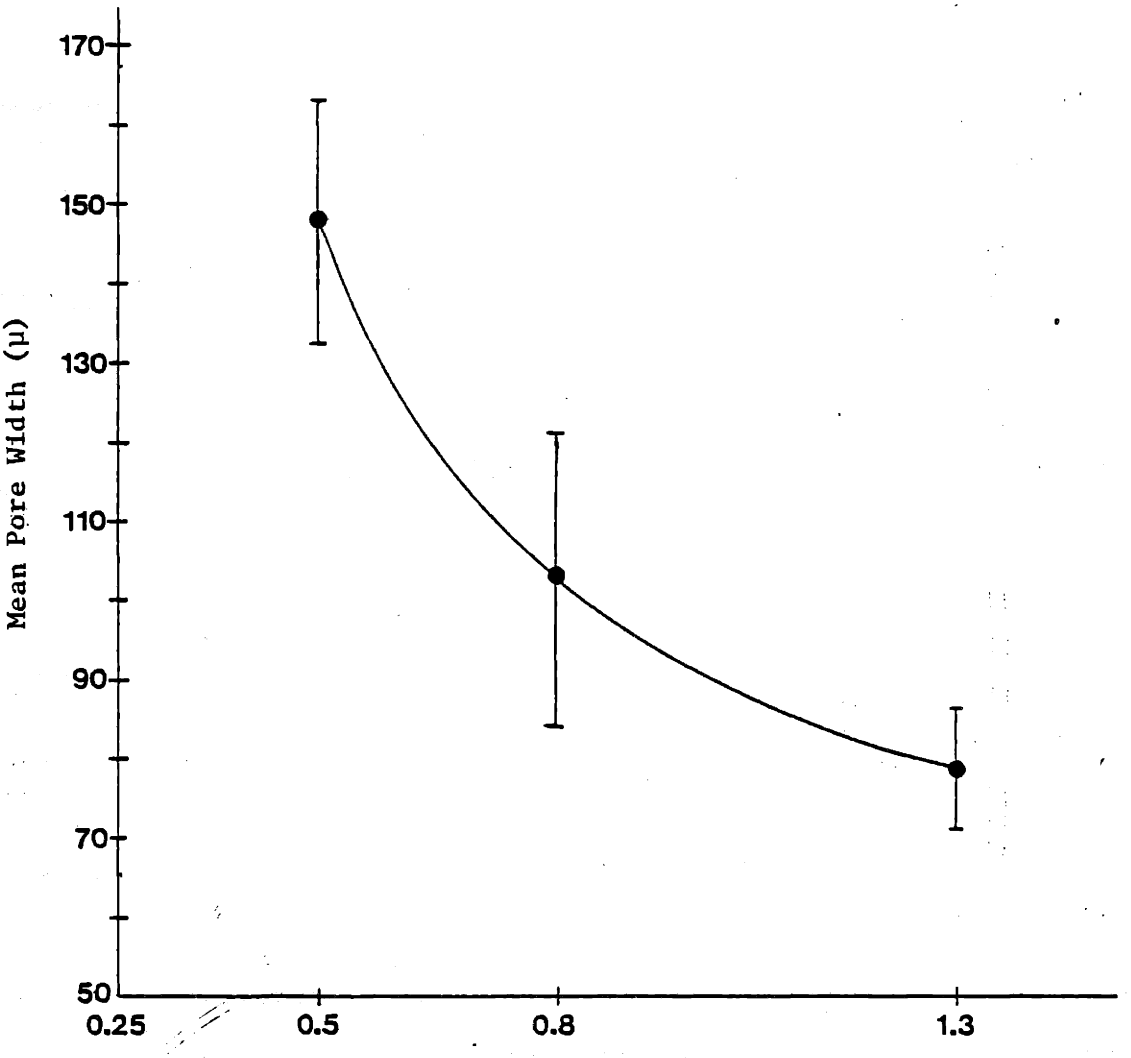

Figure 3.4.7 Pan Mean Pore Width versus Collagen Concentration

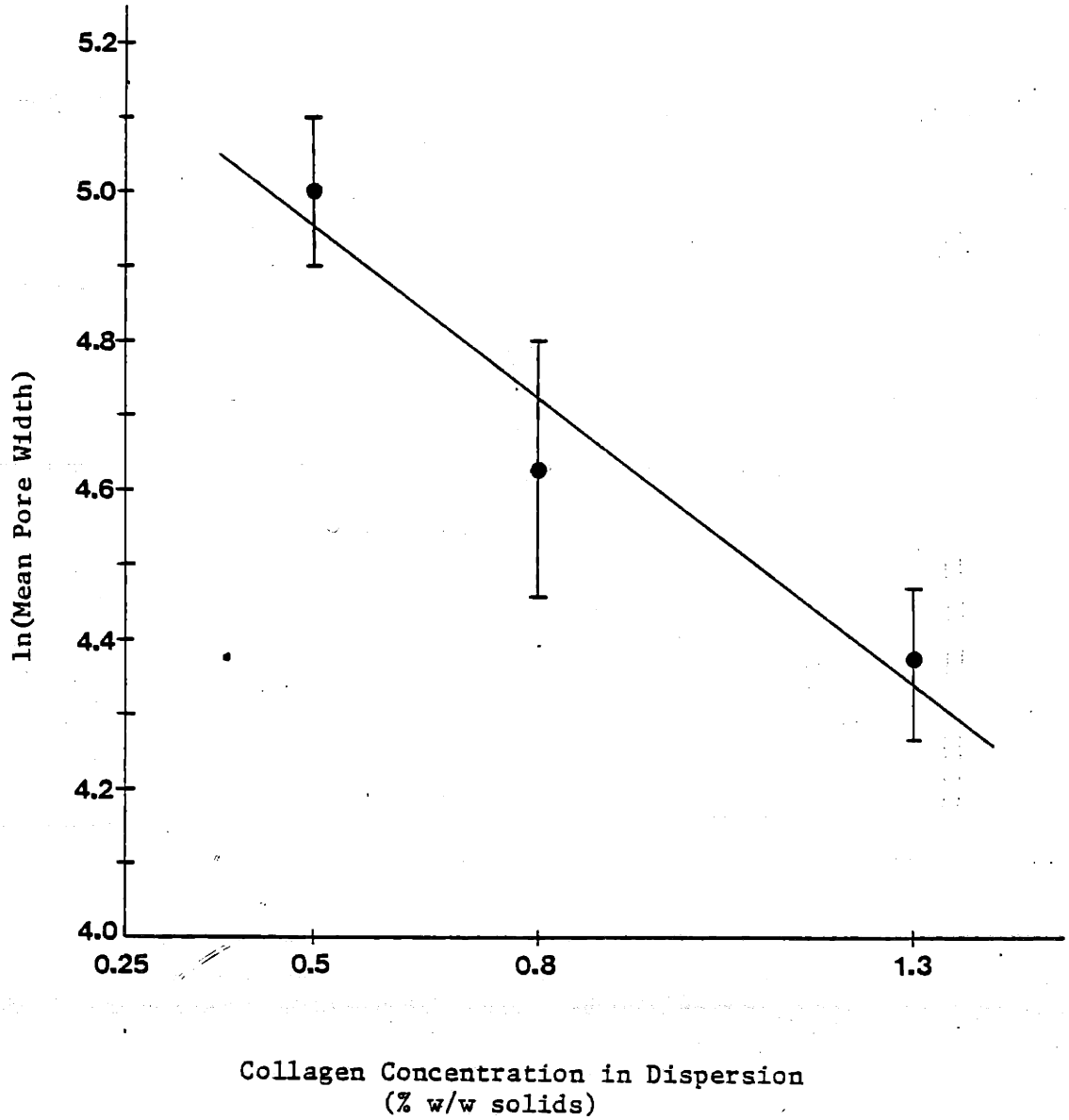

Figure 3.4.8 ln(Pan Mean Pore Width) versus Collagen Concentration

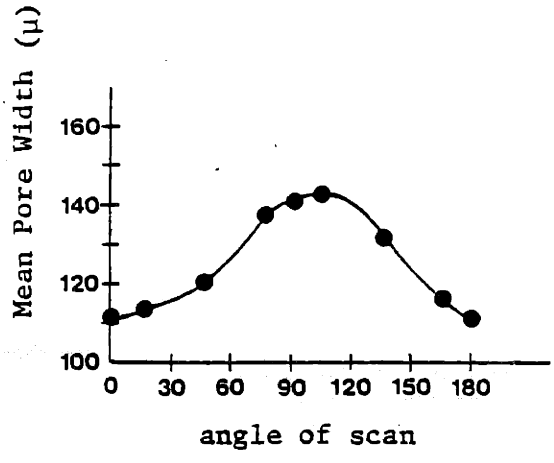

a) 1.0x edge view

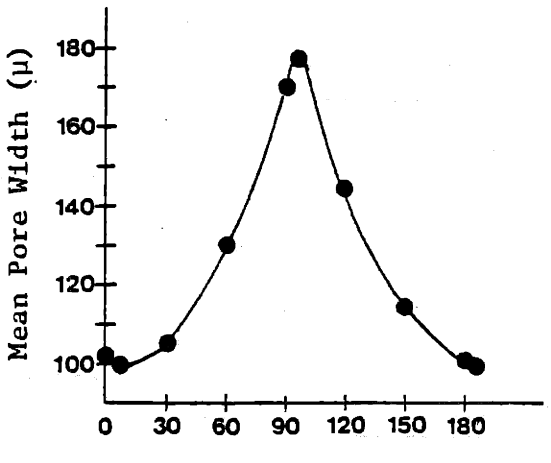

b) 1.6x edge view

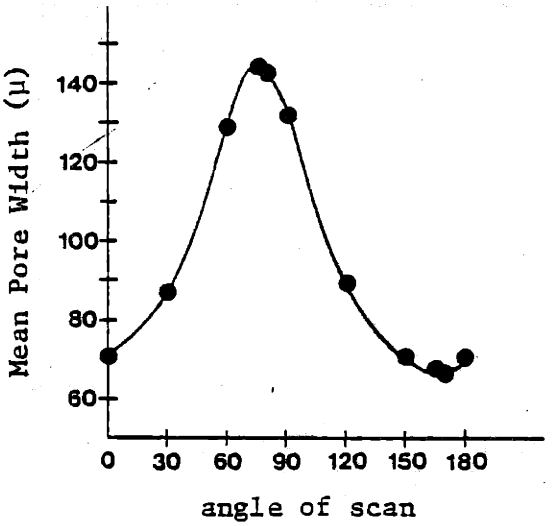

c) 2.6x edge view

Figure 3.4.9 Orientation: Mean Pore Width versus Angle of Scan

indicating a higher degree of orientation. This trend is indicated by a larger peak height, smaller standard deviation of the peak, and a larger value of kurtosis for the 1.6x and 2.6x foams as listed in Table 3.4.2. For these three measurments the 1.6x material was not significantly different from the 2.6x material when compared in a two-tailed t-test ($p > 0.2$). The values for the 1.6x and 2.6x foams were then grouped together and tested against the 1.0x foam in a contrast test [31] (H_o: $(\bar{X}_{1.6} + \bar{X}_{2.6})/2 - \bar{X}_{1.0} = 0$). The values of peak height, peak standard deviation, and kurtosis for the 1.6x and 2.6x foams were significantly different from the 1.0x foam ($p < 0.005$).

The average of the mean pore widths of all scans were calculated for the 1.0x, 1.6x, and 2.6x foams and are also shown in Table 3.4.2. The values for the 1.0x and 1.6x materials were not significantly different when compared in a two-tailed t-test ($n = 5, 11$, $p > 0.2$). These values were combined and compared to the average for the 2.6x material in a contrast test (H_o: $(\bar{X}_{1.0} + \bar{X}_{1.6})/2 - \bar{X}_{2.6} = 0$). They were significantly different from the 2.6x foam ($p < 0.05$). The collagen concentration had a larger effect on the mean pore width of the pan side than the edge view.

3.4.2 Pore Volume Fraction

The pore volume fraction was measured for the 1.0x, 1.6x, and 2.6x materials. Table 3.4.3 shows the mean values and their respective standard deviations. As expected pore volume fraction decreased with increasing concentrations of collagen-GAG. Values were compared using an unpaired, two-tailed t-test and all were significantly different from

Table 3.4.2 Porosity: Edge View

	1.0x		1.6x		2.6x	
	Mean	Std. Dev.	Mean	Std. Dev.	Mean	Std. Dev.
Mean pore width (μ)	145	16	135	19	123	18
Aspect Ratio	1.24	0.09	1.73	0.50	1.87	0.28
Height of Peak (μ)	30	12	70	40	76	22
Peak Standard Deviation (μ)	1.07	0.12	0.91	0.06	0.90	0.09
Kurtosis	2.30	0.19	2.72	0.34	2.79	0.18

each other, see Table 3.4.4.

Table 3.4.3 Mean Volume Fractions

Type of Material	Pore Volume Fraction	Std. Dev.	Collagen Volume Fraction	Std. Dev.
1.0x	0.9940	0.0002	0.0056	0.0002
1.6x	0.9928	0.0002	0.0072	0.0002
2.6x	0.9860	0.0020	0.0140	0.0020

Table 3.4.4 Pore Volume Fraction: Unpaired, one-tailed, t-test results

Pairs Tested	n_1, n_2	t	p
1.0x vs. 1.6x	7,10	12.7	0.001
1.0x vs. 2.6x	7,9	9.16	0.001
1.6x vs. 2.6x	10,9	9.07	0.001

3.5 Histology

3.5.1 Histology: Crosslinked versus Noncrosslinked

Histological sections were taken at days 15, 21, and at the "long term" stage. When there is no longer any substantial change in the external appearance of the graft site, the scar is described as "long term." Descriptions of these sections are listed in Table 3.5.1. The epithelial migration over the graft occurred at approximately the same rate for both the crosslinked and noncrosslinked materials. Initially it appears that the mesenchymal cells migrated more rapidly into the noncrosslinked material. By day 21 the cell concentrations within the two types of grafts were roughly equal. Both grafts became well vascularized.

Table 3.5.1 Histology: Crosslinked and Noncrosslinked

	Crosslinked	Noncrosslinked
Day 15	Epidermis growing over 40% of the width of the graft, some contraction beginning, collagen becoming more dense at the wound edges, extensive cellular migration.	Epidermis growing over 40% of the the width of the graft, normal dermis growing under graft, more cells infiltrated into noncrosslinked graft than with crosslinked graft.
Day 21	Epidermis growing over 50% of width of the graft, collagen becoming densely packed, high cell concentration in graft, graft well vascularized.	Epidermis covering entire graft, very thin epidermis in center, graft has dense appearance throughout the entire graft, high mesenchymal cell concentration, well vascularized.
Long Term	Uniform epidermis completely covering neodermis, densely packed collagen aligned parallel to external surface, slightly birefringent in polarized light (90°), normal dermis migrating under neodermis along panniculus carnosus, granuloms containing multinucleated giant cells and graft collagen apparent near panniculus carnosus in some but not all long term animals.	Uniform epidermis covering neodermis, neodermis has densely packed, remodelled collagen aligned parallel to external surface, birefringent in polarized light (90°), normal dermis migrating into neodermis midway between epidermis and adipose layer, less densely packed collagen than crosslinked graft site.

The major difference between the two materials is the rate of resorption and remodelling of the collagen graft. At day 21 the crosslinked material was beginning to be degraded and remodelled, whereas these processes were already occurring throughout the noncrosslinked material by day 21, see Figure 3.5.1 a, and b. The silicone had come off the noncrosslinked graft site and the surface of the wound was entirely covered with epithelial cells at day 21 while 50% of the section of the crosslinked graft remained open. The distances that the epithelial cells migrated were equal in the two cases and the difference in amount of closure may be attributed to a difference in contraction rates.

The long term histological sections of both the crosslinked and noncrosslinked grafts contained densely packed, aligned collagen (neodermis) that was birefringent in polarized light. However, a smaller quantity of neodermis was apparent in the noncrosslinked graft site. The only other difference between the noncrosslinked and crosslinked long term histological sections was the location of the normal, intact dermis migrating from the original wound edge. In the crosslinked graft site, the normal dermis was migrating under the densely packed collagen, while the normal dermis in the noncrosslinked graft site was migrating through the dense collagen, roughly midway between the epidermis and the adipose tissue.

A distinct difference between the neodermix and normal intact dermis can be seen. The fibers of the normal dermis have a random woven appearance and are more loosely packed than the neodermis. No epidermal appendages are regenerated in the neodermis. Any appendages apparent in

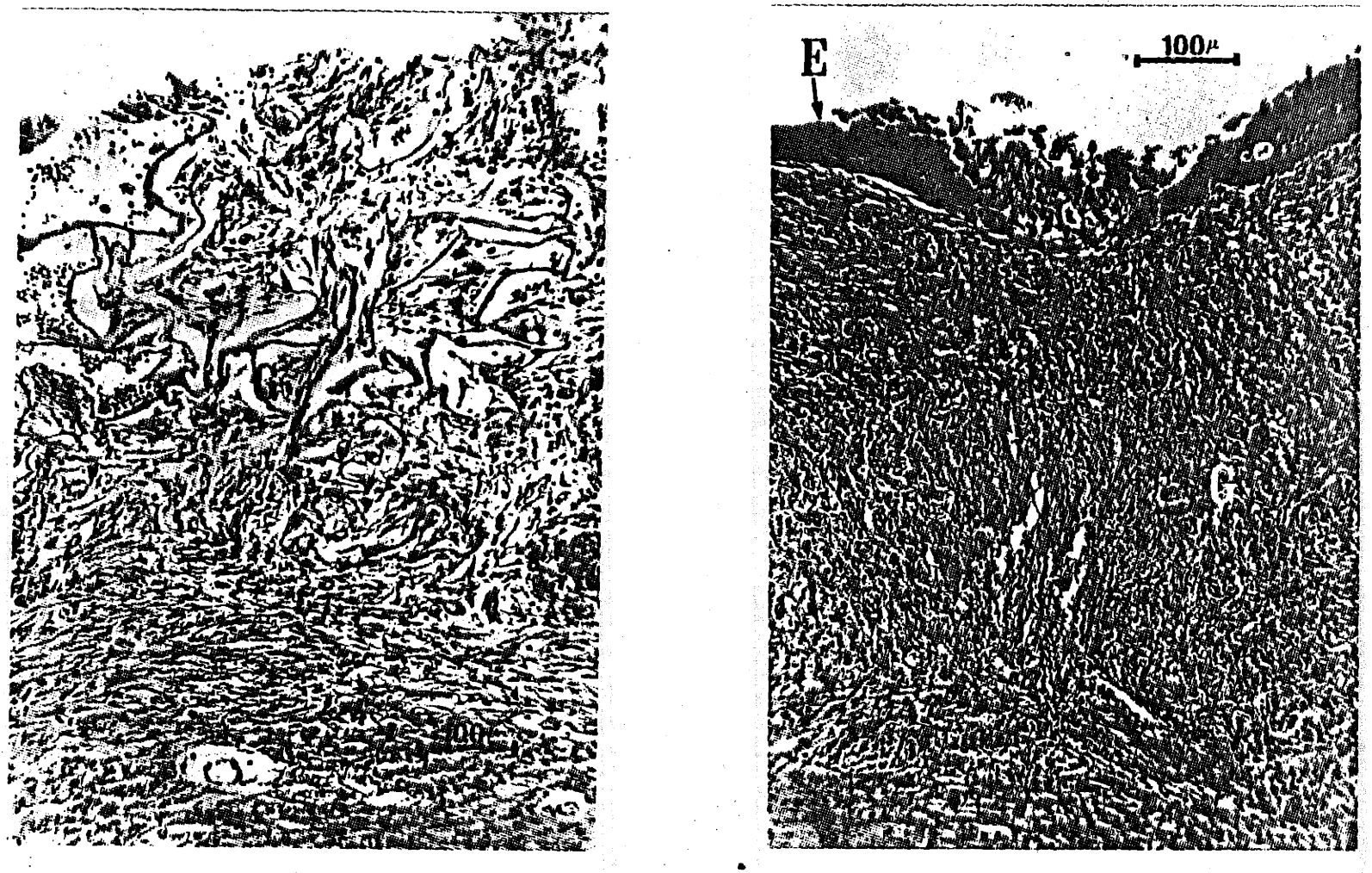

(a) (b)

Figure 3.5.1 Histological Section, hematoxylin and eosin stain, center of graft, G - graft, E - epidermis, a) crosslinked graft day 21, b) noncrosslinked graft, day 22

the graft site have most likely migrated from the wound edges. The dense parallel alignment of the collagen fibers and the lack of epidermal appendages in the neodermis make it easy to establish the difference between the two regions.

Approximately half of the long term sections of both materials contained a region where a small part of the collagen foam had not remodelled and was not birefringent in polarized light. This region was well infiltrated with cells. Often but not always these cells were multinucleated giant cells. Some cells around the region were aligned parallel to the surface of this region. It is unclear whether a fibrotic sac was beginning to form around the region. No significant fibrotic sac formation was found in any sections. These regions have been labelled as granulomas. The granulomas always occurred in the neodermis near or next to the adipose tissue. The cause of these granulomas is unknown. In general granulomas may result from the reaction of the animal to aseptic foreign bodies such as silk suture threads [32]. The sutures used in these experiments were nylon and have a very low incidence of initiating an inflammatory response [33]. Therefore, the probability that the sutures are the cause of the granulomas is small. Another possible cause is small impurities in the collagen foam from either the processing steps or from the original source of the collagen. Again the probability that there were that many impurities in the grafts is small. The collagen-GAG itself may be the cause of the inflammatory response. In some cases it may initiate an aseptic foreign body response. There is no conclusive evidence for the cause of the granulomas.

3.5.2 Histology: Concentration/Porosity Variation

Histological sections for the 1.0x, 1.6x, and 2.6x material were taken at days 7, 14, 22, and long term. The results are listed in Table 3.5.2. A distinct difference in the thickness of the collagen fiber aggregates in the graft were observed in days 7, 14, and 22. The thickness of the fiber aggregates increased with increasing collagen concentration in the foam. The collagen aggregates of the 2.6x grafts were 15 - 25μ wide, roughly three times the thickness of the 1.0x aggregates (5 - 10μ). The 1.6x aggregate thickness was approximately 10 - 20μ.

At day 7 the 1.6x and 2.6x grafts were poorly adhered to the wound bed and very little cellular migration into the grafts had taken place. The 1.0x material was more firmly adhered to the wound bed and cellular infiltration was evident. A cell concentration gradient can be seen in the 1.0x graft with a greater number of cells near the adipose tissue and fewer near the silicone layer. The epidermis was just beginning to thicken and become hyperplastic at the wound edges in all three types of grafts. In the 1.6x graft it is not clear whether the epidermis was going to migrate under or over the graft material. All three materials were becoming vascularized.

At day 14 both the 1.0x and 2.6x grafts were well adhered with the epidermis migrating over approximately 40% of the graft. A 1.6x histological sample was not obtained. The 1.0x material was uniformly infiltrated with cells throughout the graft, the difference in cell concentration gradients withing the graft had been eliminated. The 2.6x graft was infiltrated with cells; however, there was a greater concentration

Table 3.5.2 Histology: Variation with Concentration/Porosity

	1.0x	1.6x	2.6x
Day 7	Cell infiltration evident, cell concentration gradient with more cells near adipose tissue and at wound edges, hyper-plastic epidermis beginning to migrate over graft, well vascularized.	Separation of graft from wound bed, some cell infiltration, epidermis becoming hyperplastic at edge, beginning to grow both over and under graft in some sections, graft becoming vascularized.	Separation of graft from wound bed, very few mesenchymal cells in graft, thickening of epidermis at edge and beginning to grow over graft, highly vascularized.
Day 14	Epidermis covering 40% of width of graft, high cell concentration in graft, beginning to vascularize, collagen becoming densely packed and filled with cells at wound edges and at bottom of graft (possibly a result of resorption and remodelling.	No specimen.	Graft well adhered to wound bed, epidermis covering 35% of graft width, good cellular infiltration, cell concentration gradient, more cells at bottom of graft, highly vascularized, cells in adipose tissue, thick fibers of collagen in graft, original intact dermis migrating beneath graft.
Day 22	High cell concentration, epidermis growing over 50% of graft width, collagen partially remodelled and more dense.	40% of width has epidermal coverage, graft adhered to wound bed, high cell concentration, collagen fibers thick, cells in adipose tissue, normal dermis beginning to migrate beneath graft, graft more dense with collagen and cells (resorption and remodelling?), well vascularized.	Epidermis grown over 40% of width of graft, hyperplastic at edges, normal dermix beginning to migrate beneath graft, collagen fibers thick, graft becoming dense at wound edges and near wound bed, well vascularized.

Table 3.5.2 Histology: Variation with Concentration/Porosity continued

	1.0x	1.6x	2.6x
Long Term	Uniform epidermis completely covering neodermis, densely packed collagen aligned parallel to external surface, birefringent in polarized light (90°), normal dermis migrating under neodermis along panniculus carnosus, granuloma containing multinucleated giant cells and loosely packed collagen most likely graft collagen apparent near panniculus carnosus in some but not all long term animals.	Uniform thick epidermis completely covering neodermis, dense remodelled collagen aligned parallel to external surface, birefringent in polarized light (90°), single granuloma present in 50% of sections with non-remodelled collagen, high cell concentration, multinucleated giant cells, and nonbirefringent.	Uniform epidermis completely covering neodermis, densely packed collagen aligned parallel to external surface, neodermis birefringent in polarized light (90°), granuloma as described in 1.0x and 1.6x present in 60% of sections.

of cells near the adipose layer than near the silicone layer. The 1.0x material was beginning to remodel at the wound edges whereas the 2.6x graft showed no evidence of remodelling.

At day 22 all three materials were well vascularzied. The 2.6x graft had a slightly larger concentration of capillaries than the other materials. For each type of material, epidermal migration had proceeded over 40% to 50% of the lateral section of the graft surface, normal dermis was migrating beneath the graft, and the graft was highly infiltrated with cells. The major difference between the three materials was the extent of the resorption and remodelling of the collagen fibers of the graft. The 1.0x material was extensively resorbed and remodelled. The collagen was becoming more densely packed. Remodelling of the 1.6x graft was occurring throughout the graft, but the collagen fibers were still loosely arranged. The 2.6x material was just starting to become dense at the edges of the graft. The fibers of collagen were still thick and loosely packed in the center. Figures 3.5.2 a, and b through 3.5.4 a, and b show histological sections of the 1.0x, 1.6x, and 2.6x grafts.

There was a large variation in response from animal to animal for the high concentration materials. This variation may be a result of some nonuniformity of the pores of the grafts. Figure 3.5.5 a, and b shows the varied response of two animals to the same kind of graft material.

In long term histological sections the amount of densely packed collagen in the graft site increased with increasing collagen concentration. The 2.6x graft site had the most dense collagen aligned parallel to the skin surface. The dense collagen was birefringent in polarized light (90°). All three types of grafts had normal dermis migrating underneath and

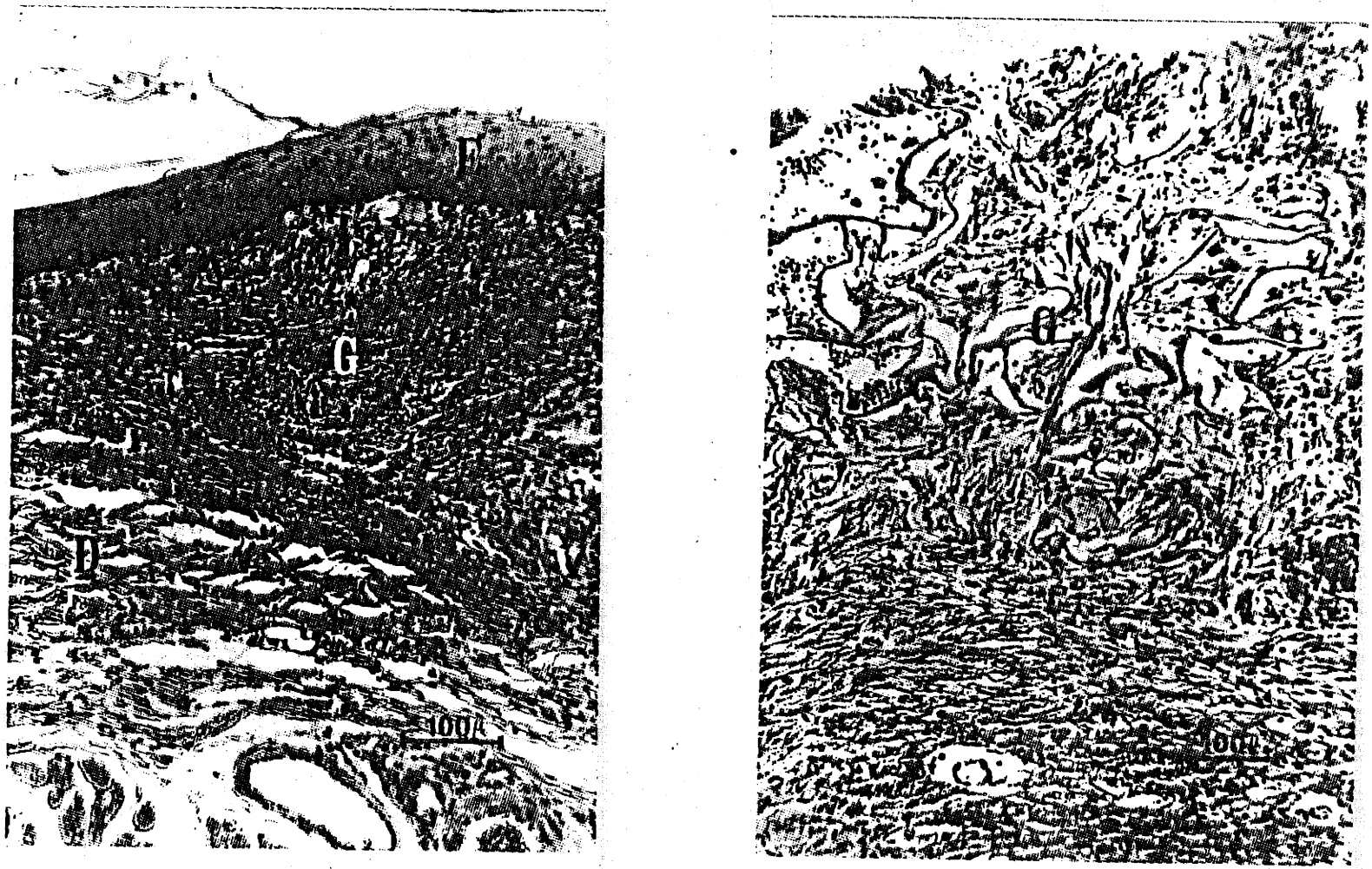

(a) (b)

Figure 3.5.2 Histological Section, 1.0x, day 21, hematoxylin and eosin stain, G - graft, E - epidermis, D - normal dermis, a) edge of graft, b) center of graft

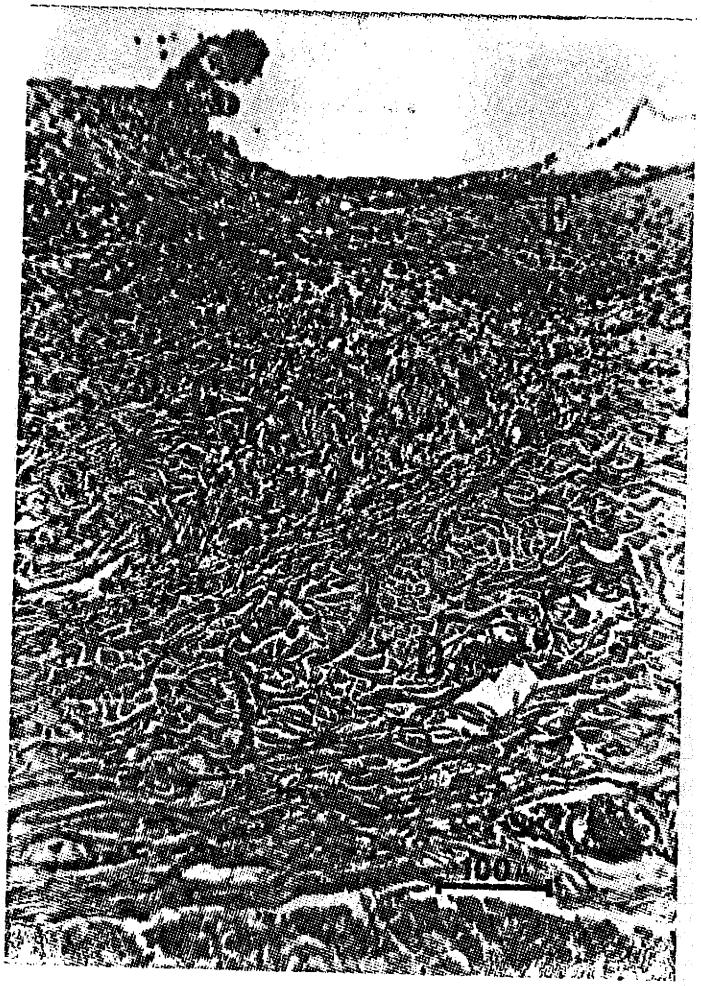

(a)

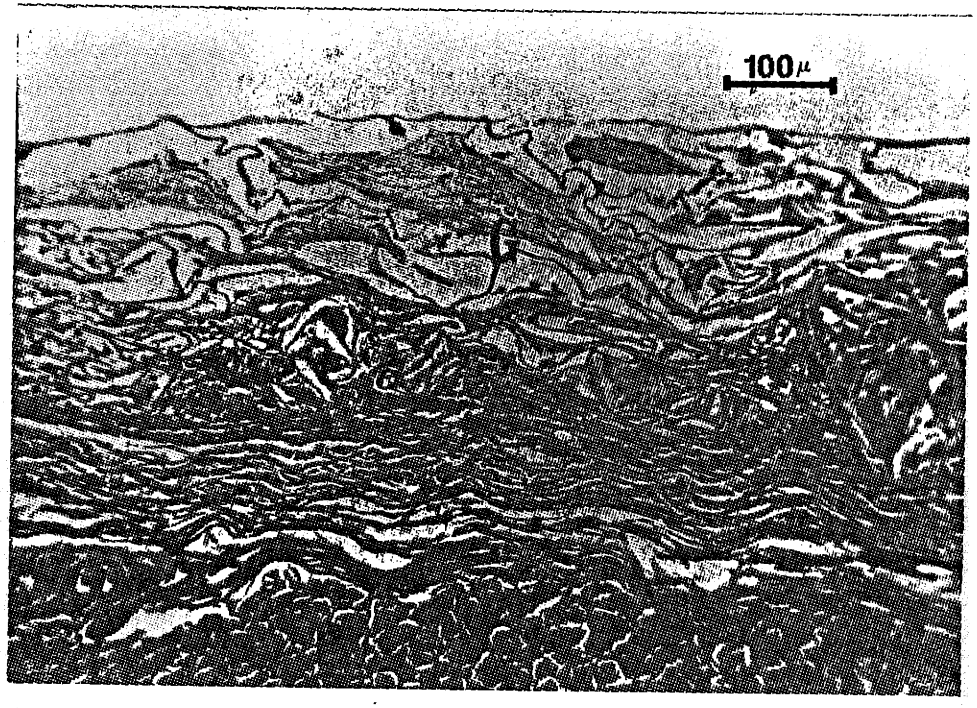

(b)

Figure 3.5.3 Histological Section, 1.6x, day 22, hematoxylin and eosin stain, G - graft, E - epidermis, D - normal dermis, P - panniculus carnosus, a) edge of graft, b) center of graft

(a)

(b)

Figure 3.5.4 Histological Section, 2.6x, day 18, hematoxylin and eosin stain, G - graft, E - epidermis, D - normal dermis, a) edge of graft, b) center of graft

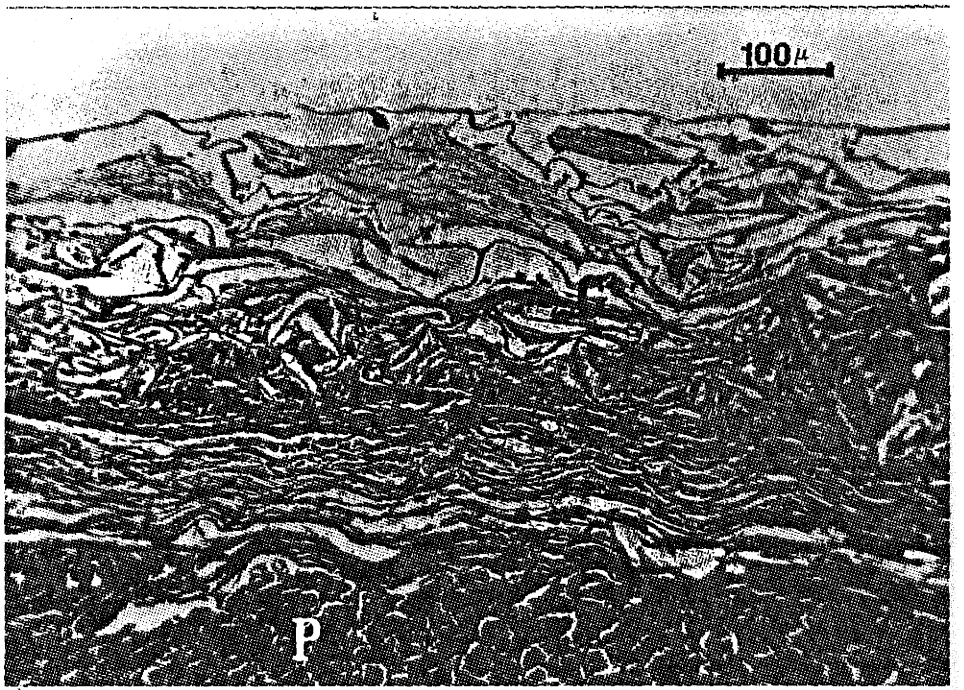

(a)

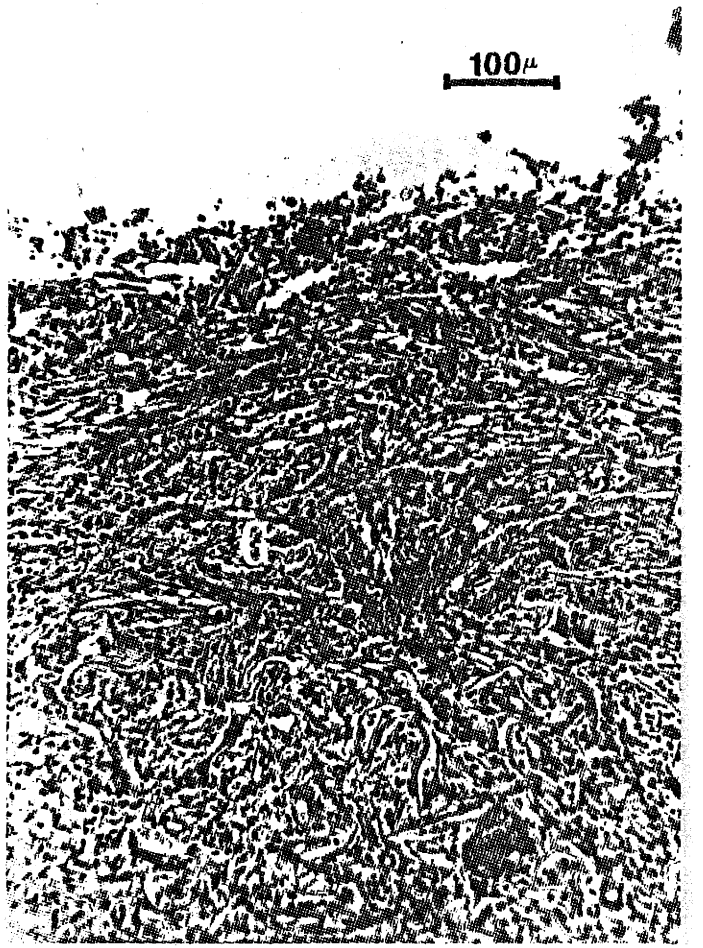

(b)

Figure 3.5.5 Comparison: Variation of Response from animal to animal, histological section, 1,6x, hematoxylin and eosin stain, G - graft, P - Panniculus carnosus, a) day 22, b) day 21

uniform thick epidermis over the graft site. The long term histological sections of all three materials contained many granulomas with and without multinucleated giant cells (as described above), see Figure 3.5.6. A higher incidence of granulomas was observed in the 2.6x grafts.

3.6 Contraction/Epithelialization (C/E)

3.6.1 C/E: Crosslinked versus Noncrosslinked

In vivo C/E was measured and calculated for the crosslinked and noncrosslinked materials grafted on guinea pigs. Curves of % original area remaining open versus time are shown in Figures 3.6.1 through 3.6.4. Figures 3.6.1 and 3.6.2 show each material alone with their respective ranges (bars). Each data point represents the average of atleast three guinea pigs. The population sizes are listed in Table 3.6.1. Figure 3.6.3 is a curve of the C/E of an open wound. This wound was prepared identically to the grafted wounds but no graft was placed in the wound bed. This work was previously done by researchers, Susan L. Hanson and Eugene Skrabut at MIT (unpublished data). Figure 3.6.4 is a composite graph comparing the effects of the two materials and the open wound. The curves in all four graphs were fitted by eye.

The onset of C/E occurred at day 6 for the crosslinked and noncrosslinked materials. In contrast the open wound had contracted to approximately two thirds of its original area by day 3.

The crosslinked and noncrosslinked C/E data were fitted with linear regression lines from the onset of C/E to the day of closure. The open wound data was fitted with a linear regression line from day 0 to day 10 forced through 100% at day 0. After day 10 the open wound data begins

Figure 3.5.6 Granuloma in a long term histological section, day 52.

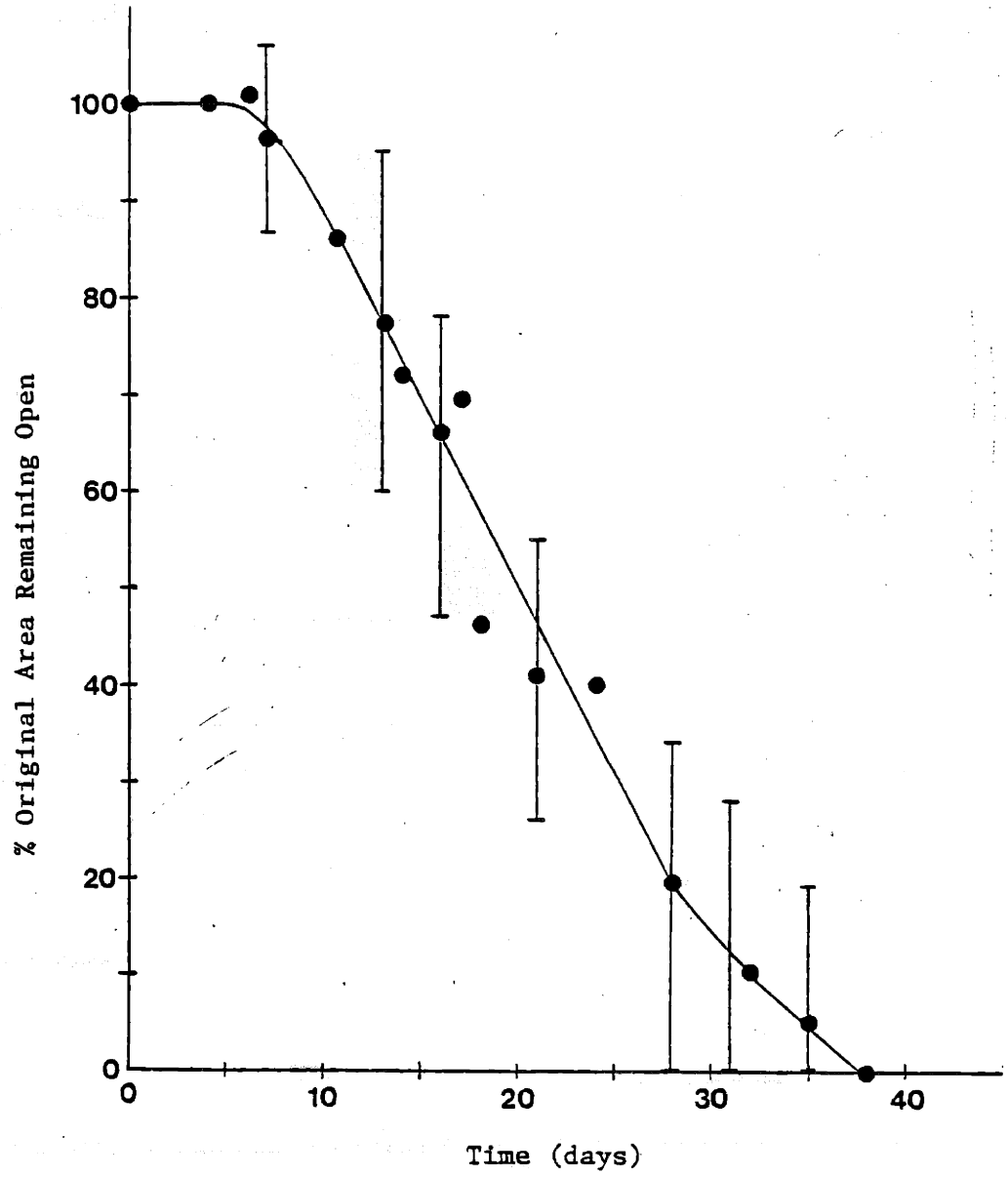

Figure 3.6.1 Crosslinked graft; Wound Closure: Reduction of open area under the silicone layer, Bars - ranges of values

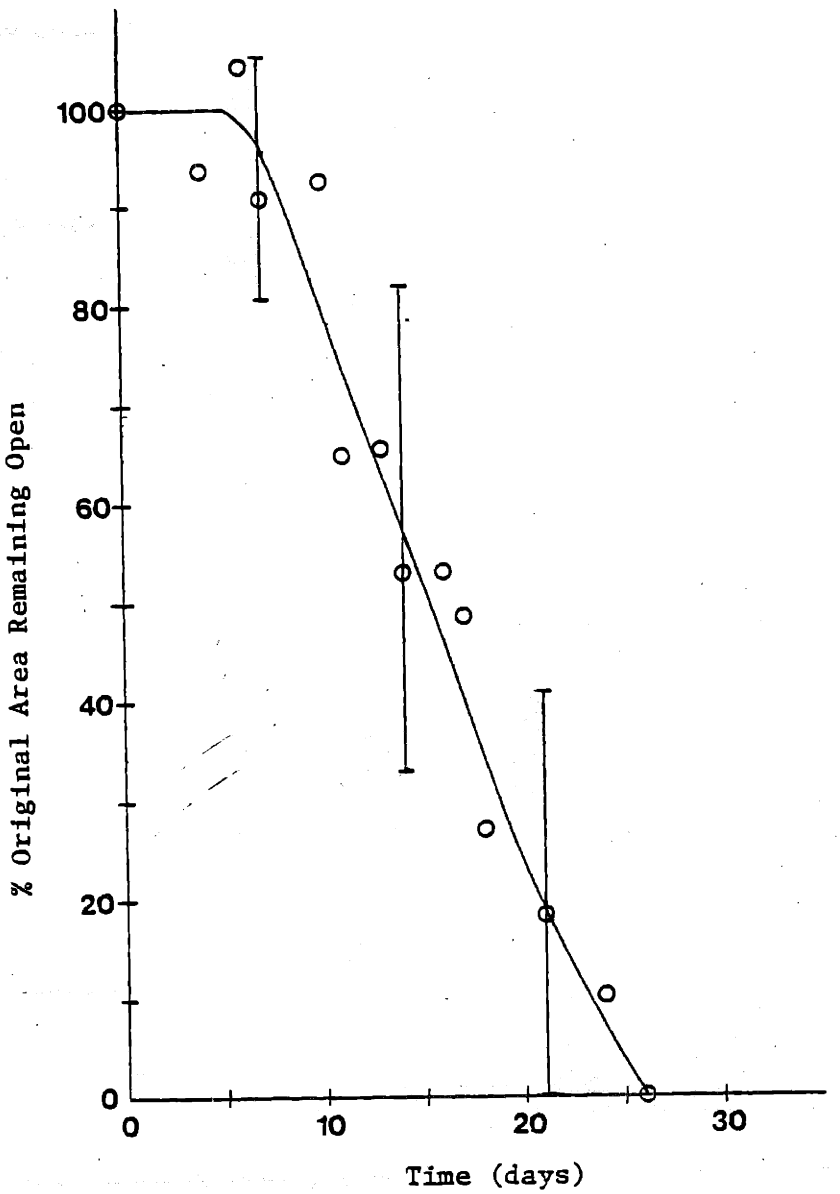

Figure 3.6.2 Noncrosslinked graft; Wound Closure: Reduction of open area under the silicone layer, Bars - ranges of values

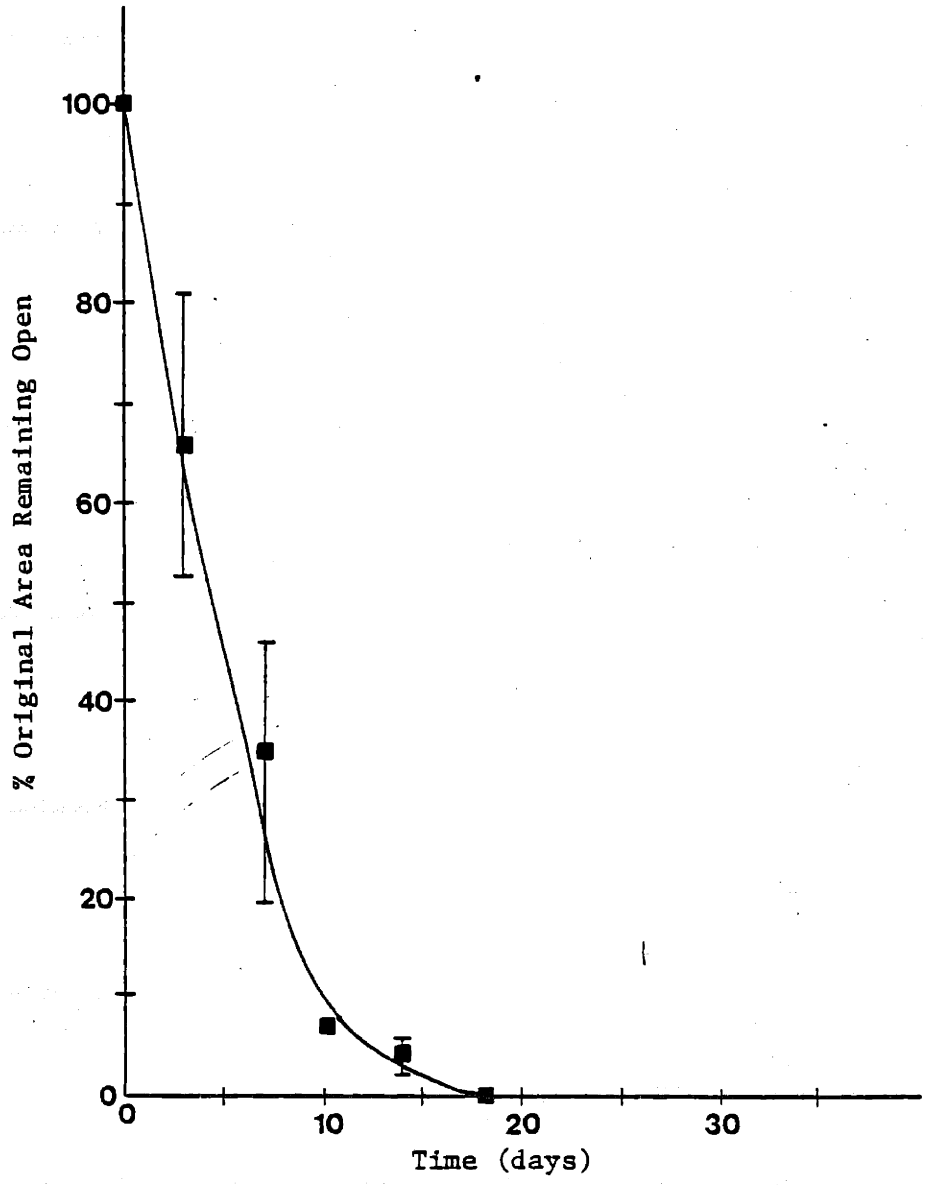

Figure 3.6.3 Open Wound; Wound Closure: Reduction of open area, Bars - ranges of values

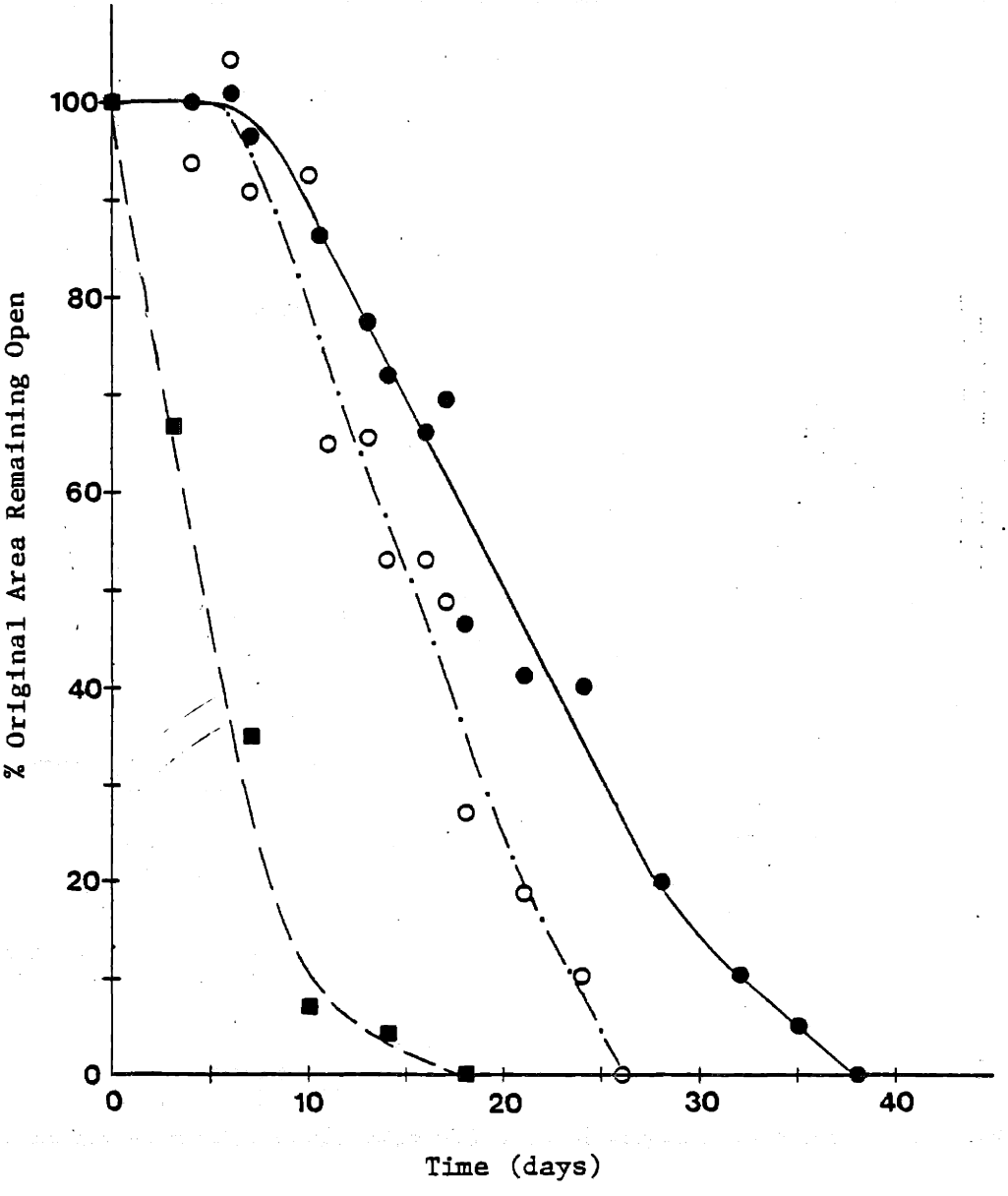

Figure 3.6.4 Composite Wound Closure Curves, ■—open wound, ●—crosslinked, ○—noncrosslinked.

to plateau, and data after day 10 was not used to compute the linear regression. The results of the linear regressions and time in days to obtain 50% closure (50% pink area) of the wounds measured from the regression lines are listed in Table 3.6.2 and shown in Figure 3.6.5. The correlations were greater than or equal to $|-0.97|$ for all three types of materials. Individual animals rather than the averages were also fitted with linear regression lines for the crosslinked and non-crosslinked materials. A paired, two-tailed t-test ($n = 8$) was performed on these data. The slopes of the crosslinked and noncrosslinked materials were found to be significantly different ($p < 0.01$). An unpaired, two-tailed t-test ($n = 5, 10$) was also performed on the open wound and non-crosslinked data. A significant difference between these two was also determined ($p < 0.005$). A distinctly different rate of closure was demonstrated by the variation in the 50% day also in Table 3.6.2. The crosslinked material achieves 50% closure 6 days later than the noncrosslinked material and 16 days later than the open wound. The difference in reduction of closure rate (i.e., the rate of reduction of pink area visible under the silicone layer) can easily be seen in the animal model. Figure 3.6.6 a, and b show a comparison of the crosslinked and noncrosslinked grafts at day 18. The difference between the pink area is roughly one square centimeter of 26% of the original area.

The average times for closure of the wounds (zero open area, zero pink area) for the crosslinked and noncrosslinked materials and the open wound were 38 days (std. dev. = 8.5), 26 days (std. dev. = 3.7), and 18 days (std. dev. = 3.0) respectively. A comparison of the ranges of the day of closure shows small overlapping, see Table 3.6.3. Closure times

Table 3.6.1 Population Sizes for C/E Data

	Total # of Animals	#Long Term Animals*
crosslinked	10	6
noncrosslinked	11	7
open wound	5	5

*Long term refers to animals that were observed for more than 50 days.

Table 3.6.2 Linear Regression of C/E Data

	Slope (%/day)	50% Day*	Intercept (%)	Correlation
crosslinked	-3.3	21	119	-0.98
noncrosslinked	-5.1	15	129	-0.97
open wound	-9.6	5	100	-0.99

*Day on which 50% original area is reached calculated from the regression line.

Table 3.6.3 Data of Day of Closure (zero pink area)

	Average (days)	Range (days)	Std. Dev. (days)
crosslinked	38	25 - 45	8.5
noncrosslinked	26	21 - 31	3.7
open wound	18	14 - 21	3.0

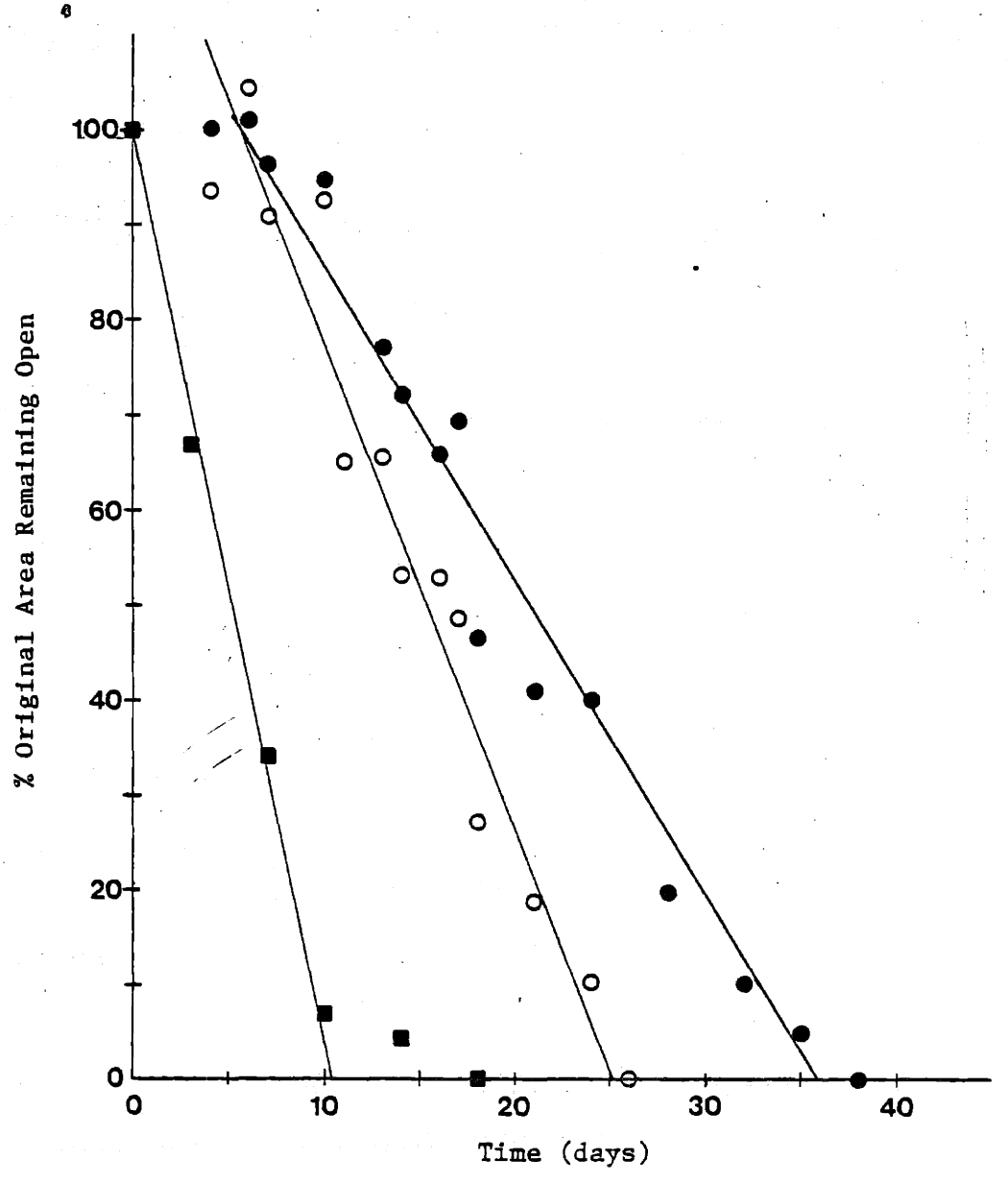

Figure 3.6.5 Composite Wound Closure Curves fitted with Linear Regressions, ■—open wound, ●—crosslinked, ○—noncrosslinked

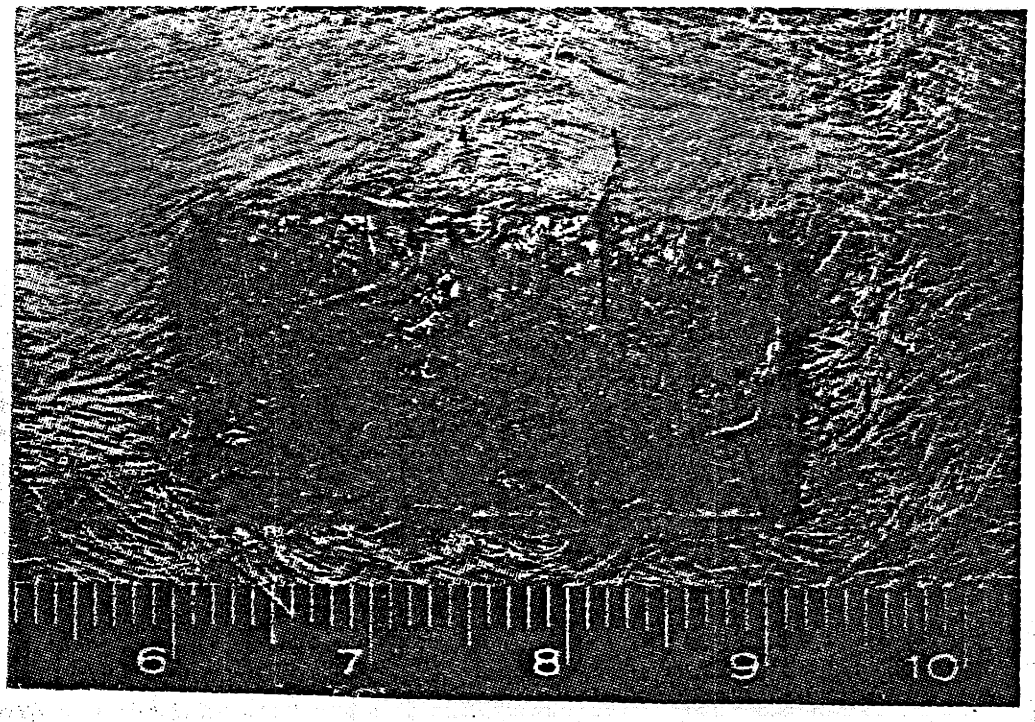

a) left graft; crosslinked, 35% original area

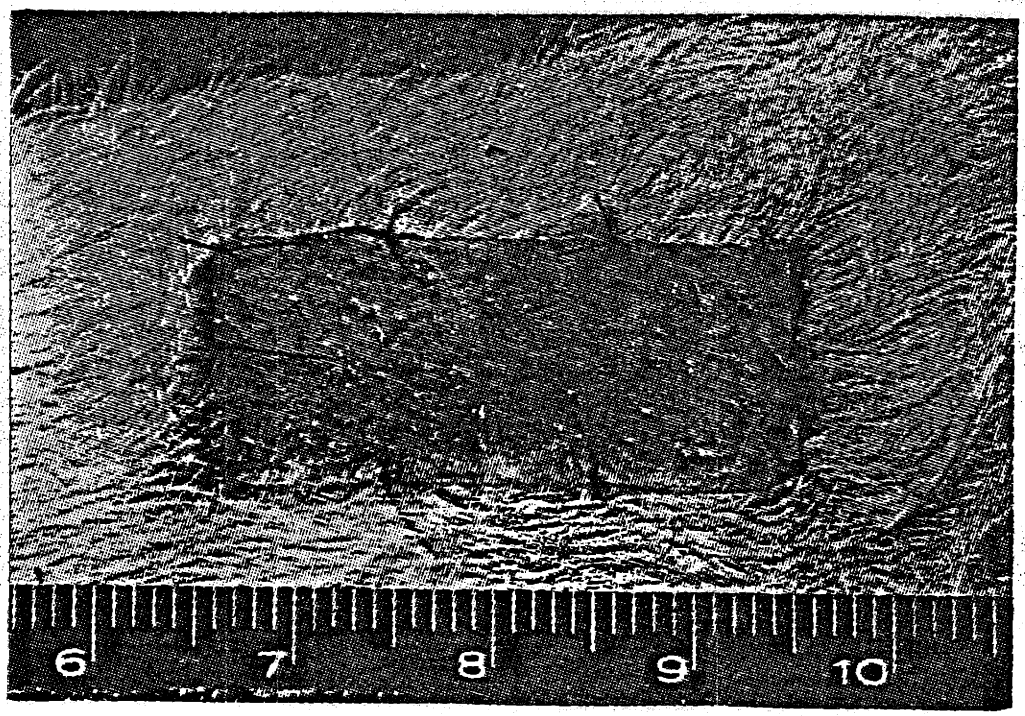

b) right graft; noncrosslinked, 9% original area

Figure 3.6.6 Comparison of Wound Closure, day 18, grafts are from the same animal

for the animals double grafted with the crosslinked and noncrosslinked materials were compared with a paired, two-tailed t-test (n = 6). The test concluded that the crosslinked material closes the wounds at significantly later times ($p < 0.01$).

The mean of the areas of the long term scars (average time, day 70) for the crosslinked and noncrosslinked materials were 27.4% (std. dev. = 4.6%) and 23.8% (std. dev. = 7.0%) respectively. These values showed no significant difference in a paired, two-tailed t-test ($n = 6$, $p > 0.3$). A greyish pink area remained longer in the center of the crosslinked scar than in the noncrosslinked scar. By day 60, the appearances of the external surface of the scars were the same for both materials. Data for the open wounds was not obtained, but is most likely not much different from the crosslinked and noncrosslinked scars [29].

3.6.2 C/E: Effects of Concentration/Porosity

In vivo C/E was measured and calculated for the 1.0x, 1.6x, and 2.6x materials. The results are plotted as % original area versus time with ranges (bars) in Figures 3.6.7 through 3.6.10. Each material is presented individually in Figures 3.6.7 through 3.6.9. Each data point represents the average of atleast three guinea pigs. Population sizes are listed in Table 3.6.4. Figure 3.6.10 is a composite graph of all three materials. The curves in all four graphs were fitted by eye. Due to an error, a set of 6 male guinea pigs were grafted. The results from these animals were not significantly different from the females in either C/E of histology and the results from these animals were combined with the results from the female animals.

During the lag phase before C/E begins, the wound edges of the 1.0x

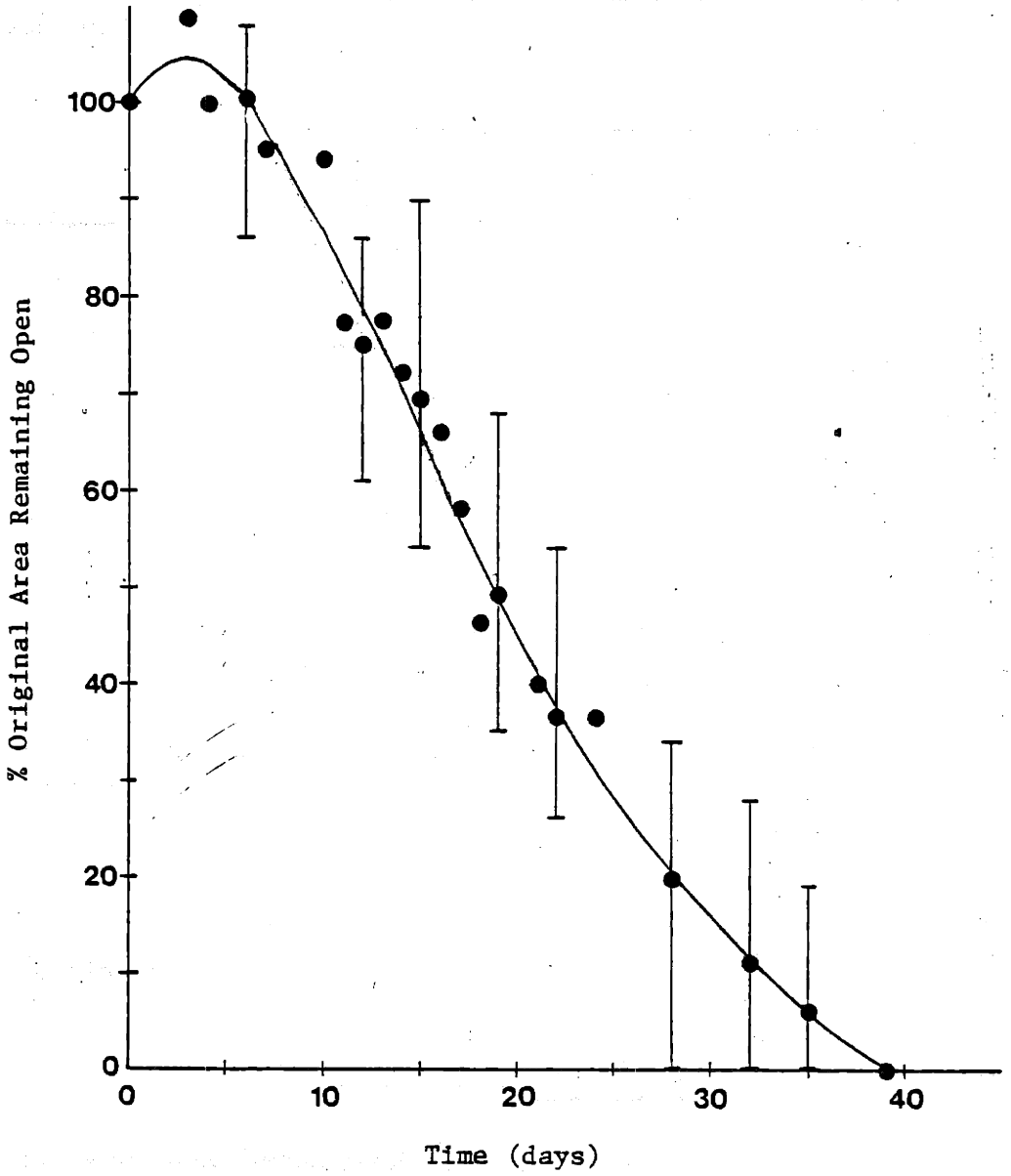

Figure 3.6.7 1.0x graft; Wound Closure: Reduction of open area under the silicone layer, Bars - ranges of values

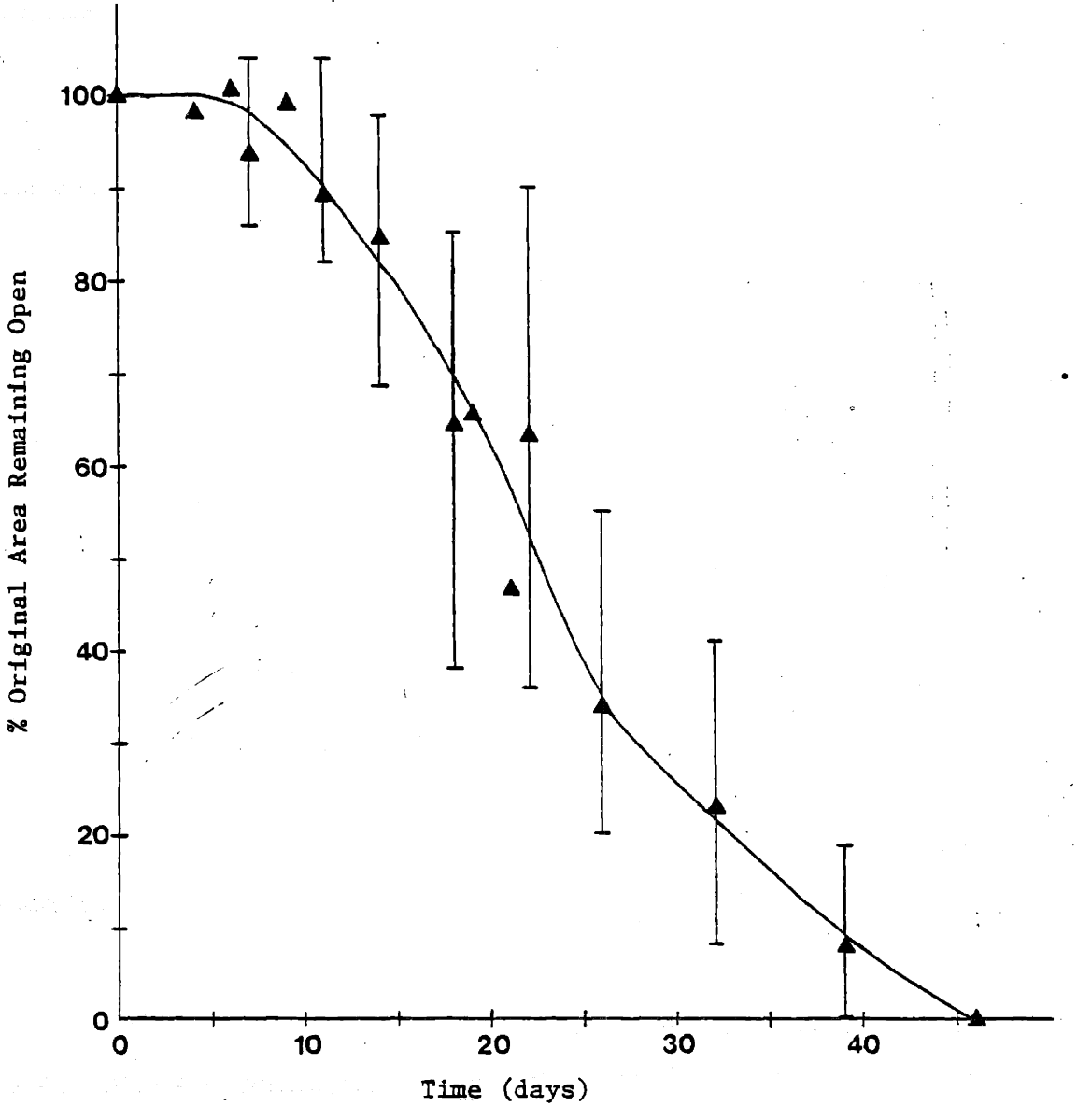

Figure 3.6.8 1.6x graft; Wound Closure: Reduction of open area under the silicone layer, Bars - ranges of values

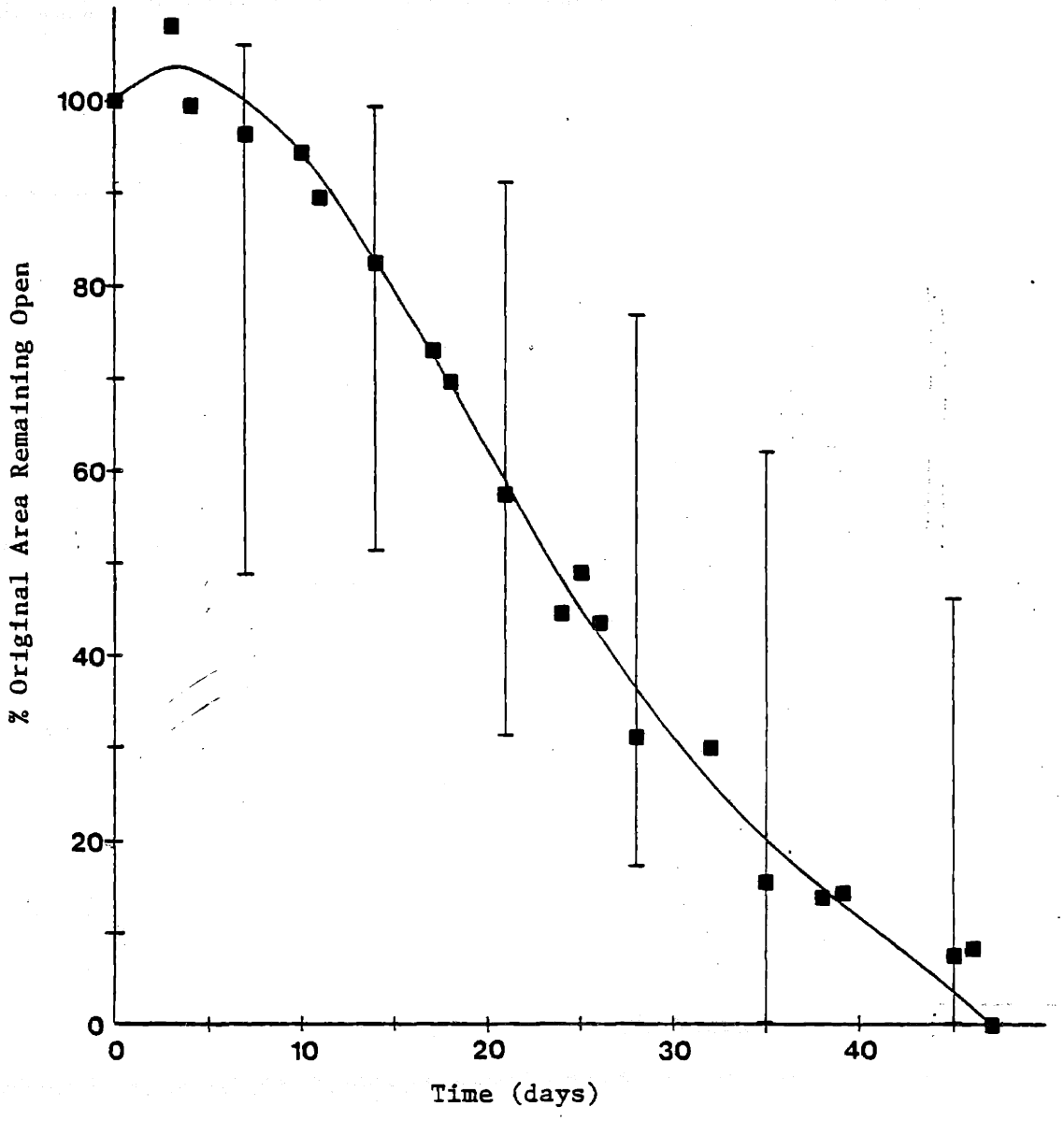

Figure 3.6.9 2.6x graft; Wound Closure: Reduction of open area under the silicone layer, Bars - ranges of values

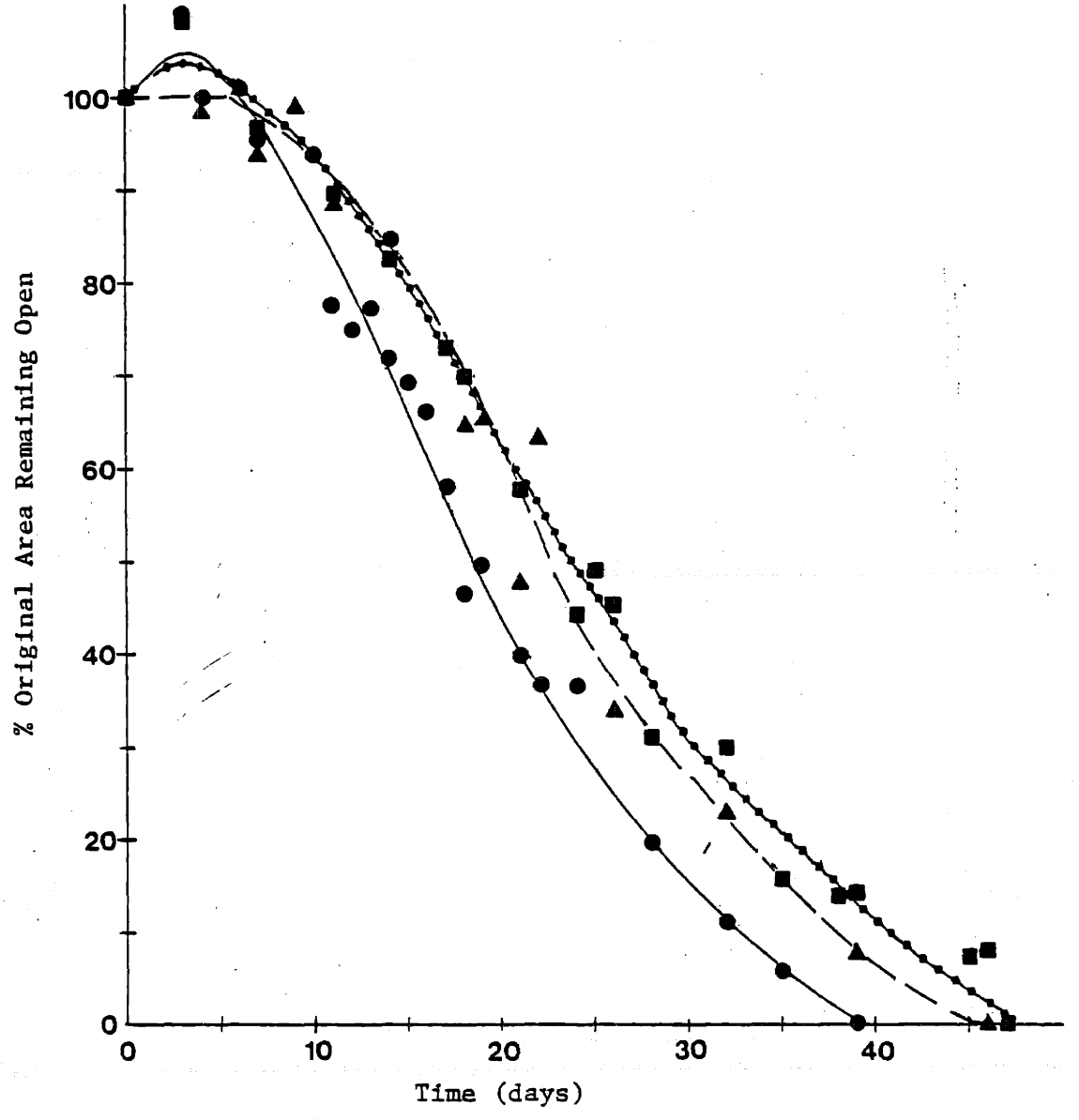

Figure 3.6.10 Composite Wound Closure Curves, ●—1.0x, ▲—1.6x, ■—2.6x

Table 3.6.4 Population Sizes for C/E Data

Type of Material	Total # of Animals	#Long Term Animals
1.0x	16	7
1.6x	13	4
2.6x	16	10

Table 3.6.5 Linear Regression of Averaged C/E Data

Type of Material	Slope (%/day)	50% Day	Intercept (%)	Correlation
1.0x	-3.2	20	113	-0.98
1.6x	-2.7	25	116	-0.98
2.6x	-2.5	25	116	-0.98

Table 3.6.6 Mean Linear Regression of Individual Animal C/E Data

Type of Material	Slope (%/day)	Std. Dev. (%/day)	50% Day (days)	Std. Dev. (days)
1.0x	-3.9	1.2	19	3.0
1.6x	-3.0	1.4	23	4.6
2.6x	-2.8	0.8	26	7.5

Table 3.6.7 Data of Day Closure (zero pink area)

Type of Material	Average (days)	Range (days)	Std. Dev. (days)
1.0x	39	25 - 45	8.0
1.6x	46	39 - 53	8.1
2.6x	47	32 - 73	14.8

and 2.6x materials gaped. Inspite of the difference in the gaping of the wounds between the three different materials, C/E begins between day 6 and 7 for all three concentrations.

The higher concentrated grafts exhibited a subtle decrease in the rate of closure (rate of reduction of pink area under the silicone) when compared with the 1.0x grafts. The 1.6x and 2.6x curves are very similar. All three curves were fitted with linear regression lines from the onset of C/E to the day of closure. The results of the linear regressions and the time in days to obtain 50% closure (50% original pink area) of the wounds calculated from the regression lines are listed in Table 3.6.5 and are shown in Figure 3.6.11. The correlation was -0.98 for each material.

C/E data from each guinea pig was also fitted with a linear regression and the average slopes, 50% day and their standard deviations were calculated for each kind of material. These values are shown in Table 3.6.6. There was no significant difference in the C/E rates of the 1.6x and 2.6x grafts when they were compared using an unpaired, two-tailed, t-test ($n = 10, 12, p > 0.5$). Thus, it was assumed that the closure rate of the 1.6x and 2.6x materials were the same and were grouped together. When the combined closure rate of the concentrated materials and the 1.0x material were compared with a contrast test, they were significantly different ($p < 0.0005$). The 50% day was also significantly extended from 20 days for the 1.0x grafts to 25 days for the concentrated grafts (contrast test, $p < 0.01$). There was no significant difference between the 50% day for the 1.6x and 2.6x grafts. Figure 3.6.12 shows a comparison of the closure rate for all three materials. A distinct difference in the pink area of the graft can be seen.

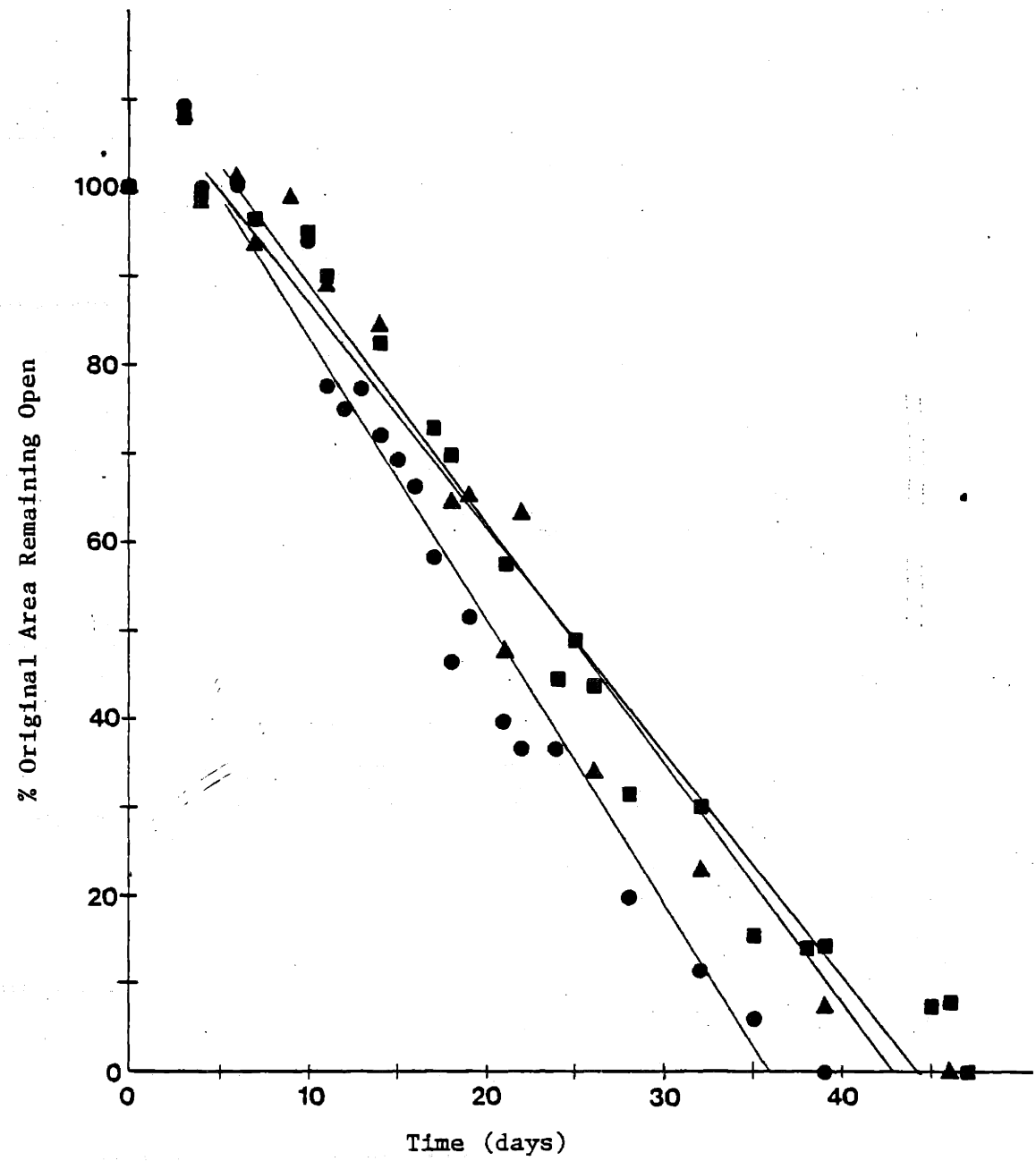

Figure 3.6.11 Composite Wound Closure Curves fitted with Linear Regressions, ●—1.0x, ▲—1.6x, ■—2.6x

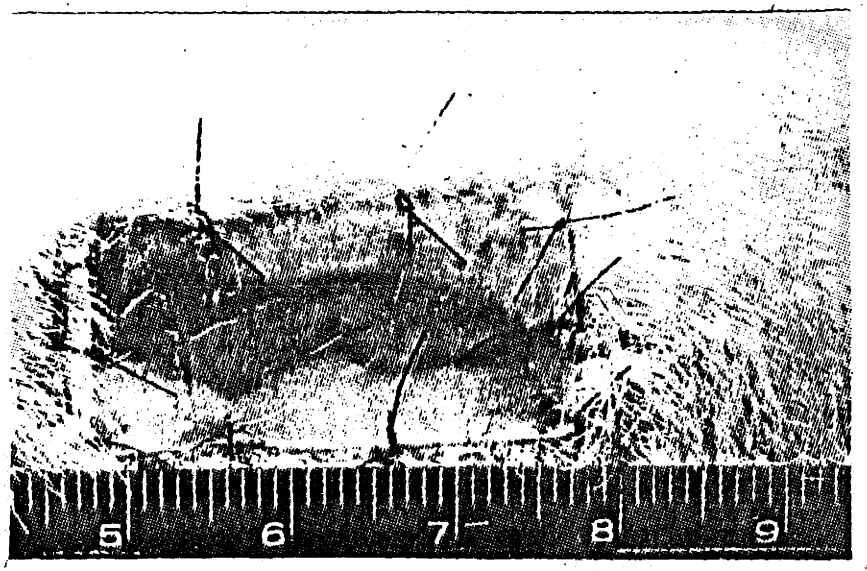

(a)

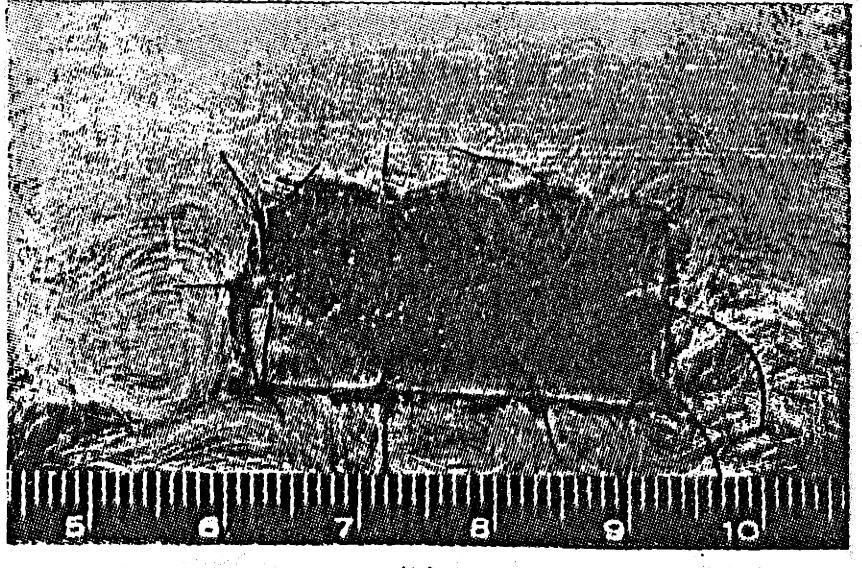

(b)

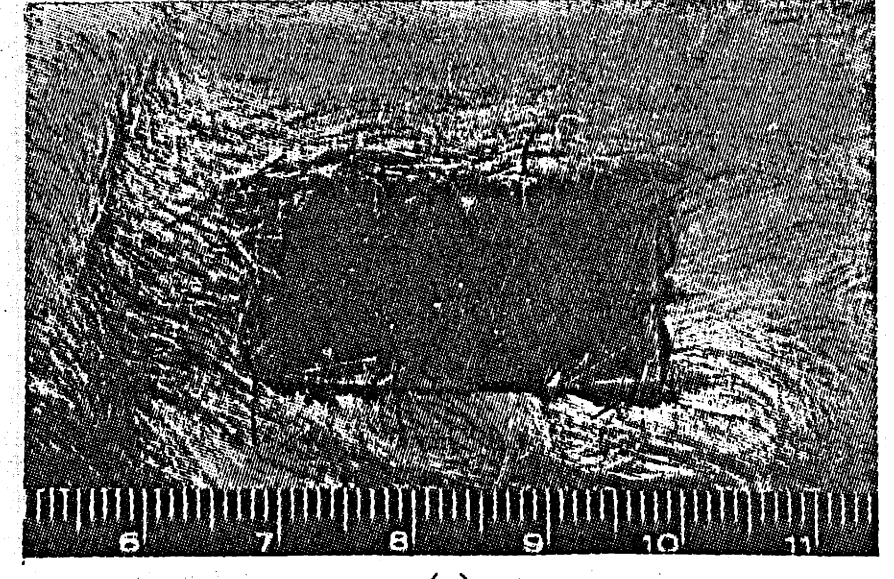

(c)

Figure 3.6.12 Comparison of Rate of Closure a) 1.0x, day 24, 34% original area, b) 1.6x, day 26, 55% original area, c) 2.6x, 54% original area

The average times for closure for the 1.0x, 1.6x, and 2.6x materials were 39 days (std. dev. = 8 days), 46 days (std. dev. = 8 days), and 47 days (std. dev. = 15 days) respectively. A comparison of the ranges of the days of closure shows a large overlapping for all three materials. The ranges are listed in Table 3.6.7. When the 1.6x and 2.6x materials were compared with an unpaired, two-tailed, t-test, it was concluded that they did not close the wounds at significantly different times ($n = 4, 9$, $p > 0.5$). The 1.6x and 2.6x closure times were compared against the 1.0x material in a contrast test and were not significantly different ($p > 0.05$).

The mean of the areas of the long term scars (times ranging from 67 days to 87 days) for the 1.0x, 1.6x, and 2.6x materials were 27.4% (std. dev. = 4.6%), 28.6% (std. dev. = 6.1%), and 24.2% (std. dev. = 6.9%) respectively. No significant difference in long term scar area was found using a one-way analysis of variance ($p > 0.7$). Figure 3.6.13 shows a typical long term scar.

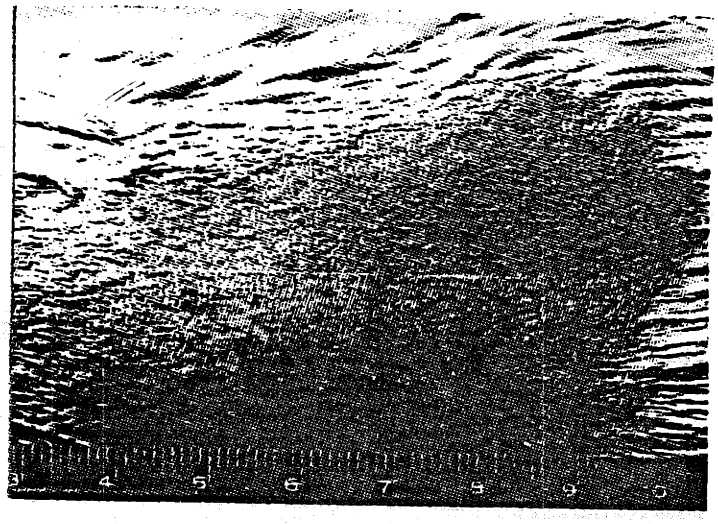

Figure 3.6.13 Typical Long Term Scar, 2.6x concentration, day 66.

4. DISCUSSION

4.1 Crosslinked versus Noncrosslinked

A strong difference in the wound healing responses for the noncrosslinked materials has been demonstrated. The major physiochemical difference between these two materials is their crosslink densities. The noncrosslinked foam had undergone only one crosslinking procedure, dehydrothermal treatment (DHT). Interchain crosslinks were most likely introduced during this process, due to the excessive removal of water from the sample [23, 34]. The number of crosslinks formed was not large, but was of sufficient quantity to insolubilize the collagen in aqueous solutions and to produce a measureable average molecular weight between crosslinks. M_c tests of noncrosslinked material exhibited an equilibrium stress greater than zero after 30 minutes [35]. It cannot be inferred from this data what would occur at infinite time.

The crosslinked material was subject to two crosslinking treatments, DHT and a glutaraldehyde bath. Glutaraldehyde reacts with the lysyl residues of collagen forming intramolecular and intermolecular crosslinks [36]. This additional crosslinking treatment reduced the M_c from 3.9×10^4 to 7.9×10^3 daltons, a five fold decrease.

From histological sections it was easily seen that the collagen of the noncrosslinked grafts were resorbed, remodelled, and became birefringent in polarized light more quickly than the crosslinked grafts. A decrease in the resorption rate of collagen *in vivo* with increased crosslink density has been demonstrated previously. Yannas, et al [37] showed this reciprocal relationship between crosslinking and degradation *in vivo*

with subcutaneous implants of collagen. Huang and Yannas [38] demonstrated that increased crosslinking of a reconstituted collagen tape decreased the rate of degradation by bacterial collagenase. Chvapil, et al found that the rate of *in vivo* resorption of extruded collagen tubes could be controlled by crosslinking [14]. A definite inverse relationship between resorption rate and crosslink density was observed. White, et al showed that collagen became more resistant to bacterial and mammaliam collagenase with increased crosslinking for collagen films [15]. Harris, et al demonstrated via radioactive labelling that the crosslinking of collagen gels decreased degradation both *in vivo* and *in vitro* [39]. Hijar [12] has shown that the rate of *in vitro* degradation of filtered, dense collagen-GAG sheets via bacterial collagenase was reduced as the crosslink density was increased.

There are two plausible reasons for the effect of crosslinking on degradation. 1) It is possible that additional crosslinking hinders the penetration of collagenase reducing the rate of degradation. Mammalian collagenase is responsible for the break down of collagen *in vivo*. It cleaves the collagen molecule at a specific site producing helical fragments [40]. These "cleavage" sites may be partially blocked by crosslinks causing inhibition of enzyme-substrate interaction [39]. Bacterial collagenase may also be obstructed by crosslinks. 2) When cleavage does take place, the crosslinks serve to retain most of the structure, retarding further degradation by other proteolytic enzymes, see Figure 4.1.1. Many proteases require some denaturation of collagen before they can degrade it [40]. These enzymes may be inhibited by the retention of the collagen structure via crosslinks. Thus, the collagen matrix would be broken

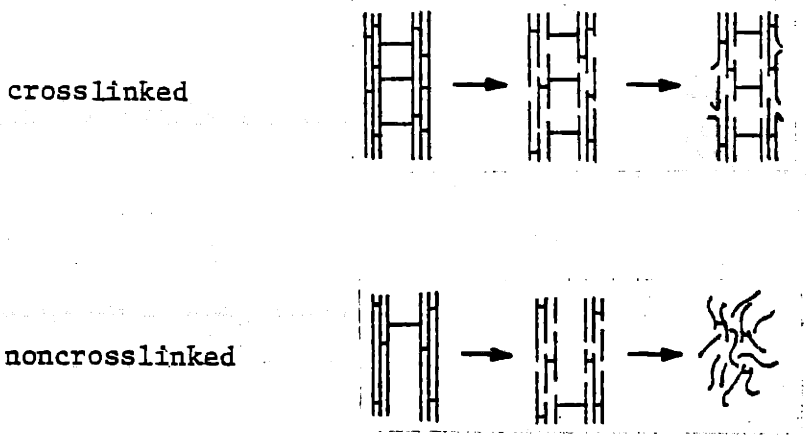

Figure 4.1.1 Schematic diagram of the stabilization of the collagen structure via crosslinking, from Bowes and Cater [36].

down more slowly and remain a stable structure for a longer period of time.

Oliver, et al [41] have performed elegant experiments with crosslinked and noncrosslinked collagen grafts in rats. Full thickness skin without the panniculus carnosus was excised from a radioactively labelled rat and all cellular elements were removed without damaging the collagen structure. Some of these cell-free dermal collagen grafts were also treated with 0.01% glutaraldehyde at pH 7.2 and 15°C for 16 hours. These crosslinked and noncrosslinked radioactive dermal grafts were sutured under a skin flap of another rat (not labelled with radioactivity). Three to four weeks later, the overlying skin was removed and a split thickness isograft was sutured over the collagen. Collagen turnover was monitored by the loss of radioactively labelled hydroxyproline from the graft site. From the measurements of the amounts of radioactive hydroxyproline remaining in the graft area at 22 weeks, Oliver determined that

the crosslinked dermal grafts only lost approximately 20% of the original collagen, while a loss of approximately 70% of original collagen content was demonstrated in the noncrosslinked dermal grafts. They concluded that the crosslink density had a profound effect on collagen degradation. Oliver's results agree with and support the histological findings of the crosslinked and noncrosslinked grafts of the artificial skin bilayer.

The increased crosslink density also reduced the C/E rate of the grafts on guinea pigs from 5%/day for the noncrosslinked grafts to 3%/day for the crosslinked grafts. Histological sections showed that the migration of the epidermis from the wound edge occurred approximately at the same rate (see Table 3.6.1) independent of crosslink density. The contribution of epidermal migration to the C/E rate was probably equivalent for the crosslinked and noncrosslinked grafts. Therefore, the decrease in the C/E rate was most probably due to an increase in the contraction rate of the wound. Contraction kinetics for Oliver's dermal grafts [41] were not reported. Results of final contracted area in Oliver's experiments were roughly the same for the crosslinked and noncrosslinked dermal grafts, but these values cannot be realistically compared to the results of the artificial skin bilayer due to the large difference in grafting procedure.

Although the noncrosslinked graft contracted much more rapidly than the crosslinked material, the response was not at all similar to the open wound response. The open wound contracted to two thirds of its original area by the third day and proceeded to contract at a rate twice that of the noncrosslinked graft and three times that of the crosslinked material.

Since crosslink density affects both the collagen degradation and

contraction rates of the grafts on guinea pigs, these two effects may be related. This experiment was not designed to reveal the mechanism of contraction. One may only speculate on the relationship. One possible explanation for the reduced rate of contraction is that the more stable crosslinked collagen foam acts as a weak internal splint. Previous studies by Stone and Madden [42] and Zahir [43] have shown that inert splinting of open wounds with polymethylmethacrylate suppressed contraction. Once the splints were removed, contraction resumed to form the usual stellate scar. It was observed qualitatively in this work that the noncrosslinked material had a lower modulus and tensile strength than the crosslinked material. However, both the crosslinked and noncrosslinked foams are very weak in compression and tension, and the silicone layer governs the mechanical properties of the bilayer in both types of grafts. Therefore, the splinting effect of the crosslinked collagen foam would be negligible.

Another explanation is that the silicone layer acts as a more effective splint with the crosslinked material than the noncrosslinked foam. The silicone rubber is attached to the collagen foam by mechanical interlocking. The extent to which chemical bonding occurs is unknown but is most likely small. Since the pore structures of the crosslinked and noncrosslinked foams are roughly the same, the mechanical interlocking or attachment of the silicone will be the same. Therefore, there is no difference in the mechanical properties of the two bilayers or in the splinting effect between the two types of collagen foams due to their interaction with the silicone layer.

It is unknown whether the collagen foams manufactured with or without

glutaraldehyde treatment are thrombogenic. The type of banding structure the collagen has after it has been processed into the artificial skin is also unknown. A direct relationship between the amount of banding and the thrombogenicity of collagen has been shown by Sylvester (1982) [44]. The bovine hide collagen when swelled at pH 3, treated with glutaraldehyde at pH 3 and dialyzed to pH 7 is not banded and nonthrombogenic when contacted with platelets in vitro. Presumably the pH 3 collagen which is freeze dried into a porous sheet, dehydrothermally crosslinked, rehydrated in pH 3 acetic acid, and crosslinked in pH 3 glutaraldehyde has a nonbanded structure. The crosslinks from the reaction with pH 3 glutaraldehyde will "lock in" the nonbanded structure when the material is dialyzed to pH 7 in deionized water and then in isopropanol [44 - 45]. The noncrosslinked material may or may not have sufficient crosslinking from the DHT crosslinking treatment to retain the pH 3 structure of collagen. The noncrosslinked material may be thrombogenic. Previous platelet aggregation tests of crosslinked foams by Forbes [45] showed no aggregation. However, these foams had not been placed in isopropanol before testing. Forbes also tested a tube of crosslinked pH 3 collagen-GAG stored in ethanol. It was thrombogenic with an asymptote (maximum per cent aggregation) of 50%. Due to the lack of standardization, the dosage levels of these two samples used in the tests are not known. These two tests imply that alcohol storage may affect the thrombogenicity of a material. Further investigation of this area is necessary.

In spite of the lack of understanding of the thrombogenicity of the graft materials, no difference in the external appearance of the grafts was observed and no blood clots or adverse blood reactions were detected

in histological samples.

4.2 The Effect of Concentration/Porosity

The variation of pore size and structure of the final freeze dried material is a function of the freezing kinetics. The size and alignment of ice crystals formed in the frozen collagen dispersion will determine the size and orientation of the pores after lyophilization. The formation of ice crystals depends on the rate of nucleation of ice crystals and on the diffusion of water molecules through the dispersion to add to the growing crystal. The most significant process that limits ice crystal growth is the inability of the water molecules to diffuse through the increasing viscosity of the freezing dispersion. Thus, the initial viscosity of the dispersion is an important parameter in the formation of the final pore structure. A higher viscosity will decrease the rate of diffusion of water molecules through the dispersion and smaller ice crystals and pores will form.

The collagen concentration will greatly affect the viscosity and the freezing of the dispersion. As the collagen concentration is increased, the viscosity also increases, inhibiting the rate of ice crystal growth. As expected on the basis of this simple model, the mean pore width decreased as the collagen concentration was increased. The thermal conductivity and freezing point of the dispersion also change as the concentration is increased, but these effects on porosity are probably small.

Occasionally in edge views of the collagen foams, a dense region was formed along the pan surface, see Figure 3.3.3 c. Since the pan surface is closest to the temperature regulated shelf, these regions

were most likely adjacent to one of the freezing coils within the shelf. This area would have frozen more rapidly causing a smaller pore size and a more dense area.

The structure of the foam consists of many interconnecting pores. A planar section through the structure reveals pores of irregular shape. Measurement of the cross sectional area of each enclosed pore, a region entirely surrounded by collagen, would be misleading. A very large area does no necessarily indicate a wide pore through which a cell may easily pass. A pore with a very large area may be a narrow, winding pore with a very large surface area to volume ratio. Particulary for the 1.0x material, where collagen walls are not continuous throughout the planar section (see Figure 3.4.1 a and b), an area measurement would be meaningless. It would ignore these walls that obstruct the path of the cell through the collagen foam. The distance between collagen walls will determine whether a cell may be able to pass through the material and is the appropriate measurement for our particular application of the collagen foam.

Each material was embedded so that the pore structure through a plane intersecting the foam could be evaluated. The embedding did not significantly alter the structure of the collagen foam. Figure 4.2.1 a and b show a comparison of the embedded edge view photographed in reflected light microscopy and a SEM photograph of an edge view which was not embedded. The two section were taken from different regions of the same foam. Similar pore structures are seen in the two photographs. The embedded photograph characterizes the pore structure in two dimensions whereas the SEM photograph reveals the three dimensional pore structure.

The photomicrographs of the polished embedded foams were traced to

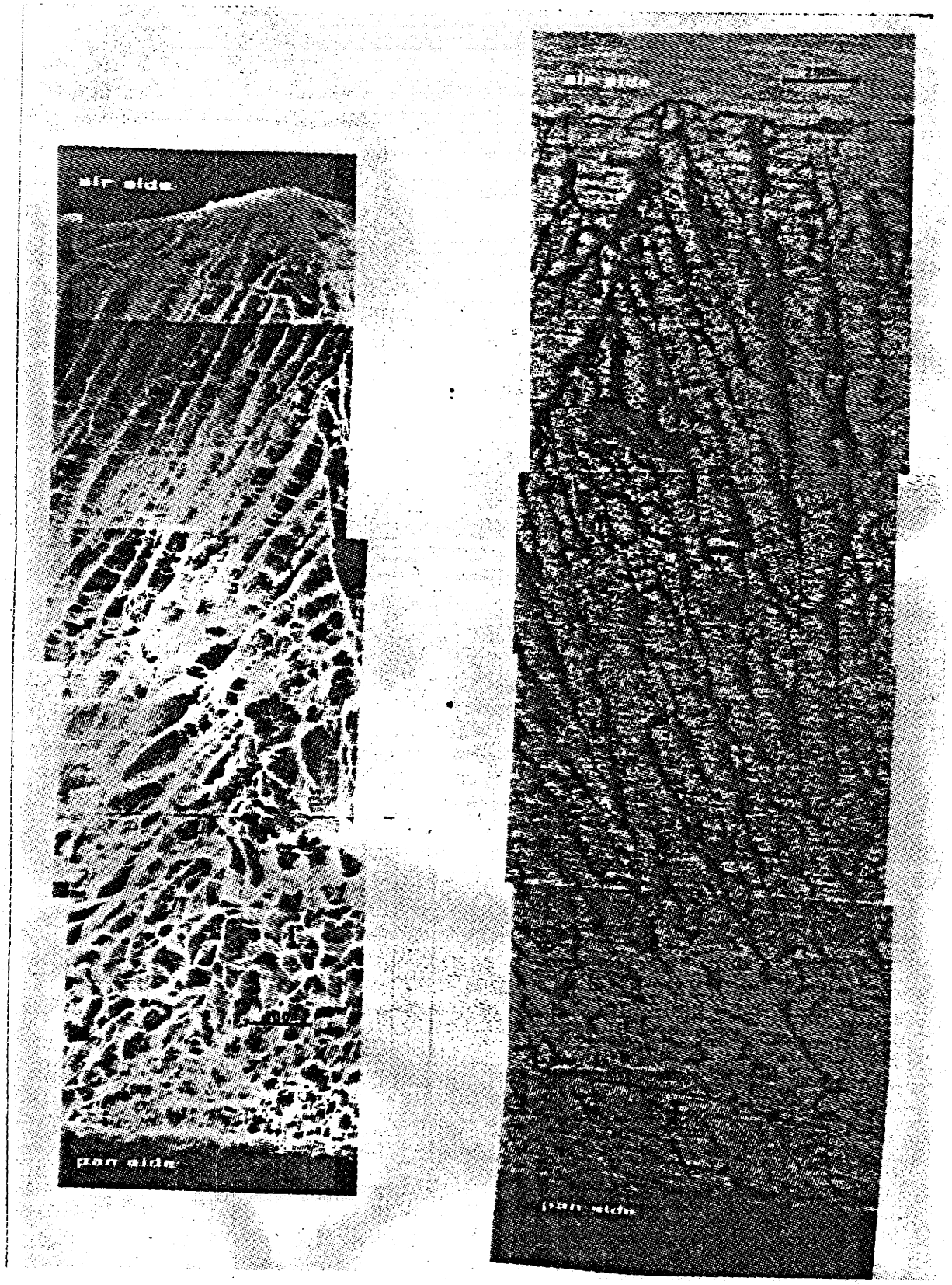

(a) (b)

Figure 4.2.1 Comparison of a) scanning electron photomicrograph and b) reflected light photomicrograph of embedded foam. The two sections were taken from nonadjacent sections of the same 2.6x foams.

increase the contrast for the computer digitization. The thickness of the collagen wall was then the thickness of the line of the pen. Since the pore width is much larger than the thickness of the collagen wall, the error introduced into the pore width measurement from this transformation is small.

Pore volume fraction was measured using gravimetric methods. If this quantity were measured using stereological methods, a large error would be introduced from the traced pore. Stereological pore volume fraction is measured by the ratio of the area of collagen to the total area of the reflected light photomicrograph. In the tracings the pore volume fraction would be the ratio of the black area to the total area. The transformation of the thickness of the collagen wall which varies to the thickness of the pen line which is relatively constant would produce a large difference between the actual collagen area and the black area of the tracing. Significant error would be introduced in pore volume fraction measurements by the tracings. Therefore, gravimetric methods were used to measure the pore volume fraction even though the values obtained by this method would not correlate with accurate stereological measurements.

The distributions of pore widths show a large number of widths of only a few microns. These low values do not indicate that there are a large number of very small pores. They are measurements in the corners and irregular walls of pores, see Figure 4.2.2. Since the computer made 256 scans per sample, these smaller width measurements are emphasized. The histogram is skewed towards the lower values and the mean of the histogram is smaller. Thus, the true mean pore width is most likely higher than the mean measured by this method.

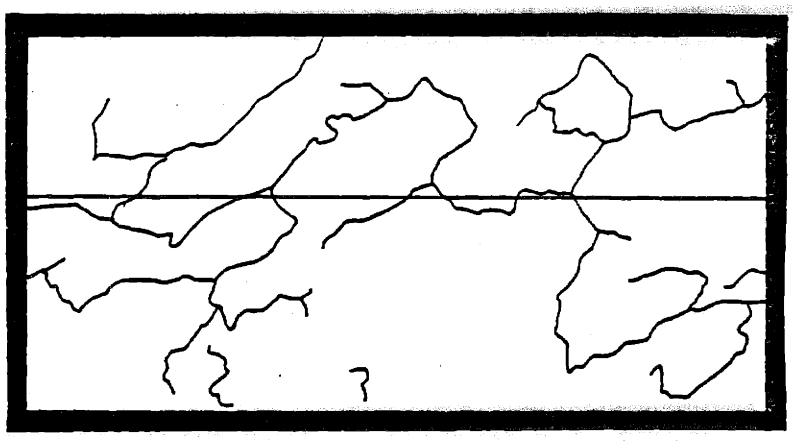

Figure 4.2.2 Computer scan showing emphasis of small pore width measurements.

The porosity had a profound effect on the initial infiltration of the mesenchymal cells from th wound bed into the pan surface of the foam. From the qualitative observations, the grafts of the 1.6x and 2.6x materials did not become well adhered to the wound bed until day 8 or 9. Histology of these materials supports these clinical observations. In histological section taken before day 8, the graft material was torn from the wound bed during sectioning of the parafin embedded sample indicating poor adhesion. After day 8 cellular infiltration of the 1.6x and 2.6x graft materials was observed and good adhesion to the wound bed was obtained. In the 1.0x graft, good adhesion and migration of cells were obtained by day 4. The grafts that became well adhered and infiltrated with cells more rapidly had a mean pore width of the pan surface before rehydration of 150μ and a broad distribution of pore widths with pore widths as large as 500μ. The reduction of the mean pore width to 100μ or 80μ and the narrowing of the distributions of pore widths seriously obstructed the path of migrating cells. Since the porosity for all materials did not consist of many pores of the same size, but a distribu-

tion of pore widths, it is most likely the distribution not the mean that controls the penetration of cells into the collagen matrix. The 1.6x and 2.6x materials had narrower distributions with fewer large pore widths and inhibited cellular migration. The minimum pore width through which a cell may pass is not known from this experiment. However, it is clear that the presence of larger pore widths on the order of 500μ facilitate the infiltration of cells into the graft.

There was no significant difference in cellular migration between 1.6x and 2.6x grafts. Thus, decreasing the mean pore width on the pan surface from 100μ as in the 1.6x foam to 80μ as in the 2.6x foam had very little effect on cell infiltration.

Measurements of the pore widths of the 1.0x, 1.6x, and 2.6x materials were performed on the foams after DHT and before rehydration. Pore widths in the rehydrated materials are most likely slightly different from the pores of the dry foam. Therefore, all measurements of pore widths are estimates of the actual dimensions of the pores of the rehydrated, grafted materials.

The values of the pore widths necessary for good cellular penetration agree with the work of Chvapil, et al [20]. From the results of subcutaneous implants of collagen-glycol methacrylate composite sponges, Chvapil stated that the pores should exceed 100μ for quick infiltration by connective tissue. His porous samples that were "biologically acceptable" had pore diameters of 450μ with a maximum of 1300μ. No description of the methods of pore measurements were made.

Dagalakis, et al [24] measured the mean pore size of the collagen-GAG foam freezed dried from dispersions of 1 - 3 w/w % solids. Mean pore

size was measured from SEM photographs using the same stereological method as in this work but with fewer scans per picture. A mean pore size of 100μ ± 80μ was measured. The % solids in Dagalakis' experiment [24] was not precisely stated. The 1 - 3 w/w % solids is similar to the 1.6x and 2.6x materials. Mean pore widths of 80μ and 100μ for the 1.6x and 2.6x materials correlates well with the values obtained by Dagalakis.

It is clear that reduction of the pore widths delays good adhesion and cellular migration. Clinically these delays would not be acceptable. Pore widths which are larger than those of the 1.0x foam may possibly speed up cellualr infiltration and adhesion. However, the increase in pore width may mechanically weaken the material and cause difficulty in handling. This area merits more investigation.

Cellular migration at the wound edges through the edge of the graft occurred more rapidly than migration from the wound bed through the pan surface of the graft for the highly concentrated materials. This observation coincides with the variation in pore size of the edge views with concentration. The increase in concentration had a much smaller effect on the mean pore width of the edge than the pan surface. The mean pore width of the pan surface decreased from 150μ for the 1.0x foam to 80μ for the 2.6x foam while the mean pore width of the edge only decreased from 145μ for the 1.0x to 123μ for the 2.6x. It is not understood why collagen concentration affects the porosity on various regions differently. There is a temperature gradient through the thickness dimension of the collagen sheet as it freezes, which may result in a difference in the porosities of the pan surface and the edge once the sheet is freezed dried into a foam.

The pore volume fraction of the 1.0x, 1.6x, and 2.6x materials decreased with increasing concentration of collagen. However, the change was small and probably did not have a large effect on cell infiltration.

The volume fraction of collagen measured in the dry foam agrees with the w/w % solids data. As the w/w % solids was increased 1.6 and 2.6 times, the collagen volume fraction increased 1.3 and 2.5 times. These values are slightly different. The difference is expected since one value is a weight percentage and the other is a volume percentage.

Both pore and collagen volume fractions were obtained from the collagen foam before rehydration. Since the collagen foam shrank less than 15% upon rehydration, these measurements of pore volume fraction are upper limits of the rehydrated values. The pore volume fractions measured, 99%, are well above the 50 - 70% value reported by Chvapil, et al [20] for a "biologically acceptable" collagen foam.

Once the mesenchymal cells entered the collagne-GAG foam, there appeared to be little inhibition of cellular migration. Since the collagen concentration did not have as large an effect on the pore widths of the edge views as on the pore widths of the pan side, the resistance to cell migration was much less once the cells had entered the graft. The columnar orientation of pores may have facilitated the migration of cells toward the silicone layer in the 1.6x and 2.6x materials. In vitro studies of cell infiltration, where basal cells were centrifuged into the graft, showed larger clusters of cells in the oriented material as compared with the random structure [33].

In the graphs of % original area remaining open versus time the gaping of grafted wounds during the first week has been observed with all materials. This phenomenon is most likely a function of the prepar-

ation of the wound bed prior to grafting rather than the type of graft material. The angle of the cut when the full thickness skin is excised may vary and produce different initial reactions at the wound edge. Therefore, the gaping shown for the 1.0x and 2.6x materials in Figure 3.6.10 is not particular to those materials.

The 1.6x and 2.6x materials significantly reduced the rate of wound closure when compared with the 1.0x grafts. Epithelialization of the grafted wound did not appear to be affected by the concentration variations. Epithelial cells migrated at roughly the same rate over all three types of material. Thus, the reduction of wound closure rate for the 1.6x and 2.6x grafts was most likely due to a decreased contraction rate.

There was no significant difference in the average C/E rate between the two more highly concentrated materials. The role of increased collagen concentration of the graft material in the mechanism of contraction is not clear. The effect is subtle and the difference between the 1.6x and 2.6x grafts may be obscured by the wide variation in biological response from animal to animal.

Since rapid cellular penetration of the graft is inhibited by the smaller pores of the 1.6x and 2.6x grafts, the concentration of collagenase produced by invading cells may increase more slowly, and resorption and remodelling of the collagen graft would be delayed. This delay in collagen degradation was observed in histological sections. There is also a higher concentration of collagen in the graft site of the 1.6x and 2.6x materials than the 1.0x material. This increase in collagen may result in a longer time for the collagenase to degrade the entire graft.

It is possible that the rate of contraction is related to the rate

of collagen degradation. Zeitz, et al have measured collagen metabolism in the healing open wound with radioactive tracers [46]. They observed a decrease in collagen catabolism in the first few days of healing. At later times the collagen degradation rate increased during wound contraction and scar tissue remodelling. Studies of the effect of cortisone treatment on wound healing have shown a decrease in wound contraction as well as the reduction in collagen formation in the wound bed [47]. A similar relationship between contraction and collagen degradation was observed for the crosslinked and noncrosslinked grafts. The crosslinked grafts degraded as well as contracted more slowly than the noncrosslinked grafts. In contrast Abercrombie, et al [48] measured the collagen content in open wounds and found that collagen formation continued after contraction had ceased. However, their measurements were overestimations of the collagen content, since their specimens taken at later stages of healing contained a significant amount of the surrounding normal skin. Klein and Rudolph [49] studied the collagen turnover and contraction in full thickness skin wounds grafted with split thickness, and thin and thick full thickness isogenic skin grafts. Collagen turnover was detected by the loss of radioactively labelled hydroxyproline form the isogenic grafts. The grafts, that had the largest loss of collagen mass with a relatively small amount of new collagen synthesis, contracted most.

It appears that there is a relationship between the rates of collagen degradation and wound contraction. This observation does not reveal the actual mechanisms of wound contraction but presents another aspect of the complicated total picture.

Although the collagen concentration/porosity and crosslink density

have an effect on the contraction kinetics in wound healing, the extent of the contraction and the appearance of the external surface of the scar is independent of these two variables. It is clear that these parameters do not prevent contraction but only delay the process. The chemistry of the system is not appreciably changed by the alterations of the porosity or the crosslink density. Certainly chemical crosslinks are formed with glutaraldehyde but the chemical interactions between the collagen and the tissue enzymes are not significantly changed; they are only delayed. Thus, the lack of substantial change in the long term scars is not surprising nor unsuspected.

It has been proposed that the epithelial cells at the wound edges partially regulate the collagen deposition in scar formation [46]. Since the epithelialization of the 1.0x, 1.6x, 2.6x, and noncrosslinked grafts appeared the same, this mechanism is consistent with the observed similarity in the external surface area and the density of collagen of the long term scar observed in all the graft materials.

4.3 Comparison of the Effect of Crosslink Density and Collagen Concentration/Porosity

It appears that the crosslink density has a larger effect on contraction and collagen degradation than the porosity or collagen concentration. There were large distinct differences between the crosslinked and noncrosslinked materials in wound closure rates and day of closure. The variation in collagen concentration had a much smaller effect. The 2.6x dispersion (1.3 w/w % solids) was very viscous and was the highest concentration that could be used without drastically changing the manufacturing protocol. The

2.6x grafts produced a smaller change in the wound healing response than the variation in crosslink density and some clinically negative results in the context of the effort to treat a patient population with massive burns.

The varied response in both histological and C/E from animal to animal was much larger for the concentrated grafts than the others. This range of data may be a result of nonuniformities in the material or the orientation of pores in relation to the wound bed. More subtle differences caused by increased collagen concentration may be observed. The day of closure is a possible example. Roughly 20% of the 2.6x animals showed a marked decrease of contraction rate, and closure did not occur until day 70, 23 days later than the average. Histological samples showed no difference in specific cellular reaction, only the kinetics were altered. A larger population of tests would need to be done to clarify the effects of concentration on rate of closure and day of closure.

Since the crosslink density clearly exhibited a larger effect on the wound response with less variation, it should be chosen over the collagen concentration as the parameter to alter degradation rate of graft material and the rate of closure.

5. SUMMARY

1. Crosslinked and noncrosslinked collagens have been grafted on full thickness skin wounds in the form of a bilayer membrane. Rates of wound closure and collagen degradation decreased with increasing crosslink density. Epithelialization rate was approximately the same for the crosslinked and noncrosslinked grafts. Therefore, the decrease in the rate of wound closure is due to a decrease in the rate of contraction. No significant differences between the appearance or areas of the external scar at day 70 were observed.
2. A method of quantitating the porosity of the dry collagen foams was developed, using reflected light microscopy and stereological measurements. The collagen foams were embedded, sectioned, and polished to reveal the pan surface and the edge views. The embedding medium reflects light without scattering whereas the rough surface of the collagen scatters light. The collagen appears black and the embedding medium appears white in reflected light. These polished samples were photographed in a reflected light microscope. The photomicrographs are traced to enhance the contrast for computer digitization. Stereological measurements of pore widths were performed with a computer, resulting in measurements of the mean pore width and distribution of pore widths.
3. Measurements of pore widths and orientations for three different concentrations of collagens (1.0x, 1.6x, and 2.6x) in the pan side and edge views were performed. Mean pore width on the pan side decreased and the distribution of pore widths became more narrow with increasing collagen concentration. Orientation of the pores of the edge

sections were observed and quantitated. A higher degree of orientation was measured for the more concentrated materials.

4. A highly porous collagen surface with a broad distribution of pore widths and mean pore width of 150μ before rehydration allowed more rapid cellular infiltration than more narrow distributions of pore width with mean pore widths of 80μ and 100μ. The 1.0x grafts, containing a significant fraction of large pores (500μ), had the best cellular infiltration.

5. Increased collagen concentration (smaller pore widths) reduced the rates of wound closure and collagen degradation.

6. The effect of crosslink density over the possible range of variables may be larger than the effect of porosity and collagen concentration on the rate of wound closure and collagen degradation.

REFERENCES

1. Peacock, E.E., and Van Winkle, W., Wound Repair, 2nd ed., Philadelphia: W.B. Saunders Co., 1976

2. Montagna, W. and Parakkal, P.F., The Structure and Function of Skin, 3rd ed., New York: Academic Press, 1974

3. Montgomery, B.J., "Consensus for Treatment of the Sickest Patients You'll Ever See," J. Am. Med. Assoc., 241:345 (1979)

4. Guildalian, J., "A Comparative Study of Synthetic and Biological Materials for Wound Dressing," J. Trauma, 13(1):32 (1973)

5. Abbenhaus, J.I. and Donald, P., "The Use of Collagen Graft for Replacement of Major Skin Loss," Laryngoscope, 81:1650 (1971)

6. Pickerell, K.L., "A New Treatment for Burns," Bull. Johns Hopkins Hosp., 69:217 (1941)

7. Person, E.A., "An Evaluation of Methyl 2-Cyanoacrylate as a Burn Dressing," Amer. Surgeon, 33(4):344 (1967)

8. Chardack, W.M., et al, "Synthetic Substitutes for Skin," Plas. Recon. Surg., 30(5):554 (1962)

9. Burke, J.F., et al, "Successful Use of a Physiologically Acceptable Artificial Skin in the Treatment of Extensive Burn Injury," Annals of Surgery, 194(4):413 (1981)

10. Yannas, I.V., "Prompt, Long Term Functional Replacement of Skin," Trans. A.S.A.I.O., 27:19 (1981)

11. James, D.W. and Newcombe, J.F., "Granulation Tissue Resorption During Free and Limited Contraction of Skin Wounds," J. Anat., 95:247 (1967).

12. Yannas, I.V., "Use of Artificial Skin in Wound Management," in The Surgical Wound, Peter Dineen, ed., Philadelphia: Lea & Febiger, 1981, p.184

13. Hijar Fernandez, P.G., "Mechanical Properties and Rate of Enzymatic Degradation of Collagen-Mucopolysaccharide Composite Materials," S.M. Thesis, Mechanical Engineering, MIT, 1979.

14. Chvapil, M., et al, "Effect of Collagen Crosslinking on the Rate of Resorption of Implanted Collagen Tubing in Rabbits," J. Biomed. Mater. Res., 11:297 (1977)

15. White, M.J., et al, "Collagen Films: Effect of Crosslinking on Physical and Biological Properties," Biomat., Med. Dev., Art. Org., 1(4):703 (1973)

16. Leighton, G., et al, Science, 155:1259 (1967)

17. Wanke, M., et al, Melsunger Med. Mitteilungen, 41:108 (1967)

18. Taylor, D.F. and Smith, F.B., "Porous Methyl Metacrylate as an Implant Material," J. Biomed. Mater. Res. Symp., 2(2):467 (1972)

19. Stasikelis, P. "Burn Dressing Based on Collagen: Structural Parameters Affecting Performance," S.M. Mechanical Engineering, MIT, 1979

20. Chvapil, M., et al, "Some Chemical and Biological Characteristics of a New Collagen-Polymer Compound Material," J. Biomed. Mater. Res., 3:315 (1969)

21. Komanowsky, M., et al, "Production of Comminuted Collagen for Novel Applications," J. Am. Leather Chem., 69:410 L91974)

22. Yannas, I.V. and Burke, J.F., "Design of an Artificial Skin. I. Basic Design Principles," J. Biomed. Mater. Res., 14:65 (1980).

23. Yannas, I.V., et al "Design of an Artifical Skin", Part II. Control of Chemical Composition," J. Biomed. Mater. Res., 14:107 (1980)

24. Dagalakis, N, et al, "Design of an Artificial Skin, Part III. Control of Pore structure," J. Biomed. Mater. Res., 14:511 (1980)

25. Weiderhorn, N.M., J. A. L. C. A., 48:77 (1955).

26. Weiderhorn, N.M. and Reardon, G.V., J. Polym, Sci., 9:315 (1952)

27. Snyder, B. and Hayes, W. C., "Stereology of Trabecular Bone," Technical Report OBL 80-2, Orth. Biomech. Lab., Beth Israel Hosp., 1980

28. Catsimpoolas, N. and Griffiths, A.L., Methods of Cell Separation, N. Catsimpoolas ed., New York: Plenum, 1978

29. Skrabut, E., Personal communication, 1982.

30. Snedecor, G.W. and Cochran, W.G., Statistical Methods, 6th ed., Ames, Iowa: Iowa State University Press, 1967, Chap. 4, p.91

31. Brown, B.W. and Hollander, M., Statistics: A Biomedical Introduction, New York: John Wiley & Sons, 1977, p. 230

32. Ryan, G.B. and Majno, G.M., Inflammation, Kalamazoo, MI: Upjoh, 1977, p. 62

33. Orgill, D.P., Personal Communication, 1982

34. Yannas, I.V. and Tobolsky, A.V., "Crosslinking of Gelatin by Dehydration," Nature, 215: 509 (1967)

35. Skrabut, E. and Flynn, S., Personal Communication, 1982

36. Bowes, J.H. and Cater, C.W., "The Interaction of Aldehydes with Collagen," Biochim. Biophys. Acta, 168:341 (1968)

37. Yannas, I.V., et al, "Correlation of in vivo Collagen Degradation Rate with in vitro Measurements," J. Biomed. Mater. Res., 9:623 (1975)

38. Huang, C. and Yannas, I.V., "Mechanical Studies of Enzymatic Degradation of Insoluble Collagen Fibers," J. Biomed. Mater. Res., 8:137 (1979)

39. Harris, E. D. and Farrell, M. D., "Resistance to Collagenase: A Characteristic of Collagen Fibrils Crosslinked by Formaldehyde," Biochim. Biophys. Acta, 287:133 (1972)

40. Peacock, E.E., "Collagenolysis: The Other Side of the Equation," World J. Surg., 4:297 (1980)

41. Oliver, R.F., et al, "Hydroxyproline Turnover in Collagen Grafts," Conn. Tiss. Res., 9:59 (1981)

42. Stone, P.A. and Madden, J.W., "Biological Factors Affecting Wound Contraction," Surg. Forum, 26:547 (1975)

43. Zahir, M., Contraction of Wounds," Brit. J. Surg., 51:456 (1964)

44. Sylvester, M., "Thrombogenicity of Collagen," S. M. Thesis, Mechanical Engineering, MIT, 1982

45. Forbes, M., S. M. Thesis, Mechanical Engineering, MIT, 1982

46. Zeitz, M., et al, "Collagen Metabolism in Granulating Wounds of Rat Skin," Ach. of Derm. Res., 263:207 (1978)

47. Billingham, R.E., et al, "Effect of Cortisone on Survival of Skin Homografts in Rabbits," Brit. M. J., 1:1157 (1951)

48. Abercrombie, M., et al "Collagen Formation and Wound Contraction during Repair of Small Excised Wounds in the Skin of Rats," J. Embryol. Exp. Morph., 2(3):264 (1954)

49. Klein, L. and Rudolph, R., "^{3}H-Collagne Turnover in Skin Grafts," Surg. Gyn. Obst., 135:49 (1972)